Final Report

Understanding Arsenic Mobilization in Groundwater of Haridwar and Formulating its Remediation Measures

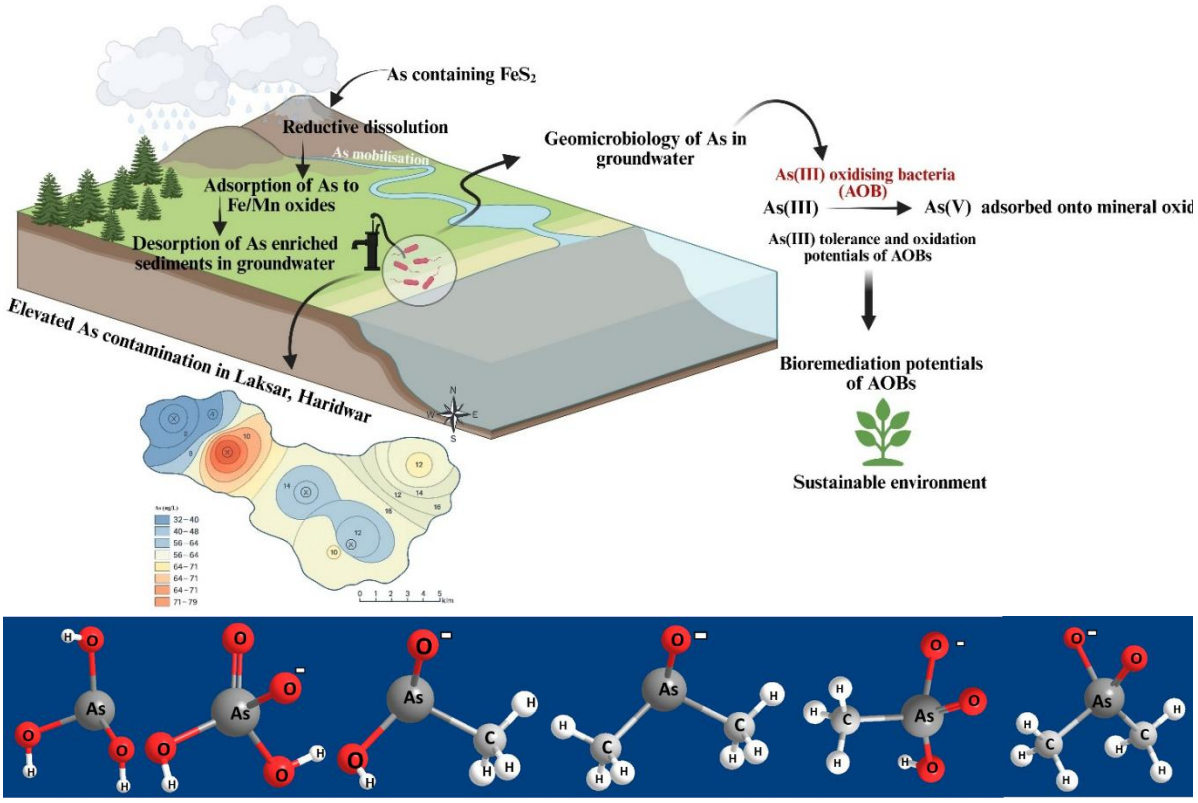

NATIONAL INSTITUTE OF HYDROLOGY
JAL VIGYAN BHAWAN
ROORKEE - 247667

2025-26

DIRECTOR

Dr. Y. R. Satyaji Rao

DIVISIONAL HEAD

Dr. Y. R. Satyaji Rao

STUDY TEAM

Dr. Rajesh Singh, Sc. E, EHD
Dr. Sumant Kumar, Sc. E, GWHD
Dr. Pradeep Kumar, Sc. E, EHD
Dr. M.K. Sharma, Sc. G, EHD
Dr. Vinay Kumar Tyagi, Sc. D, EHD
Dr. Kalzang Chodden, Sc. C, EHD

PROJECT STAFF

Ms. Shubha Dixit, Dr. Sandeep Singh, Dr. Kaptan Singh

PREFACE

Groundwater remains a lifeline for billions, particularly in developing nations like India, where it serves as the primary source of drinking and irrigation water. However, the growing incidence of groundwater contamination by naturally occurring arsenic poses a severe environmental and public health challenge. Traditionally considered geogenically safe, aquifers in parts of Uttarakhand—especially in Haridwar district—are now showing alarming levels of arsenic. Motivated by the increasing reports of arsenic occurrence in the region, this study was conceptualized to explore the hydrogeochemical processes that control its mobilization, assess its health risks, and propose informed mitigation strategies.

This research focuses on the Laksar and Khanpur blocks of Haridwar, situated in the Upper Indo-Gangetic Plain and characterized by recent alluvial deposits, shallow aquifers, and intensive agricultural and industrial activity. A total of 420 groundwater samples were collected from both shallow and deep aquifers and analyzed using advanced instrumentation such as Inductively Coupled Plasma Mass Spectrometry (ICP-MS) and Ion Chromatography. Field parameters like pH, electrical conductivity, and redox potential were recorded in situ. The integration of GIS-based mapping, statistical analysis (including PCA and Pearson correlation), and hydrochemical modeling enabled a comprehensive assessment of groundwater quality.

Results reveal that approximately 17% of the groundwater samples exceed the WHO permissible limit for arsenic, with some locations reporting concentrations as high as 102 µg/L. Geochemical analysis suggests that the mobilization of arsenic is predominantly driven by reducing conditions, reductive dissolution of Fe/Mn oxides, and microbial activity, exacerbated by anthropogenic factors such as fertilizer use and industrial discharge.

This study contributes to the growing body of knowledge on groundwater contamination in Himalayan foothill regions and provides a foundation for sustainable groundwater management in arsenic-prone areas. It is hoped that the findings will inform both policy and practice, guiding future water safety planning and public health interventions.

The report has been prepared by Dr. Rajesh Singh, Sc. E; Dr. Sumant Kumar, Sc. E; Dr. Pradeep Kumar, Sc. E; Dr. M. K. Sharma, Sc. F; Dr. Vinay Kumar Tyagi, Sc. D; and Dr. Kalzang Chodden Sc. C under the guidance of the Head of the Environmental Hydrology Division.

(Y. R. S. Rao)
Director

CONTENTS

LIST OF FIGURES

LIST OF TABLES

1. INTRODUCTION

The degradation of groundwater quality has emerged as a critical environmental and public health challenge, particularly in regions experiencing rapid urbanization, industrialization, and agricultural intensification. Among the various contaminants of concern, arsenic (As) poses a significant threat due to its toxicity, mobility, and widespread occurrence in aquifer systems. While groundwater has traditionally been viewed as a reliable and safe source of freshwater, growing evidence suggests that both anthropogenic activities and natural geochemical processes are contributing to its deterioration.

In South Asia, the Indo-Gangetic Plain, one of the world's most extensive and densely populated alluvial aquifer systems, has reported increasing incidences of groundwater contamination. Although historically considered water-rich, the region is now facing rising levels of geogenic contaminants such as arsenic, fluoride, and uranium, often exceeding safe drinking water standards (Kumar et al., 2021a, 2021b; Nijesh et al., 2021; Pant et al., 2021; Pal et al., 2022; Gautam et al., 2022). The mobilization of these elements is often exacerbated by large-scale groundwater abstraction, which alters redox conditions and enhances the release of arsenic and other trace elements from aquifer sediments (Lapworth et al., 2017).

Anthropogenic factors further compound the problem. Unregulated discharge of industrial effluents and untreated sewage into surface water bodies, coupled with intensive agricultural practices and use of agrochemicals, can lead to the infiltration of contaminants into shallow aquifers. Additionally, irrigation return flows and induced vertical hydraulic gradients facilitate the downward migration of pollutants, triggering complex biogeochemical interactions that can mobilize arsenic and other toxic elements (Appelo and Postma, 2005; Lapworth et al., 2017, 2018).

In the Haridwar district of Uttarakhand, groundwater is the primary source of water for domestic and agricultural use. Traditionally regarded as safe, the region’s groundwater is now under threat from rising population pressures, expanding industrial activities, and poor waste management. Recent concerns have highlighted the presence and potential mobilization of naturally occurring arsenic, attributed to both abiotic and biotic weathering of primary and authigenic minerals.

Globally, groundwater accounts for approximately 95% of the accessible freshwater supply (Lall et al., 2020) and plays a crucial role in supporting domestic, agricultural, and industrial needs, as well as maintaining ecological balance (Grogan et al., 2017). However, its quality is increasingly compromised by the interplay of human activities and natural processes. Since the Industrial Revolution, arsenic contamination of groundwater has become a significant environmental hazard, with severe implications for human health, especially in developing countries (Burri et al., 2019).

This study aims to investigate the hydrogeochemical characteristics of groundwater in the Haridwar region, with a particular focus on the occurrence, mobilization pathways, and potential health risks associated with arsenic contamination.

1.1. Occurrence of Arsenic in GW and Its Human Health Impacts

Arsenic contamination of groundwater is a global concern, affecting millions of people who rely on untreated groundwater for drinking and cooking. Chronic ingestion can lead to arsenicosis, a condition characterized by skin pigmentation changes, hyperkeratosis, and various cancers, especially of the skin, lungs, bladder, liver, and kidneys (Shankar et al., 2014). The International Agency for Research on Cancer (IARC) classifies arsenic as a Group 1 carcinogen (IARC, 2012), with exposure linked to multiple health disorders including developmental abnormalities and cardiovascular diseases (Hughes et al., 2011; Saint-Jacques et al., 2014; Madhukar et al., 2016; Health Canada, 2017). An estimated 220 million people worldwide are exposed to arsenic concentrations exceeding the WHO guideline of 10 µg/L (Amini et al., 2008a; Fendorf et al., 2010).

1.1.1. Geochemical Forms and Mobility

In groundwater, arsenic primarily occurs in two inorganic forms: Arsenite [As(III), H_3AsO_3] and Arsenate [As(V), $HAsO_4^{2-}$]. Their mobility and toxicity are strongly influenced by redox conditions, pH, and microbial activity. As(III), dominant under reducing (anoxic) conditions, is more toxic and mobile, up to 60 times more, than As(V), which prevails in oxidizing environments (Jain & Ali, 2000; Parul & Saraswat, 2024; Baloch et al., 2020).

Arsenic is naturally present in the Earth's crust and is released into groundwater mainly through the weathering of arsenic-bearing minerals such as pyrite (FeS_2), which can contain up to 2300 µg/g of arsenic (Smedley & Kinniburgh, 2002). Mobilization occurs through abiotic redox reactions and microbial processes, including the reductive dissolution of iron oxides that often adsorb or incorporate arsenic (Dixit & Hering, 2003; Missimer et al., 2018; Malakar et al., 2016).

Under anoxic conditions, microorganisms utilize Fe(III) oxides as electron acceptors, promoting their dissolution and releasing co-associated arsenic into groundwater. This process also facilitates the reduction of As(V) to the more toxic As(III) (Herbel & Fendorf, 2006; Fendorf et al., 2010). In contrast, under oxic conditions, arsenic may be adsorbed onto newly formed Fe-oxyhydroxides, effectively removing it from solution (Straub et al., 2001; Bissen & Frimmel, 2003). These redox-driven adsorption-desorption mechanisms, along with microbial mediation, are central to arsenic's environmental mobility and bioavailability.

1.1.2. Global and Regional Distribution

Arsenic-contaminated groundwater is prevalent in South and Southeast Asia, Latin America, parts of Europe, and the United States (Podgorski & Berg, 2020). Countries such as Bangladesh, India, China, Vietnam, Mexico, and Chile report widespread contamination, often with severe public health consequences (Table 1.1).

Table 1.1. Occurrence of the Arsenic in the groundwater across the world

Country	Study Area	Max As conc. (µg/L)	References
Afghanistan	Santiago del Estero Province	14,969	Bhattacharya et al. 2006
Australia	Stuarts Point coastal	85	Smith et al. 2003
Bangladesh	Noakhali	4730	Chakraborti et al. 2010
Bolivia		364	Bundschuh et al. 2010
Brazil		2980	
China	Datong Basin	1932	He et al. 2021
	Hetao Basin	572	Guo et al. 2008
	Yinchuan	177	Guo et al. 2014
Cambodian		1610	Berg et al. 2007
Ecuador		969	Bundschuh,2021
Ethiopia	Southwestern Ethiopia	184.5	Berg et al. 2007
Ghana		1760	Kusimi et al. 2012
Hungary	Southern Hungary	260	Rowland et al. 2011
India	Bhair	1466	Dhillon, 2020
	Shahpur block, Bhojpur district, Bihar state	1805	Chakraborti et al. 2009
	Punjab	3192	Dhillon, 2020
	Haridwar	0.10 to 102	Khan and Rai, 2022
	Haridwar	12.5	Sharma et al. 2024
Iran	Kurdistan Some villages	1500	Hamidian et al. 2019
	Isfahan Mutehgold mining district	1061	
Japan		38	Tashdedulet al.2022
Korea	Geumsan County	113	Jadhav et al. 2015
Nigeria	Warri-Port Harcourt, Ogun State, Kaduna	750	Shaji et al. 2021
Myanmar	Ayeyarwady	630	Wang et al. 2021
Mexico	La Laguna Region	5000	
Nepal	Nawalparasi	2620	
Spain	Duero Cenozoic Basin	613	Gómez et al. 2006
Thailand	Suphan Buri	5000	Shaji et al. 2021
USA	Lahontan Valley, in Churchill County, Nevada	4100	Walkera et al. 2008

In India, arsenic has been detected at elevated levels in states like West Bengal, Bihar, Uttar Pradesh, and Uttarakhand. Within Uttarakhand, Laksar and Khanpur blocks in Haridwar district are identified arsenic hotspots (Khan & Rai, 2022). The Ganga–Meghna–Brahmaputra (GMB) basin, characterized by Holocene alluvial sediments rich in organic matter and fine-grained materials, is particularly vulnerable to arsenic mobilization under reducing conditions (Chakraborti et al., 2004; Mukherjee et al., 2019).

Additionally, iron (Fe) and manganese (Mn) are frequently co-mobilized due to similar geochemical behaviors. Their elevated concentrations further deteriorate groundwater quality and are associated with industrial waste discharge, urban runoff, and solid waste mismanagement (Kumar et al., 2024).

1.1.3. Implications for Public Health

Arsenic exposure via contaminated drinking water remains one of the most pressing environmental health threats worldwide. The speciation, bioavailability, and toxicity of arsenic are governed by dynamic interactions between redox conditions, iron mineralogy, organic matter, and microbial communities (Sorg et al., 2014; Malakar et al., 2016).

In groundwater systems where anoxic conditions dominate, the prevalence of As(III) increases the risk to human health due to its higher toxicity and bioaccumulation potential. Understanding these geochemical mechanisms is essential for developing effective mitigation strategies, especially in vulnerable regions like Haridwar where reliance on groundwater is high and regulatory controls are limited.

1.2. Factors Influencing Arsenic Mobilization

The mobilization of arsenic in aquifers is governed by a complex interplay of physicochemical and hydrogeological factors, including:

- Redox conditions
- pH and ionic competition
- Presence of organic matter
- Microbial activity
- Adsorption–desorption dynamics
- Aquifer recharge processes

Under reducing conditions, iron-reducing bacteria can dissolve iron (Fe) oxides, thereby releasing adsorbed or co-precipitated arsenic into groundwater. One of the primary mechanisms driving this process is the reductive dissolution of Fe/Mn (oxy)hydroxides, often triggered by the presence of labile organic matter (Smedley & Kinniburgh, 2002; Hug et al.,

2020). Competitive desorption due to the presence of bicarbonate and phosphate ions further contributes to arsenic mobilization.

Arsenic release is mediated by both geochemical transformations and microbial metabolism, which are in turn strongly influenced by the geochemical characteristics of the aquifer system (Dowling et al., 2002; Oremland & Stolz, 2003). Reductive dissolution of arsenic-bearing Fe minerals has been widely identified as a dominant pathway for arsenic release into groundwater (McArthur et al., 2001; Chakraborty et al., 2015). In anoxic environments, dissimilatory Fe/Mn-reducing microorganisms utilize Fe/Mn (oxy)hydroxides as terminal electron acceptors during anaerobic respiration, leading to the dissolution of these minerals and the subsequent release of arsenate (Islam et al., 2004). Furthermore, arsenate itself can act as a terminal electron acceptor; certain microbial species are capable of reducing As(V) to the more mobile and toxic arsenite as part of their respiratory processes (Fan et al., 2008; Slyemi & Bonnefoy, 2012). Changes in redox potential and pH can also facilitate the abiotic dissolution of arsenic-bearing minerals, further enhancing arsenic mobility in groundwater systems (Jiang et al., 2019).

1.3. Context, Justification, and Objective of the Study

Arsenic contamination in groundwater has historically been concentrated in the aquifers of the Lower Gangetic Plain (Kulkarni et al., 2017; Singh & Singh, 2015). However, recent evidence highlights its emergence in the Upper Gangetic Plain, particularly within Holocene-aged aquifers (Khan & Rai, 2022). One such vulnerable region is the Laksar block in the southeastern part of Haridwar district, located within the Khadar tract. This area is geologically characterized by recent alluvial deposits resulting from periodic riverine flooding (Ministry of Water Resources, 2016).

The unconfined aquifers in Laksar are composed mainly of fine sand, silt, and clay, and are marked by high permeability and shallow water tables. These hydrogeological conditions, combined with intense agricultural activity and an expanding industrial footprint, make the region susceptible to groundwater contamination, particularly by arsenic. Despite its significance, there has been a lack of comprehensive studies examining the coupled geochemical and microbial processes driving arsenic mobilization in this area (Kumar et al., 2019; Khan & Rai, 2023).

In Haridwar district, arsenic concentrations in groundwater have been reported with approximately 17% of samples exceeding the World Health Organization (WHO) guideline value of 10 µg/L (Sharma et al., 2024). Although other groundwater parameters, such as nitrate, fluoride, and sulfate, typically fall within permissible limits, the elevated arsenic levels observed in the Laksar and Khanpur blocks pose significant public health risks (Khan & Rai, 2022). Compounding the issue is the rapid industrialization of the region. Although several reports have flagged concerns over declining water quality and its health implications, a

systematic and integrated groundwater quality assessment, particularly one focused on arsenic, has not been conducted in over a decade. In response to these critical knowledge gaps, this study is designed with the following key objectives:

- To determine the mechanisms governing the arsenic mobility, and quantify the rate and extent of these reactions
- To design alternatives to mitigate arsenic contamination of drinking water

By addressing these objectives, the study aims to contribute a scientific foundation for groundwater management policies and intervention strategies that promote environmental sustainability and safeguard public health in Laksar, Haridwar and similar arsenic-affected regions.

2. MATERIALS & METHODS

2.1. Study Area

Haridwar district, a holy place, is located in the western part of Uttarakhand state (Fig. 2.1), between 77°42' to 78°22' E longitude and 29°35' to 30°15' N latitude, covering a geographical area of 2,360 km². It is bounded by Saharanpur district to the west, Dehradun district to the north and east, Pauri Garhwal to the east, and Muzaffarnagar and Bijnor districts to the south (District Survey Report, 2018). Geologically, the district lies beneath the Shiwalik mountain ranges and forms part of the western Indo-Gangetic Plain, composed of Pleistocene and sub-recent alluvium deposited by Himalayan rivers.

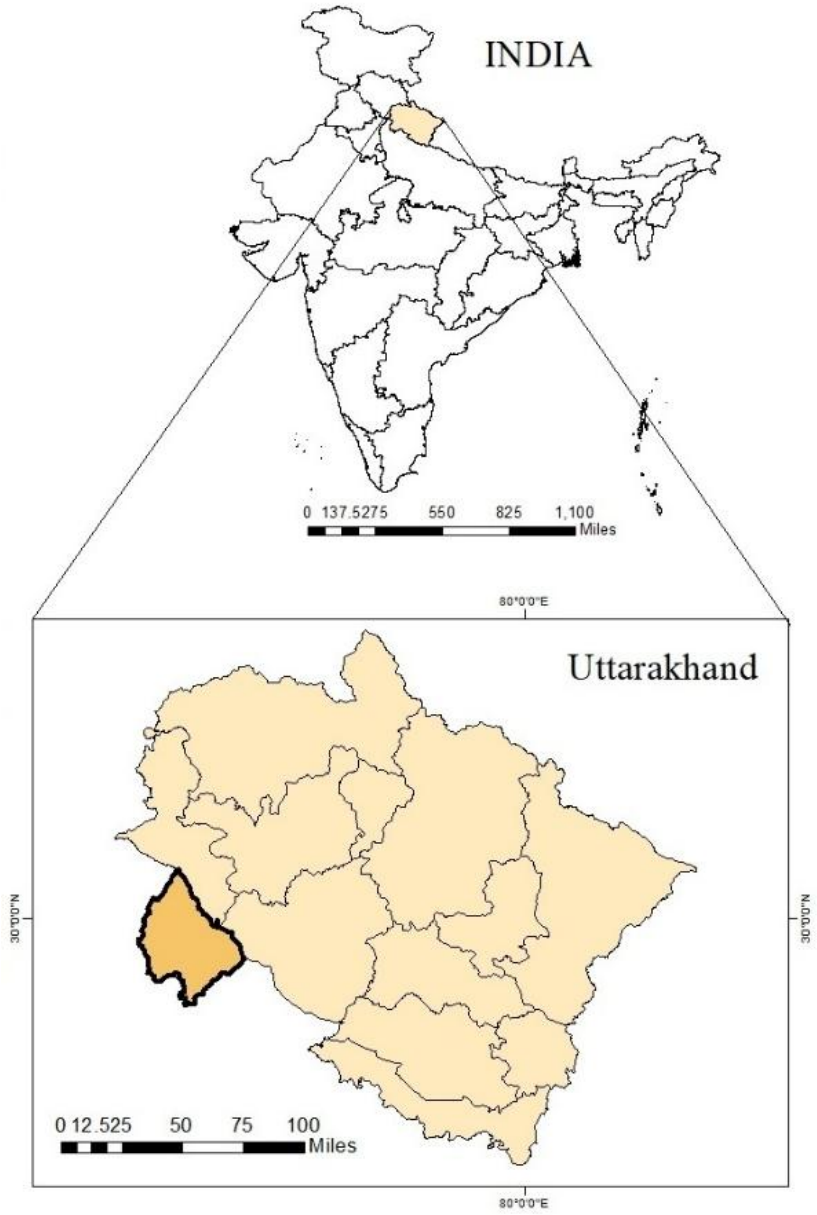

Fig. 2.1. Location map of study area

Administratively, the district comprises six blocks, Bahadrabad, Bhagwanpur, Roorkee, Narsan, Laksar, and Khanpur, and four tehsils, Haridwar, Roorkee, Bhagwanpur, and Laksar (https://haridwar.nic.in/tehsil/). According to the 2011 Census, Haridwar has a population of 1,890,422, with the Roorkee and Laksar blocks housing 238,422 and 21,760 people, respectively. General information about the district is summarized in Table 2.1.

Table 2.1. illustrate General Information about Haridwar district

Latitude	77° 42' to 78° 22' N
Longitude	29°35' to 30°15' E
Geographical Area (km^2)	2360
Average elevation (meter)	314
Total Population (Number) (censes, 2011)	1,890,422
Population density/km^2 (censes, 2011)	801
Overall Literacy rate (%)	73.43
Urbanized area (%)	36.66
Rural area (%)	63.66
Tehsils	04
Blocks	06

2.1.1. Land Use and Land Cover (LULC)

LULC data for Haridwar district were derived from Landsat-8 satellite imagery. Agricultural land constitutes approximately 54.9% of the total area, while built-up areas (including commercial, residential, and roads) cover 11.75%. Water bodies (excluding rivers) account for 1.22%, forests, vegetation, scrubs, and grasslands occupy 26.6%, and bare ground covers about 4.3% of the district (Fig. 2.2).

2.1.2. Climate

The climate of the Roorkee and Laksar blocks is subtropical and sub-humid (dry), with significant humidity. The district experiences three distinct seasons: winter, summer, and monsoon. Temperatures rise from March (average 27.6 °C), peaking in May (average 37.2 °C) before the monsoon season starts mid-June, after which temperatures decline. Winter temperatures, from December to February, range between 17.7 °C and 24.7 °C. The average annual rainfall is 1,174.3 mm, of which 84% falls during the monsoon season and 16% during the rest of the year (CGWB, 2016).

2.1.3. Drainage

The primary drainage system is the Ganga River (Fig. 2.1), which flows southward through the eastern part of the district, entering at the Haridwar boundary. Tributaries such as Ban Ganga, Kotwali Rao, Rasawan Nadi, and Pili Nadi originate from the Siwalik Hills. The perennial Solani River drains the central part of the district, with tributaries like Sipla Nadi, Mohand, Chillawal, Ratmau Rao, and Gholna Rao contributing to its flow. Seasonal rivers or nalas also feed into these systems (CGWB, 2016). The Upper Ganga Canal, originating from the Bhimgoda barrage, runs approximately 291 km with a head discharge of 370 m^3/s, dividing Roorkee into two parts (https://idup.gov.in/en/article/ganga).

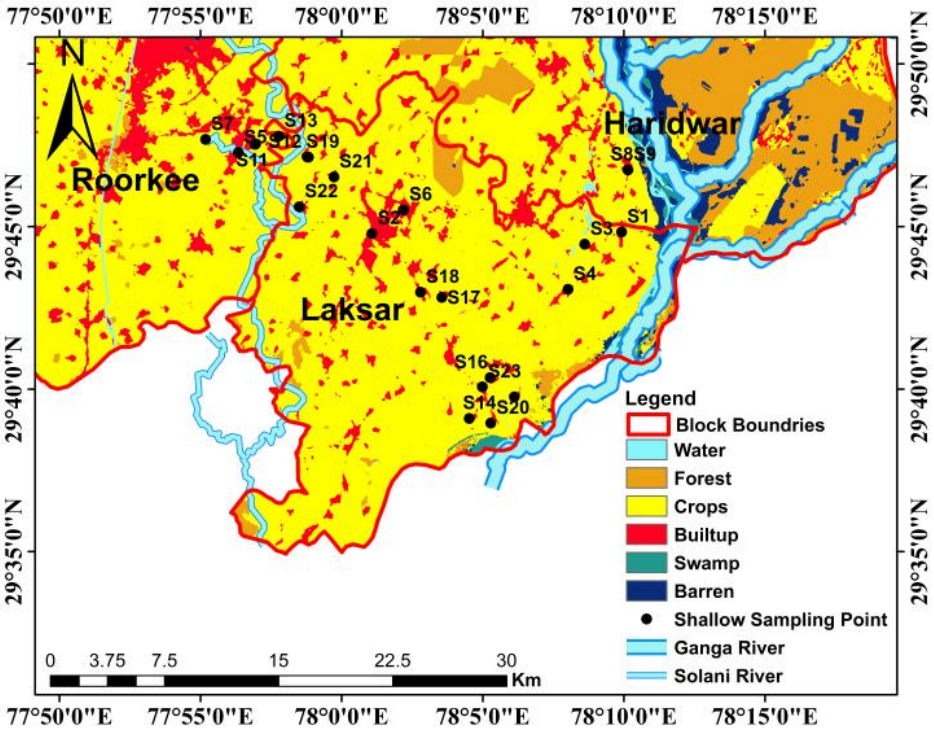

Fig. 2.2. LULC and drainage of study area

2.1.4. Groundwater

The Central Ground Water Board (CGWB) has installed 33 tube wells across the district. Water supply comes from deep tube wells, shallow tube wells, and treated surface water, with deep tube wells being the most extensively utilized (Gantait & Agarwala, 2021). The extensive Ganga alluvium supports intensive agriculture, exerting pressure on unconfined aquifers. Due to rising water demand and limited surface water availability, groundwater resources are becoming scarce. Environmental assessments indicate variable contamination with heavy metals, primarily due to anthropogenic activities (Gantait & Agarwala, 2021).

Water levels in Roorkee block vary from 3.20 to 19.39 meters below ground level (mbgl), with some tube wells recording 11 to 18 mbgl. Seasonal water level fluctuations range from 0.47 m to 3.65 m. In Laksar block, pre-monsoon and post-monsoon depths range between 4.38–5.69 mbgl and 2.32–2.53 mbgl, respectively, with fluctuations between 1.85 m and 5.69 m (CGWB, 2016).

2.1.5. Soil

Soil types significantly influence agriculture and groundwater recharge in Roorkee and Laksar blocks. The major soil orders include (CGWB, 2016):

- Ultisols (Brown Hill Soils): Predominant in northern Siwaliks, these soils have a clay accumulation horizon and low base saturation.
- Entisols (Bhabar Soils): Found in the Siwalik foothills and Tarai, characterized by absence of pedogenic horizons and high fertility despite coarse texture.
- Molisols (Tarai Soils): Located in southern parts of the district, composed of fine sand, silt, and clay, with high organic content in the surface horizon, making them very fertile.

2.1.6. Fauna and Flora

Forests cover about one-fourth of the district, rich in Ayurvedic herbs and other forest products vital for local livelihoods. Common tree species include Sal (*Shorea robusta*), Khair (*Senegalia catechu*), Shishum (*Dalbergia sissoo*), Chir Pine (*Pinus roxburghii*), Bamboo (*Bambusa vulgaris*), Sahtoot (*Morus alba*), Tun (*Toona ciliata*), and Papri (*Holoptelea integrifolia*). Many trees support industries such as paper and matchstick manufacturing.

The fauna is diverse, especially within Rajaji National Park, home to over 50 mammal species including the critically endangered Asian elephant. Haridwar also hosts over 300 bird species, with around 90 migratory species such as pockards, gulls, mallards, teals, and shells, situated within the Gangetic Plains biogeographic zone (NGT, 2019).

2.2. Sample Collection & Handling

A total of 237 shallow (20–150 feet) and 183 deep (150–660 feet) groundwater samples were collected from 23 shallow and 17 deep sampling points, respectively (Table 2.2; Fig. 2.3 & 2.4). Sampling sites were influenced by intensive agricultural and anthropogenic activities. Hand pumps were continuously operated for at least 15 minutes before sample collection to ensure representative groundwater samples.

Table 2.2. Shallow and deep groundwater sampling locations

Shallow Sampling Locations			
Location	**Location Name**	**Lat**	**Long**
S1	Fatwa School	29.74722	78.16536
S2	Laksar market	29.74644	78.01794
S3	Alawalpur	29.74095	78.14353
S4	Khanpur	29.71785	78.13369
S5	Gadhrauna	29.7879	77.939
S6	Laksar Nagar Palika Home	29.75861	78.03667
S7	Jainpur jhanjheri	29.79465	77.91964
S8	Bhogpur (home)	29.77904	78.16912
S9	Bhogpur (HOSPITAL)	29.77904	78.16911
S10	Thithola	29.79214	77.94893
S11	Khempur jojha	29.7923	77.9492
S12	Dausni Phatak	29.78564	77.97965
S13	Hazzarpur home	29.79632	77.9629
S14	Kalasiya Home	29.65163	78.07538
S15	Gangdaspur	29.6627	78.102
S16	Panditpuri road side	29.67256	78.08768
S17	Akoda Kalan	29.71368	78.05915
S18	Mundakheda khurd	29.71638	78.04662
S19	Fatwa Home	29.78556	77.98042
S20	Damanpuri	29.64925	78.08808
S21	Husainpur (Tample)	29.77543	77.9955
S22	Kuwakheda	29.76014	77.97495
S23	Kudi Habibpur	29.66781	78.08313
Deep Sampling Locations			
Location	**Location Name**	**Latitude**	**Longitude**
S1	Akodakalan	29.71274	78.061
S2	Alawalpur	29.73938	78.14028
S3	Chamanlal	29.80704	77.92767
S4	Dammanpuri	29.64915	78.08781
S5	Dausani Water Tank	29.78213	77.98424
S6	Fatwa Cattle	29.74572	78.16559
S7	Gadhrauna	29.7024	77.93973
S8	Gangdaspur	29.66233	78.10257
S9	Hazzarpur	29.79489	77.96491
S10	Jainpur jhanjheri	29.79466	77.91957
S11	Kalsiya	29.65334	78.07638
S12	Kuwakheda	29.75988	77.97502
S13	Landhaura	29.8092	77.93179
S14	Mundakheda	29.716	78.04674
S15	Panditpuri Tubewell	29.67068	78.08813
S16	Bhogpur (Tank)	29.7781	78.16906
S17	Laksar market	29.74644	78.01794

Water samples were collected using the grab sampling method in polypropylene bottles (Table 2.3) and preserved according to standard protocols (APHA, 2017). For organoleptic parameters, major ions, and trace metals including arsenic, polyethylene bottles were used. GPS coordinates were recorded for all sampling points.

Table 2.3. Samples Collection & Handling

Sr. No.	Parameter	Container	Sample Size (ml)	Preservation	Analysis Time
1	pH	--	--	--	Onsite
2	Temperature	--	--	--	Onsite
3	Conductivity	--	--	--	Onsite
4	ORP	--	--	--	Onsite
5	Major Ions	Plastic bottle	500	--	<10 days
6	Trace Metals	Plastic bottle	100	0.5 ml HNO_3	<30 days
7	Bacteriological	Plastic bottle	250	4 °C	6-8 hrs

The organoleptic parameters, major ions and trace metals following APHA's Standard Methods for the Examination of Water and Wastewater (APHA, 2017).

2.2.1. Chemical and Reagents

All chemicals used for analysis were of analytical reagent grade (Merck, BDH, Thermo Fisher). Standard solutions of metal ions, traceable to NIST, were procured from Merck (Germany). Deionized water was used throughout all analytical processes.

Glassware and containers used for trace metal analysis were thoroughly cleaned by initial washing with detergent, followed by soaking in 10% nitric acid for 48 hours, and finally multiple rinses with deionized water. For pesticide analysis (if applicable), all glassware was rinsed with chromatography-grade solvents prior to use.

2.2.2. Analytical Methodology

All water samples were analyzed following Standard Methods for the Examination of Water and Wastewater (APHA, 2017) (Table 2.4). In-situ parameters, pH, electrical conductivity, temperature, and ORP, were measured using a multi-parameter analyzer (Thermo Scientific Orion Star A329). Major ions were determined using Ion Chromatography (Metrohm 930 Compact IC Flex). Alkalinity (HCO_3^-) was measured via acid titration. Trace metals, including arsenic, were analyzed using Inductively Coupled Plasma Mass Spectrometry (ICP-MS) (Agilent Technologies). The samples for trace metals were digested in nitric acid and hydrogen peroxide for oxidation/removal of organics in Anton Paar Multiwave PRO Microwave Reaction System and filtered through 0.45-micron filter paper before injecting in ICP-MS.

Table 2.4. Analytical Methods and Equipment's used in the Study

Sr. No.	Parameter	Method	Equipment Used
A.	**Physicochemical**		
1	pH	Electrometric	pH meter – Thermo-Orion
2	Electrical Conductivity		
3	Oxidation-Reduction Potential		
4	Total Dissolved Solids	Gravimetric Method	
5	Bicarbonate	Titration by H_2SO_4	Digital Burette
6	Calcium	Conductivity Method	Ion Chromatograph (Metrohm 930 Compact IC Flex)
7	Magnesium		
8	Sodium		
9	Potassium		
10	Chloride		
11	Fluoride		
12	Nitrate		
13	Sulfate		
14	Phosphate		
B.	**Trace Metals**		
15	Arsenic	Digestion followed by Inductively Coupled Plasma Mass Spectrometry (ICP-MS)	ICP-MS (Agilent Technologies)
16	Aluminium		
17	Beryllium		
18	Chromium		
19	Cadmium		
20	Cobalt		
21	Copper		
22	Iron		
23	Lead		
24	Manganese		
25	Mercury		
26	Nickel		
27	Selenium		
28	Uranium		
29	Zinc		
C.	**Trace Metals**		
30	Total coliform	Colilert – 18 (Enzyme Substrate Coliform Test)	Biosafety cabinet, UV cabinet
31	E. coli		

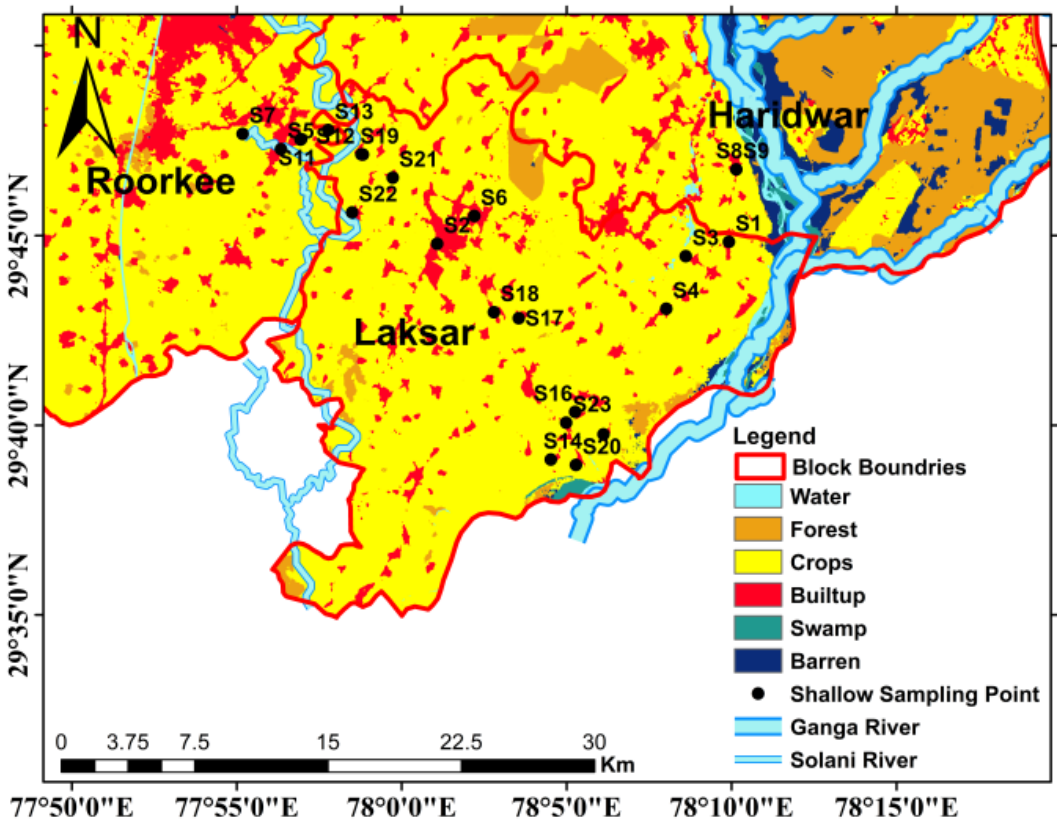

Fig. 2.3. Shallow groundwater sampling points

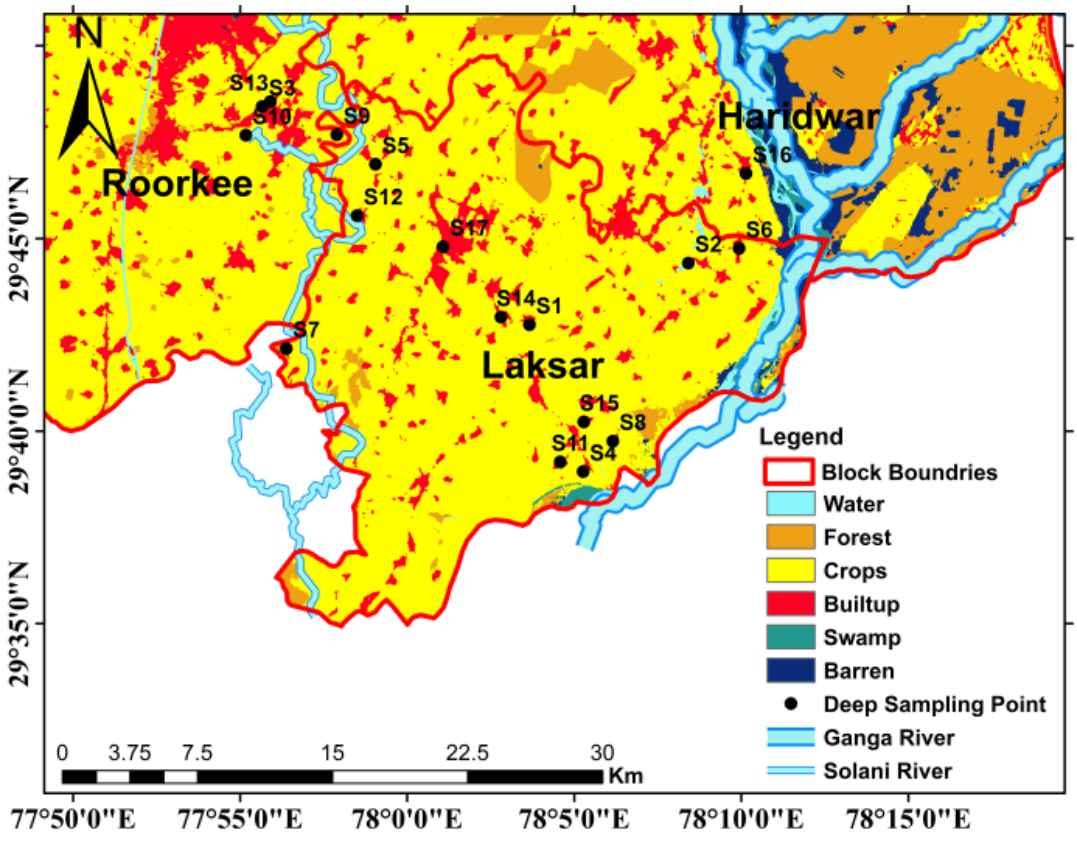

Fig. 2.4. Deep groundwater sampling points

Enumeration of E. coli and total coliforms was performed using the Colilert-18 (Quanti-Tray/2000™, IDEXX) method (APHA, 2017). This technique employs o-nitrophenyl-β-D-galactopyranoside (ONPG) and 4-methyl-umbellfieryl-β-D-glucuronide (MUG) as chromogenic and fluorogenic substrates. β-galactosidase hydrolyzes ONPG to a yellow product, while β-glucuronidase cleaves MUG to yield a fluorescent compound detectable under UV illumination.

2.3. Enrichment and Isolation of Arsenic Resistant Bacteria

Microbial abundance in groundwater is typically low, and therefore, enrichment procedures were employed to isolate As(III) resistant strains. A 300 ml volume of groundwater from each sampling site was filtered through 0.22µm membrane filters (25mm diameter) to concentrate the microbial biomass. The filter membranes were then resuspended in a minimal volume of original groundwater to enrich microbial density. For enrichment, 10 ml of this concentrated sample was inoculated into 100ml sterile crimp-sealed vials containing 50 ml of Chemically Defined Media (CDM), prepared according to the formulation described by Weeger et al. (1999). The medium was supplemented with 10 mM NaAsO2 to selectively enrich As(III) resistant bacterial strains. Cultures were incubated at 280C for 24-48 hours. Post incubation, colonies exhibiting distinct morphologies were isolated on CDM agar plates, purified, and cryopreserved in 30% glycerol -200C for further analysis.

2.4. Screening for As (III) Oxidizing Bacteria (AOB)

To differentiate between aerobic heterotrophic and chemolithotrophic arsenite oxidisers, CDM formulations were modified with appropriate carbon sources and other nutrients. Sodium acetate ($C_2H_3NaO_2$) was used as an organic carbon source in the medium for the determination of heterotrophs, whereas sodium bicarbonate ($NaHCO_3$) served as an inorganic carbon source for chemolithoautotrophs. NaAsO2 (1.3mM) was included as the sole electron donor in all formulations. Two qualitative methods, AgNO3 assay (Simeonova et al., 2004) and KMnO4 assay (Salmassi & Venkateswaren, 2010), were used to test for arsenite oxidizing capabilities. Bacterial colonies grown on As(III) supplemented agar plates were flooded with 0.1 M AgNO3 solution. The formation of a brownish precipitate around the bacterial colonies indicated the presence of oxidised arsenate. The other qualitative screening method relies on the fact that KMnO4 reacts with As(III), but not As(V). A pink coloration indicates the presence of As(V), signifying successful oxidation of As(III), whereas an off-orange coloured solution indicates unoxidised As(III).

2.5. As (III) tolerance and Oxidation potentials

As(III) tolerance was examined using 96 well microtiter plates. Each well was filled with 80µl of CDM medium and 20µl of exponentially grown cells of isolates adjusted to an initial optical density (OD600) of 0.05. NaAsO2 was added as a source of As(III) to reach final concentrations ranging from 1.3 mM to 40 mM across different wells. The final volume of each well was adjusted to 200 µl. Plates were incubated at 25oC for 48 hrs, and absorbance recorded at 600 nm at various time intervals. Specific growth rates and generation times were calculated to assess and compare As(III) tolerance among isolates.

The arsenite oxidation potential of the bacterial isolates was assessed using a modified permanganate ($KMnO_4$) based colorimetric assay (Bahar et al., 2020). This method utilizes the selective reactivity of $KMnO_4$ with As(III), leading to a measurable reduction in absorbance at 525 nm. A standard calibration curve was generated using standard As(III) concentrations (0.05 - 2 mM) in CDM growth medium (pH 7.2). After adding 2.4 mM $KMnO_4$, the mixtures were incubated at 25 °C for 30 minutes, and the absorbance recorded in triplicates (Fig. S3). CDM medium without added As(III) served as the negative control. To quantify microbial oxidation, isolates were cultured in CDM supplemented with 2 mM As(III), and the residual As(III) in the cell-free supernatants was monitored over time (Table. S3). Oxidation activity was normalized against dry cell biomass and expressed as mM As(III) oxidised per milligram dry cell weight per day (mM mg-1 d-1). Further, the effect of Di-ethyl pyrocarbonate (DEPC), a reported inhibitor of arsenite oxidase activity in cultures was tested as reported earlier(Dutta et al., 2024b; McNellis & Anderson, 1998).

2.6. DNA sequence analysis

Genomic DNA was extracted from purified bacterial isolates using the Dneasy® PowerLyzer® Microbial Kit (QIAGEN, Germany), following the manufacturer's protocol. DNA integrity and concentration were assessed via 1% agarose gel electrophoresis and UV-Vis spectrophotometry (Lambda 35, PerkinElmer). The 16S rRNA gene was amplified using universal primers 27F (5′-AGAGTTTGATCCTGGCTCAG-3′) and 1492R (5′-TACGGCTACCTTGTTACGACTT-3′) as per the protocol described by Lane (1991). The resulting PCR products were sequenced and submitted to the NCBI GenBank database for accessioning. Phylogenetic relationships were inferred using the Neighbor-Joining (NJ) algorithm (Zhao et al., 2021), and evolutionary analyses were conducted using Molecular Evolutionary Genetics Analysis (MEGA12) software.

2.3. Statistical Analysis

The descriptive analysis for minimum, maximum, range mean, standard deviation, and Pearson's correlation coefficient (r) for different chemical and physical parameters and the principal component analysis (PCA) in the study was conducted by SPSS version-22 software. Pearson's correlation analysis was used for revealing and highlighting the relationship among the parameters (Egbueri et al. 2019). Correlation coefficients ,0.5 are supposed to exhibit poor correlation. A correlation coefficient of 0.5 is termed a good correlation and .0.5 is termed to have excellent correlation (Kaiser 1958). Further, p values ,0.01, ,0.05, and ,0.1 indicate a strong, significant, and moderate correlation among the parameters respectively (Goyal et al. 2021).

PCA is a multivariate statistical analysis for reducing the dimensionality of large datasets that are often difficult to interpret, increasing the interpretability without losing information. The PCA has helped in the identification of the major variable factors responsible for pollution. Factor loading helps to arrive near the significant factor and the Kaiser Normalization scheme is used for the interpretation of the factor score on varimax rotation. The significance of a factor is deduced from the Eigen value and the factor with the highest Eigen value is most significant. Eigen value ≥1 is considered significant (Singh et al., 2022).

The hydrochemical facies represents the dominancy of the major cations and anions in the groundwater (Adimalla 2020) and is presented by the trilinear diagram (piper chart) which was prepared using Grapher software version-14. Water quality indices (WQI) for drinking and irrigation usage and health risk assessment were computed using MS-Excel 2016.The LULC and point location was made by the Arc GIS.

3. Results and Discussion

3.1. Physicochemical Characteristics

The mean, minimum, maximum, standard deviation, and % samples exceeding the prescribed limits for drinking water for the observed parameter are given in Table 3.1.

Table 3.1. Descriptive analysis of the observed Parameters in Groundwater of Laksar

Parameters	Minimum	Maximum	Mean	Std. Deviation	% Sample exceeding acceptable limit	Acceptable limit (WHO, 2022)	Acceptable Limit (BIS, 2012)
Shallow Wells							
Temp (°C)	17.0	28.4	24.4	1.5	NA	NA	NA
ORP (mv)	-195.5	914.6	161.3	172.0	NA	NA	NA
TDS (mg/L)	26.5	1342.7	523.7	280.9	43	1000	500.0
EC (µs/cm^2)	41.4	2098.0	814.4	432.4	NA	NA	NA
pH	6.6	8.8	7.3	0.4	0	6.5-8.5	6.5-8.5
TOC (mg/L)	0.0	17.6	1.0	2.6	NA	NA	NA
Silica (mg/L)	0.0	20.7	5.8	5.8	NA	NA	NA
Alkalinity (mg/L)	90.0	748.0	320.8	141.2	75	NA	200.0
HCO3	109.8	912.6	391.4	172.2	NA	NA	NA
F (mg/L)	0.0	0.6	0.2	0.1	0	1.5	1.0
Cl (mg/L)	0.6	163.6	22.0	29.7	0	250	250.0
NO2 (mg/L)	-4.6	41.3	1.2	4.9	64	0	0.0
NO3 (mg/L)	0.0	211.8	11.6	25.4	8	50	45.0
SO4 (mg/L)	0.9	172.5	31.2	30.4	0	500	200.0
Li (mg/L)	0.0	0.2	0.0	0.0	NA	NA	NA
Na (mg/L)	0.6	160.1	28.0	22.1	NA	NA	NA
NH4 (mg/L)	0.0	14.8	1.8	9.8	NA	NA	NA
K (mg/L)	0.1	219.0	28.7	94.3	NA	NA	NA
Ca (mg/L)	1.8	216.1	83.8	36.1	58	NA	75.0
Mg (mg/L)	1.1	126.1	26.1	16.0	30	NA	30.0
As (µg/L)	0.0	267.1	23.9	35.3	50	10	10.0
Pb (µg/L)	0.0	156.7	3.5	12.5	5	10	10.0
Cd (µg/L)	-0.1	2.4	0.1	0.2	0	3	3.0
Cr (µg/L)	0.0	27.9	1.3	2.3	0	50	50.0
Cu (µg/L)	0.0	161.7	5.2	13.3	2	2000	50.0
Fe (µg/L)	0.6	24737.4	2193.4	3626.3	68	NA	300.0
Mn (µg/L)	0.0	2549.9	478.5	493.0	77	0.08	100.0
Zn (µg/L)	0.0	3350.2	175.3	391.6	0	NA	5000.0
Ni (µg/L)	-0.2	44.6	1.8	4.0	0.8	70	20.0
Al (µg/L)	-228.4	1721.8	61.8	171.2	34	NA	30.0
Be (µg/L)	0.0	0.2	0.0	0.0	NA	NA	NA
B (µg/L)	0.0	125.9	26.2	25.1	0	2400	500.0
V (µg/L)	-1.2	16.8	1.3	2.4	NA	NA	NA
Co (µg/L)	-0.3	3.3	0.3	0.4	NA	NA	NA

Se (µg/L)	0.0	4422.9	19.3	287.3	1	40	10.0
Sr (µg/L)	0.0	1900.6	328.1	243.4	NA	NA	NA
Ba (µg/L)	0.1	2485.5	342.1	317.6	12	1300	700.0
Ce (µg/L)	0.0	1.4	0.1	0.2	NA	NA	NA
Hg (µg/L)	0.0	68.1	2.9	6.8	35	6	1.0
U (µg/L)	0.0	85.1	6.8	11.4	5.5	30	NA
Deep Wells							
Temp (°C)	20.1	28.0	24.5	1.3	NA	NA	NA
ORP (mv)	-160.0	713.1	156.3	156.8	NA	NA	NA
TDS (mg/L)	73.9	3560.0	400.9	337.3	18	1000	500.0
EC (µs/cm^2)	115.5	4147.0	598.6	375.1	NA	NA	NA
pH	6.6	8.6	7.4	0.4	0	6.5-8.5	6.5-8.5
TOC (mg/L)	0.0	9.7	0.6	1.3	NA	NA	NA
Silica (mg/L)	0.0	18.4	7.2	5.5	NA	NA	NA
Alkalinity (mg/L)	86.0	698.0	266.9	108.2	66	NA	200.0
HCO3	102.0	851.6	307.3	139.5	NA	NA	NA
F (mg/L)	0.0	0.7	0.2	0.1	0	1.5	1.0
Cl (mg/L)	0.2	160.2	14.9	25.4	0	250	250.0
NO2 (mg/L)	0.0	31.4	0.9	3.5	65	0	0.0
NO3 (mg/L)	0.0	111.2	6.9	15.3	4	50	45.0
SO4 (mg/L)	0.6	127.9	25.6	24.4	0	500	200.0
Li (mg/L)	0.0	0.7	0.0	0.1	NA	NA	NA
Na (mg/L)	0.5	113.4	23.5	18.5	NA	NA	NA
NH4 (mg/L)	0.0	9.8	0.7	1.2	NA	NA	NA
K (mg/L)	0.1	290.0	19.5	38.3	NA	NA	NA
Ca (mg/L)	1.5	199.1	72.2	34.4	42	NA	75.0
Mg (mg/L)	0.7	86.4	21.7	12.3	18	NA	30.0
As (µg/L)	0.0	77.1	8.8	10.4	25	10	10.0
Pb (µg/L)	0.0	46.8	2.3	5.5	4	10	10.0
Cd (µg/L)	0.0	2.9	0.1	0.3	0	3	3.0
Cr (µg/L)	0.0	12.5	1.3	1.6	0	50	50.0
Cu (µg/L)	0.0	105.8	4.9	11.5	2	2000	50.0
Fe (µg/L)	0.6	14379.3	908.8	1673.1	60	NA	300.0
Mn (µg/L)	0.7	1834.9	333.3	374.2	67.2	0.08	100.0
Zn (µg/L)	1.0	1341.2	107.6	173.3	0	NA	5000.0
Ni (µg/L)	0.0	309.5	3.4	23.0	1	70	20.0
Al (µg/L)	0.0	1972.1	69.2	227.1	32	NA	30.0
Be (µg/L)	0.0	0.1	0.0	0.0	NA	NA	NA
B (µg/L)	0.0	127.9	21.0	13.4	0	2400	500.0
V (µg/L)	0.0	14.3	0.9	1.6	NA	NA	NA
Co (µg/L)	0.0	45.7	0.4	3.4	NA	NA	NA
Se (µg/L)	0.0	4.8	0.4	0.7	0	40	10.0
Sr (µg/L)	0.7	1543.6	313.1	239.5	NA	NA	NA
Ba (µg/L)	0.7	1565.4	246.7	227.8	4	1300	700.0
Ce (µg/L)	0.0	1.0	0.1	0.2	NA	NA	NA
Hg (µg/L)	0.0	56.6	2.2	5.1	36	6	1.0
U (µg/L)	0.0	88.1	8.3	11.2	6	30	NA

3.1.1. pH

The pH of groundwater samples ranged from 6.6 to 8.8 in shallow aquifers and 6.6 to 8.6 in deep aquifers, indicating a variation from slightly acidic to alkaline conditions (Fig. 3.1a & 3.1b). In general, pH values were higher in shallow aquifers compared to deep ones. Notably, pH values exceeding 8.5 were recorded in shallow groundwater from Bhogpur, Damanpuri, Munda Khera, and Gadruana villages, and in deep groundwater from Kalasiya village in Haridwar District.

In shallow groundwater, pH showed a weak but statistically significant negative correlation with As (-0.152), Mn (-0.179), B (-0.185), Co (-0.247), Sr (-0.269), Ba (-0.284), and HCO_3 (-0.227). A positive correlation was observed between pH and ORP (0.227) in shallow aquifers, indicating possible redox control on pH variation (Table 3.2a).

In deep groundwater, pH exhibited weak negative correlations with Na (-0.190), Ca (-0.186), Mg (-0.222), Se (-0.175), Sr (-0.217), Ba (-0.217), and U (-0.186).

These correlations suggest that pH may influence or be influenced by geochemical interactions involving major and trace elements, particularly those associated with carbonate equilibria, redox conditions, and mineral dissolution/precipitation processes.

3.1.2. Electrical Conductivity (EC)

Electric Conductivity (EC) in the groundwater of study area was observed to range between 41.4–2098.0 µS/cm in the shallow aquifer, with an average of 814.4 ± 432.4 µS/cm. In the deep aquifer, EC varied from 115.5 to 4147.0 µS/cm, with an average of 598.6 ± 375.1 µS/cm (as shown in Fig. 3.1c & 3.1d). The average EC was found to be higher in shallow groundwater compared to deep aquifer samples. This is likely due to the higher rate of ion dissolution occurring during groundwater recharge, which is more prominent near the surface.

3.1.3. Major Cations and Anions

Figure 3.2 (box plot) and Table 3.1 present the range and average concentrations of major ions that influence groundwater hydrochemistry in Haridwar district. The order of ion dominance in groundwater samples was $HCO_3^- > SO_4^{2-} > Cl^- > NO_3^- > NO_2^- > F^-$ among anions and $Ca^{2+} > Na^+ > K^+ > Mg^{2+} > NH_4^+ > Li^+$ among cations.

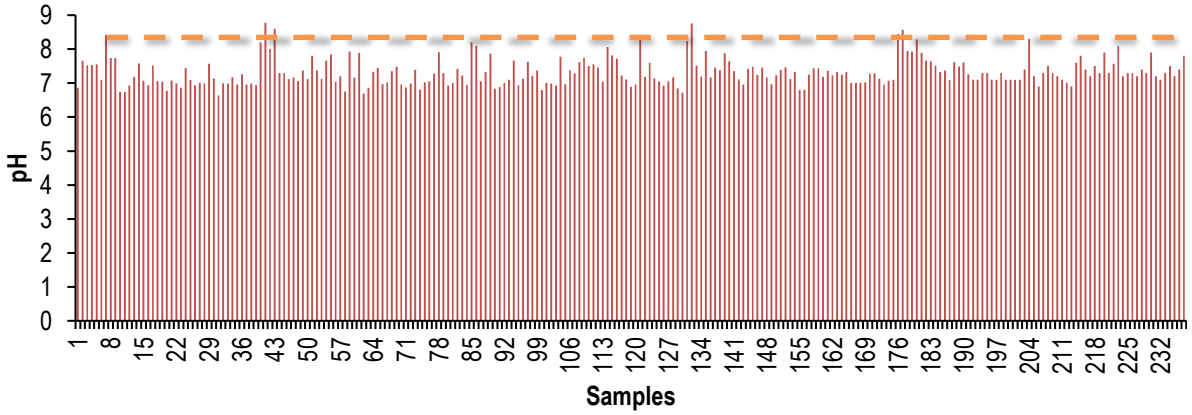

a. pH of shallow aquifer samples

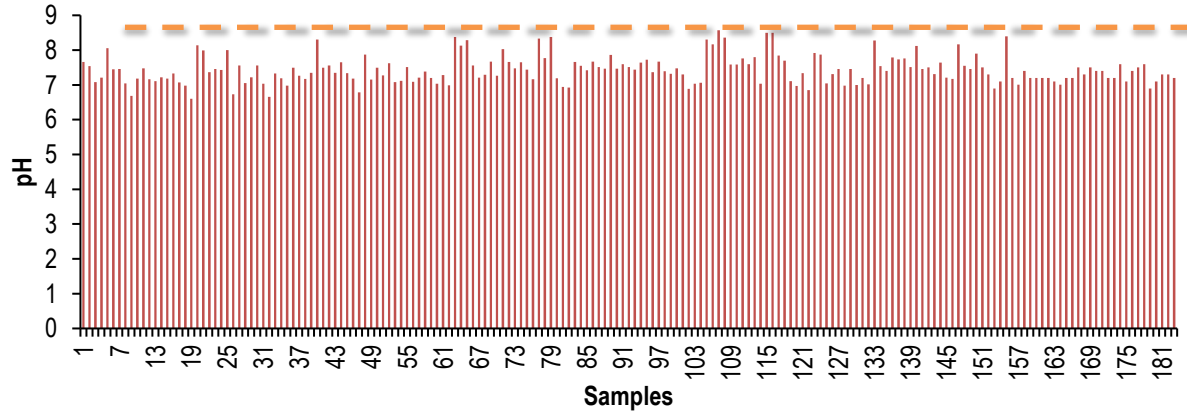

b. pH of deep aquifer samples

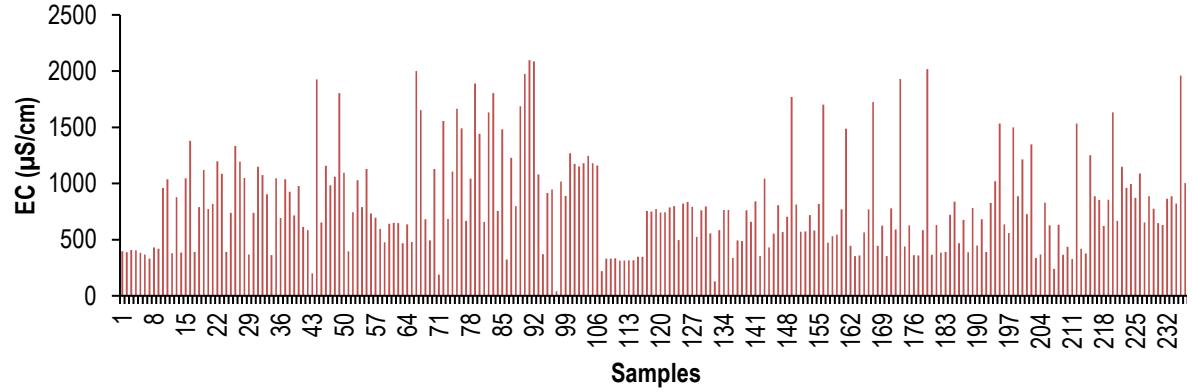

c. EC of shallow aquifer samples

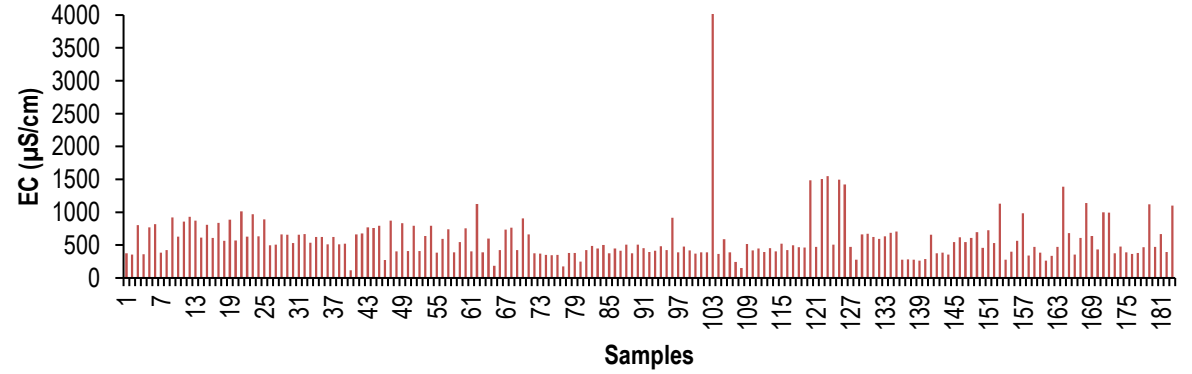

c. EC of deep aquifer samples

Fig. 3.1. pH and EC in of samples

Among the cations, Sodium (Na^+) ranged from 0.6–160.1 mg/L with an average of 28.9 ± 22.1 mg/L in shallow aquifers, and from 0.5–113.4 mg/L with an average of 23.5 ± 18.5 mg/L in deep aquifers. Potassium (K^+) was recorded at 0.1–219.0 mg/L (average 28.9 ± 94.3 mg/L) in shallow groundwater, whereas in the deep aquifer it ranged from 0.0–0.6 mg/L, with an average of 19.5 ± 38.3 mg/L.

Calcium (Ca^{2+}) concentrations varied from 1.8–216.1 mg/L (average 83.8 ± 36.1 mg/L) in shallow groundwater, where 58% of samples exceeded the BIS (2012) acceptable limit of 75 mg/L. In deep groundwater, calcium ranged from 1.5–199.1 mg/L (average 72.7 ± 34.4 mg/L), with 42% of samples exceeding the permissible limit.

Magnesium (Mg^{2+}) levels ranged from 1.1–126.1 mg/L (average 26.1 ± 16.0 mg/L) in shallow groundwater and 0.7–86.4 mg/L (average 21.7 ± 12.3 mg/L) in the deep aquifer, with elevated concentrations in 30% and 18% of the shallow and deep samples respectively. Ammonium (NH_4^+) concentrations averaged 1.8 ± 9.8 mg/L in shallow aquifers and 0.7 ± 1.2 mg/L in deep aquifers, indicating that shallow groundwater is more affected by fertilizer inputs.

Among anions, Fluoride (F^-) concentrations ranged from 0.0–0.6 mg/L (shallow) and 0.0–0.7 mg/L (deep), with average values of 0.2 mg/L in both aquifers, well below the BIS limit of 1.5 mg/L. Chloride (Cl^-) concentrations were 0.6–163.6 mg/L in shallow groundwater (average 22.0 ± 29.7 mg/L) and 0.2–160.2 mg/L (average 14.9 ± 25.4 mg/L) in deep groundwater, both within the acceptable limits of BIS (250 mg/L) and WHO (2022).

Nitrite (NO_2^-) concentrations ranged from 0.0–41.3 mg/L (average 1.2 ± 4.9 mg/L) in shallow groundwater and 0.0–31.4 mg/L (average 0.9 ± 3.5 mg/L) in deep aquifers. Notably, 64% and 65% of shallow and deep samples respectively exceeded the BIS permissible limit of 0 mg/L. Nitrate (NO_3^-) concentrations ranged from 0.0–211.8 mg/L (average 11.6 ± 25.4 mg/L) in shallow groundwater and 0.0–111.2 mg/L (average 6.9 ± 15.3 mg/L) in deep groundwater. Around 8% of shallow and 4% of deep samples exceeded the BIS permissible limit of 45 mg/L. The dominance of NO_2 over NO_3 suggests partial decomposition of nitrogenous fertilizers and organic matter in the aquifer.

Sulfate (SO_4^{2-}) concentrations ranged from 0.9–175.5 mg/L (average 31.2 ± 30.4 mg/L) in shallow groundwater and 0.6–127.9 mg/L (average 25.6 ± 24.4 mg/L) in deep groundwater, both well below permissible limits.

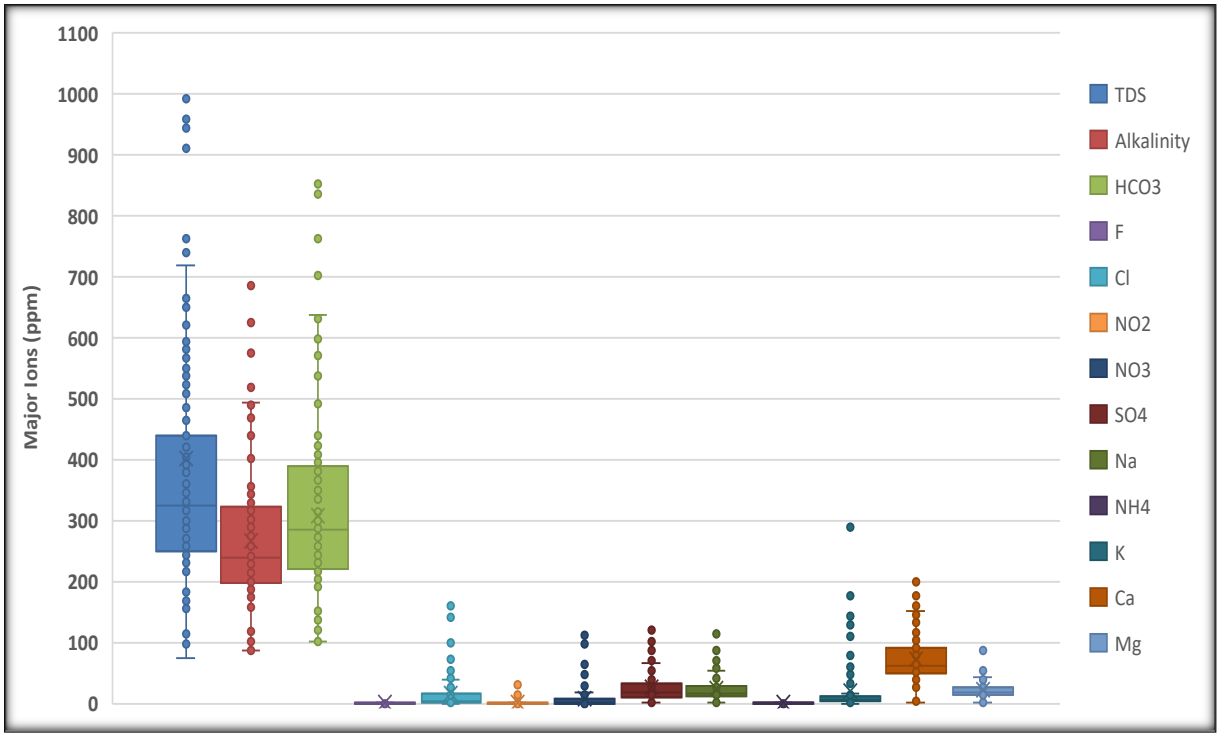

Fig. 3.2. Box plot for the major ions observed in the groundwater

3.1.4. Total Dissolved Solids (TDS)

Total Dissolved Solids (TDS) in shallow groundwater ranged from 26.5–1342.7 mg/L, with an average of 523.7 ± 280.9 mg/L. In deep groundwater, TDS ranged between 73.9–3560.0 mg/L with an average of 400.9 ± 337.3 mg/L (Figure 3.3). TDS values exceeded the BIS acceptable limit of 500 mg/L in 43% of shallow groundwater samples and 18% of deep groundwater samples (Table 4.1).

TDS was observed to be higher in shallow groundwater compared to deep aquifers (Figure 3.3). Villages such as Duasani, Fatwa, Husainipur, Akoda Khurd, Kuwa Khera, Bhogpur, Munda Khera, Thithola, Khempur, Damanpuri, Gangdaspur, Akodakalan, and Hazzarpur showed elevated TDS in shallow aquifers, while deep aquifers in Akodakalan, Kalsiya, Fatwa, Gangdaspur, Dausni, Panditpuri, Alawalpur, and Damanpuri also showed high TDS levels.

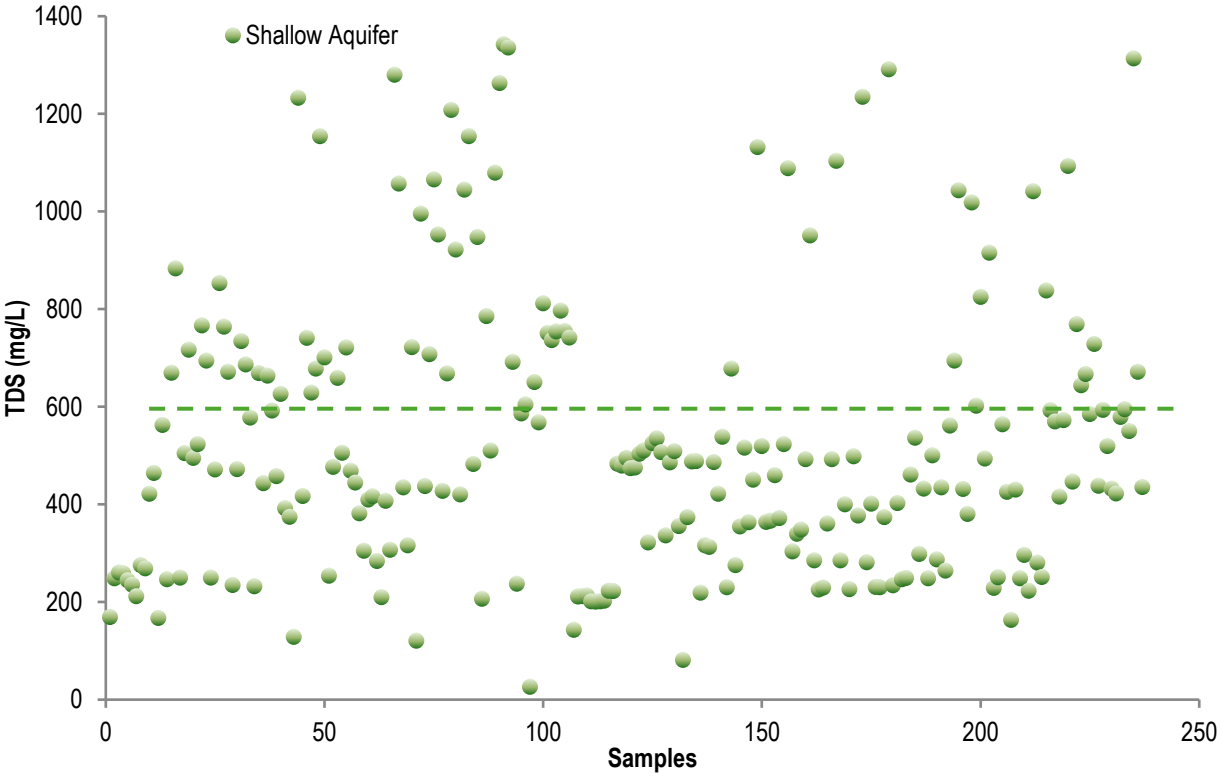

a. TDS of shallow aquifer samples

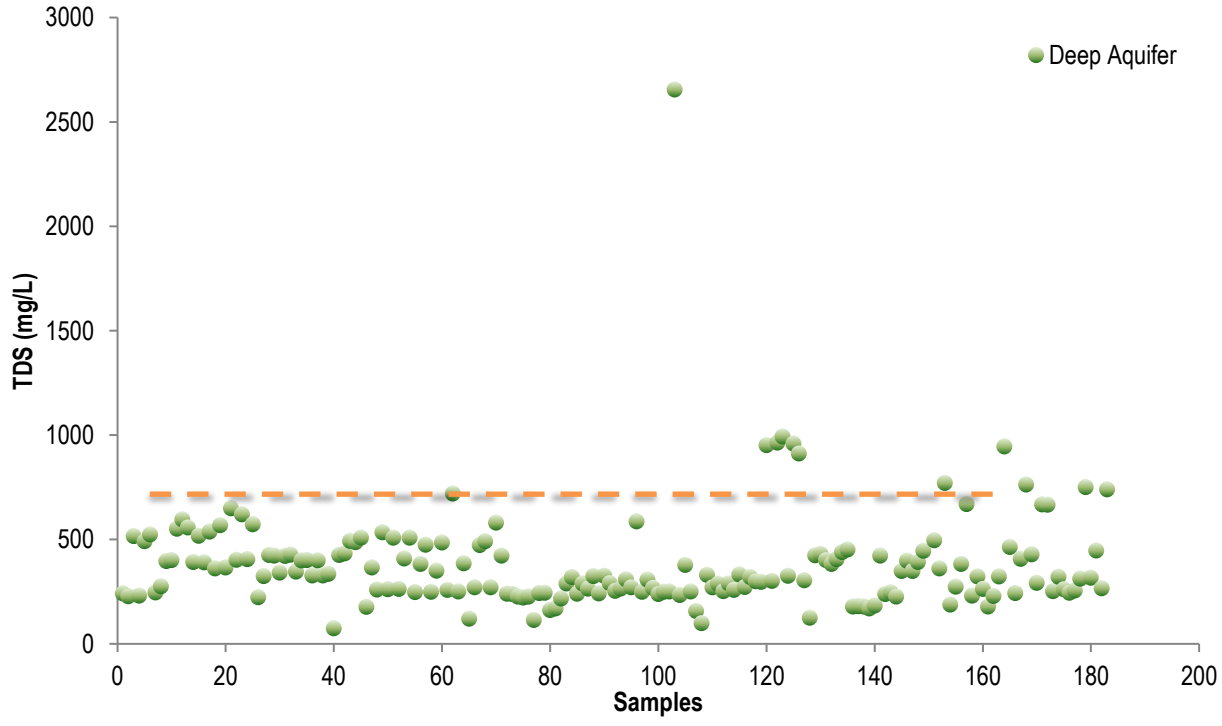

b. TDS of deep aquifer samples

Fig. 3.3. Total dissolved solids in GW samples

Table 3.2a. Pearson co-relation between the parameters in shallow groundwater

Parameters	pH	EC	ORP	TDS	Alk	HCO3	F	Cl	NO2	NO3	SO4	Na	NH4	K	Ca	Mg	As	Pb	Cd	Cr	Cu	Fe	Mn	Zn	Ni	Al	B	Co	Se	Sr	Ba	Hg	U
pH	1																																
EC	-.347**	1																															
ORP	.252**	-.197**	1																														
TDS	-.330**	.996**	-.192**	1																													
Alk	-.227**	.591**	-.122	.564**	1																												
HCO3	-.227**	.591**	-.122	.564**	1.000**	1																											
F	.025	.032	.012	.028	.220**	.220**	1																										
Cl	-.094	.547**	.077	.549**	.344**	.344**	.087	1																									
NO2	.040	.143*	.162*	.143*	.139*	.139*	.079	.531**	1																								
NO3	-.111	.333**	.114	.336**	.168*	.168*	.027	.504**	.195**	1																							
SO4	-.115	.502**	.130	.499**	.289**	.289**	.147*	.729**	.297**	.421**	1																						
Na	-.041	.512**	-.033	.512**	.417**	.417**	.235**	.737**	.400**	.430**	.536**	1																					
NH4	-.035	.139*	.030	.152*	-.078	-.078	-.006	.251**	.595**	.011	.307**	.124	1																				
K	-.120	.372**	.006	.381**	.068	.068	.049	.486**	.379**	.229**	.568**	.319**	.903**	1																			
Ca	.027	.381**	.126	.389**	.244**	.244**	.228**	.644**	.389**	.374**	.550**	.661**	.211**	.349**	1																		
Mg	-.100	.478**	.118	.480**	.258**	.258**	.083	.651**	.338**	.523**	.633**	.614**	.209**	.380**	.671**	1																	
As	-.152*	.226**	**-.212****	.198**	.230**	**.230****	.001	.030	-.061	-.012	.034	.139*	-.062	-.008	.095	.023	1																
Pb	-.032	-.042	-.019	-.045	.024	.024	-.055	-.016	.004	.139*	-.061	-.048	-.021	-.035	-.025	-.060	-.070	1															
Cd	-.126	-.083	-.077	-.100	.064	.064	.082	-.057	-.043	.074	-.022	-.102	-.047	-.018	-.100	-.119	.140*	.360**	1														
Cr	-.060	-.057	-.114	-.064	-.041	-.041	.080	-.034	.003	.074	-.064	-.067	-.033	-.038	-.101	-.125	.059	.297**	.575**	1													
Cu	.028	-.031	.038	-.035	-.028	-.028	-.045	.013	-.001	.141*	.025	-.042	-.010	-.002	-.024	-.035	-.020	.781**	.403**	.306**	1												
Fe	-.134	.389**	**-.219****	.380**	.409**	**.409****	.113	.210**	.149*	.061	.029	.259**	-.015	.019	.156*	.075	**.193****	.253**	.010	.168*	-.009	1											
Mn	-.179**	.456**	**-.241****	.423**	.408**	**.408****	.033	.234**	-.011	.057	.223**	.204**	.021	.172*	.011	.128	**.626****	-.049	.186**	.043	-.050	**.279****	1									
Zn	-.022	-.027	-.058	-.032	.027	.027	-.073	-.002	.026	.086	-.073	-.035	-.029	-.036	-.020	-.061	-.125	.869**	.256**	.283**	.550**	.401**	-.040	1								
Ni	-.028	-.002	-.047	.002	-.186**	-.186**	-.066	.000	-.003	.027	-.013	-.029	.012	.038	-.072	-.057	-.001	.108	.210**	.321**	.142*	.052	.010	.154*	1							
Al	-.081	-.049	.111	-.060	-.028	-.028	-.012	.001	-.015	.217**	-.006	-.027	-.021	-.015	-.034	-.027	-.044	.184**	.501**	.390**	.215**	.049	-.035	.078	.076	1						
B	-.185**	.703**	-.019	.680**	.699**	.699**	.138*	.464**	.168*	.367**	.450**	.431**	-.046	.188**	.280**	.333**	**.246****	.012	.097	.038	.083	.265**	.403**	.000	-.033	.064	1					
Co	-.247**	.538**	.010	.521**	.385**	.385**	.119	.461**	.115	.294**	.366**	.327**	.016	.250**	.248**	.233**	.159*	.171*	.220**	.191**	.095	.349**	.413**	.262**	.191**	.123	.569**	1				
Se	-.043	.040	-.037	.040	.022	.022	-.002	-.014	-.018	.032	.024	-.039	-.006	-.001	.022	-.005	.046	-.014	.026	-.047	-.014	-.039	.124	-.028	-.010	-.011	-.078	.007	1			
Sr	-.269**	.174*	-.230**	.124	.250**	.250**	.086	.039	-.015	-.038	.093	.117	-.042	.035	.040	.013	**.438****	.050	.395**	.248**	.096	.219**	.461**	.110	.069	.131	.311**	.218**	.032	1		
Ba	-.284**	.275**	-.182**	.242**	.328**	.328**	-.006	.073	-.014	.028	.006	.107	-.055	-.024	.072	.051	**.691****	.041	.288**	.194**	.009	.416**	.543**	.044	.014	.102	.317**	.184**	-.073	.580**	1	
Hg	.130	-.022	.116	-.027	.046	.046	.081	.018	.087	-.041	-.060	-.031	-.002	-.037	-.026	-.042	-.014	-.031	-.023	-.058	-.036	.013	.045	-.022	-.095	-.018	.024	-.055	.056	-.006	.075	1	
U	-.111	.052	.061	.058	-.099	-.099	-.114	.016	-.063	-.026	.129	-.105	.429**	.367**	.044	.125	-.060	.014	.166*	.108	-.025	-.127	-.020	.059	.054	-.020	-.083	.021	.139*	.138*	.128	.084	1

Table 3.2b. Pearson co-relation between the parameters in deep groundwater

Parameters	pH	EC	ORP	TDS	Alk	HCO3	F	Cl	NO2	NO3	SO4	Na	NH4	K	Ca	Mg	As	Pb	Cd	Cr	Cu	Fe	Mn	Zn	Ni	Al	B	Co	Se	Sr	Ba	Hg	U
pH	1																																
EC	-.295**	1																															
ORP	.073	.115	1																														
TDS	-.130	.682**	.093	1																													
Alk	-.313**	.360**	-.030	.205*	1																												
HCO3	-.131	.275**	.020	.157*	1.000**	1																											
F	-.082	.169*	.012	.109	-.016	-.028	1																										
Cl	-.089	.168*	.220**	.141	-.002	.017	.064	1																									
NO2	.099	-.046	.097	.051	-.057	-.033	-.028	.436**	1																								
NO3	.018	.077	.222**	.066	-.067	-.033	-.087	.633**	.594**	1																							
SO4	-.148	.311**	.195*	.181*	.120	.144	.229**	.664**	.310**	.538**	1																						
Na	-.190*	.252**	.193*	.208**	.068	.063	.132	.791**	.463**	.534**	.607**	1																					
NH4	-.043	.085	.239**	.064	-.112	-.069	.088	.640**	.682**	.495**	.356**	.558**	1																				
K	-.112	.380**	.232**	.258**	.091	.059	.226**	.652**	.626**	.550**	.668**	.604**	.609**	1																			
Ca	-.186*	.307**	.306**	.218**	.047	.181*	.074	.610**	.375**	.495**	.453**	.581**	.571**	.517**	1																		
Mg	-.222**	.317**	.326**	.217**	.101	.140	.045	.776**	.425**	.568**	.716**	.788**	.555**	.651**	.729**	1																	
As	.016	-.094	**-.245****	.010	-.024	.037	.162*	-.070	.005	-.086	-.028	-.063	.009	.088	-.097	-.159*	1																
Pb	-.046	.123	.044	.075	.105	.170*	.099	.150	-.005	-.017	.076	.098	.109	.031	.124	.121	.069	1															
Cd	-.004	-.012	-.233**	-.021	-.032	.041	.114	-.082	-.053	-.062	-.029	-.050	-.015	-.055	-.030	-.135	**.420****	.408**	1														
Cr	-.049	.083	-.163*	.066	.066	.043	.098	.058	-.066	-.042	.005	.024	.028	-.061	-.034	-.070	**.252****	.571**	.519**	1													
Cu	-.117	.497**	.177*	.346**	.119	.142	.145	.295**	.147	.175*	.185*	.269**	.278**	.300**	.286**	.294**	-.019	.679**	.136	.516**	1												
Fe	.107	.025	-.119	.198*	.077	.120	.040	.057	.039	-.071	-.004	.050	-.005	.039	.036	.059	.087	.204**	.045	.144	.085	1											
Mn	-.106	.264**	-.100	.160*	.238**	.265**	.236**	.015	-.081	-.086	.302**	.087	-.101	.138	-.128	.082	**.304****	.070	.109	.136	.108	**.099**	1										
Zn	-.058	.031	-.119	.028	.143	.184*	-.025	-.037	-.029	-.088	-.022	-.011	-.056	-.008	.042	-.026	.202**	.289**	.486**	.276**	.116	.440**	.144	1									
Ni	-.056	-.045	-.053	-.033	-.081	-.195*	-.016	-.048	-.018	-.041	-.064	-.052	-.034	-.043	-.101	-.085	-.010	-.021	.019	.098	.024	-.029	-.054	-.025	1								
Al	.046	-.072	-.050	-.028	-.120	-.056	.030	-.046	-.023	-.041	-.021	-.096	-.062	-.039	-.147	-.125	.073	.026	.108	.360**	.040	.167*	.162*	-.004	.033	1							
B	.002	.233**	-.022	.323**	.173*	.395**	.162*	.054	-.021	-.039	.237**	.120	.021	.080	.103	.074	**.422****	.278**	.428**	.454**	.253**	.209**	.448**	.253**	-.088	.120	1						
Co	-.095	.197*	.076	.136	.222**	.193*	.041	.160*	-.021	-.036	.077	.121	.054	-.011	.064	.125	-.031	.652**	.033	.542**	.680**	-.024	.199*	-.008	.000	.044	.197*	1					
Se	-.175*	.085	.054	.036	-.028	-.006	.045	.030	-.010	.182*	.058	.052	.140	-.030	.127	.022	.074	.098	.299**	.344**	.060	-.101	.017	.057	.002	.011	.113	-.005	1				
Sr	-.217**	.087	-.231**	.019	.121	.191*	.128	-.148	-.106	-.109	.104	-.024	-.086	-.054	-.039	-.094	**.482****	.155*	.494**	.236**	.044	.092	.389**	.448**	-.029	-.015	.386**	.011	.259**	1			
Ba	-.217**	.151	-.113	.165*	.152	.204**	.180*	.018	-.037	-.033	.144	.100	.030	.048	.030	.052	**.483****	.167*	.280**	.251**	.088	.394**	.350**	.373**	-.034	-.001	.455**	.069	.362**	.680**	1		
Hg	.018	.073	.254**	.074	.062	.135	-.036	.061	-.004	.032	.087	.057	.109	.136	.098	.140	-.076	-.007	-.040	-.054	.010	-.002	.158*	-.014	-.045	.046	.072	.016	.024	-.056	-.006	1	
U	-.186*	.241**	.013	.122	.151	.160*	.183*	.048	-.047	.123	.401**	.173*	-.026	-.008	.137	.173*	-.105	.055	.161*	.132	.050	-.104	.280**	-.034	-.030	-.005	.233**	.047	.427**	.371**	.276**	.121	1

3.2. Hydrogeochemistry

To understand the hydrogeochemical facies of groundwater in the Haridwar district, major ions from both shallow and deep aquifers were plotted using Piper trilinear diagrams (Adimalla, 2020; Kumar et al., 2021). The Piper diagram comprises triangular plots for cations and anions, along with a central diamond-shaped field that indicates overall water type. The Piper plots (Figure 4.4a & 4.4b) reveal that groundwater in both aquifers is dominated by calcium (Ca^{2+}), magnesium (Mg^{2+}), and bicarbonate (HCO_3^-) or chloride (Cl^-) ions. The two primary water types observed were Ca/Mg–HCO_3 (80%) and Ca/Mg–SO_4/Cl (20%). These results indicate the predominance of alkaline earth metals (Ca^{2+} + Mg^{2+}) over alkali metals (Na^+ + K^+), and weak acids (mainly HCO_3^-) over strong acids (SO_4^{2-} + Cl^-).

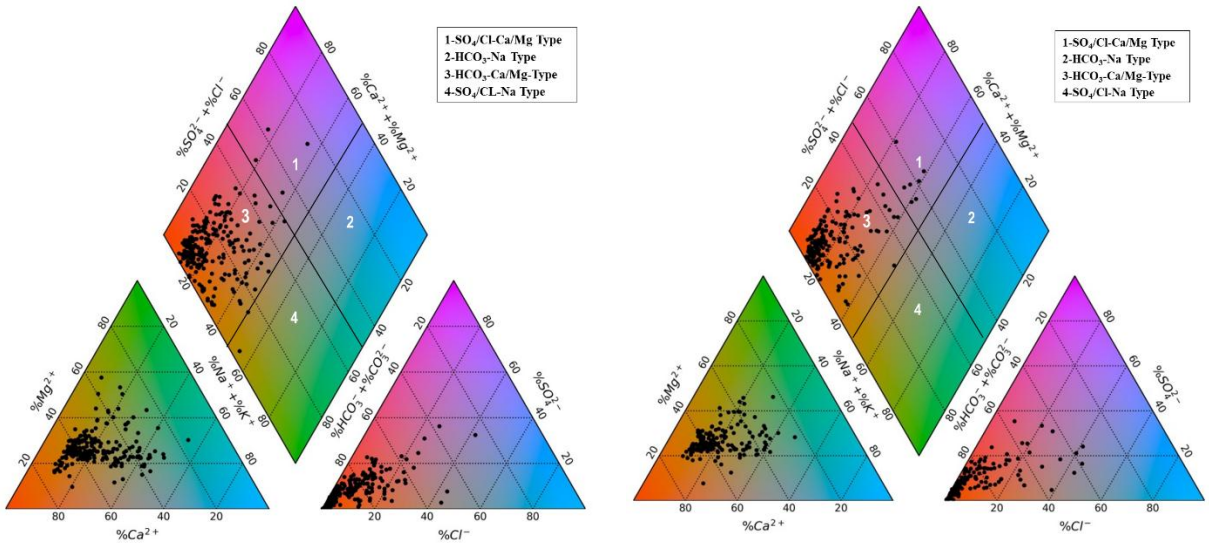

(a) (b)

Fig. 3.4. Piper Pot for (a) Shallow aquifer and (b) Deeper aquifer

Geochemical processes were further evaluated using scatter plots. The Na/Cl ratio exceeded 1 in 95.6% of shallow and 100% of deep groundwater samples (Figure 3.5a & 3.6a), suggesting a significant contribution from silicate weathering. The Ca vs. SO_4 plots (Figure 3.5b & 3.6b) showed no clear signs of gypsum dissolution in either aquifer.

The (Ca + Mg) vs. HCO_3 plot (Figure 3.5c) classifies shallow groundwater samples into three clusters: Cluster 1 samples lie above the 1:1 line, Cluster 2 between 1:1 and 1:2, and Cluster 3 aligns with the 1:2 line. These patterns, supported by Ca < HCO_3 in Fig. 3.5d, point toward carbonate weathering in the shallow aquifer. In contrast, Ca > HCO_3 in deep aquifer samples (Figure 3.6d) suggests dominance of silicate weathering.

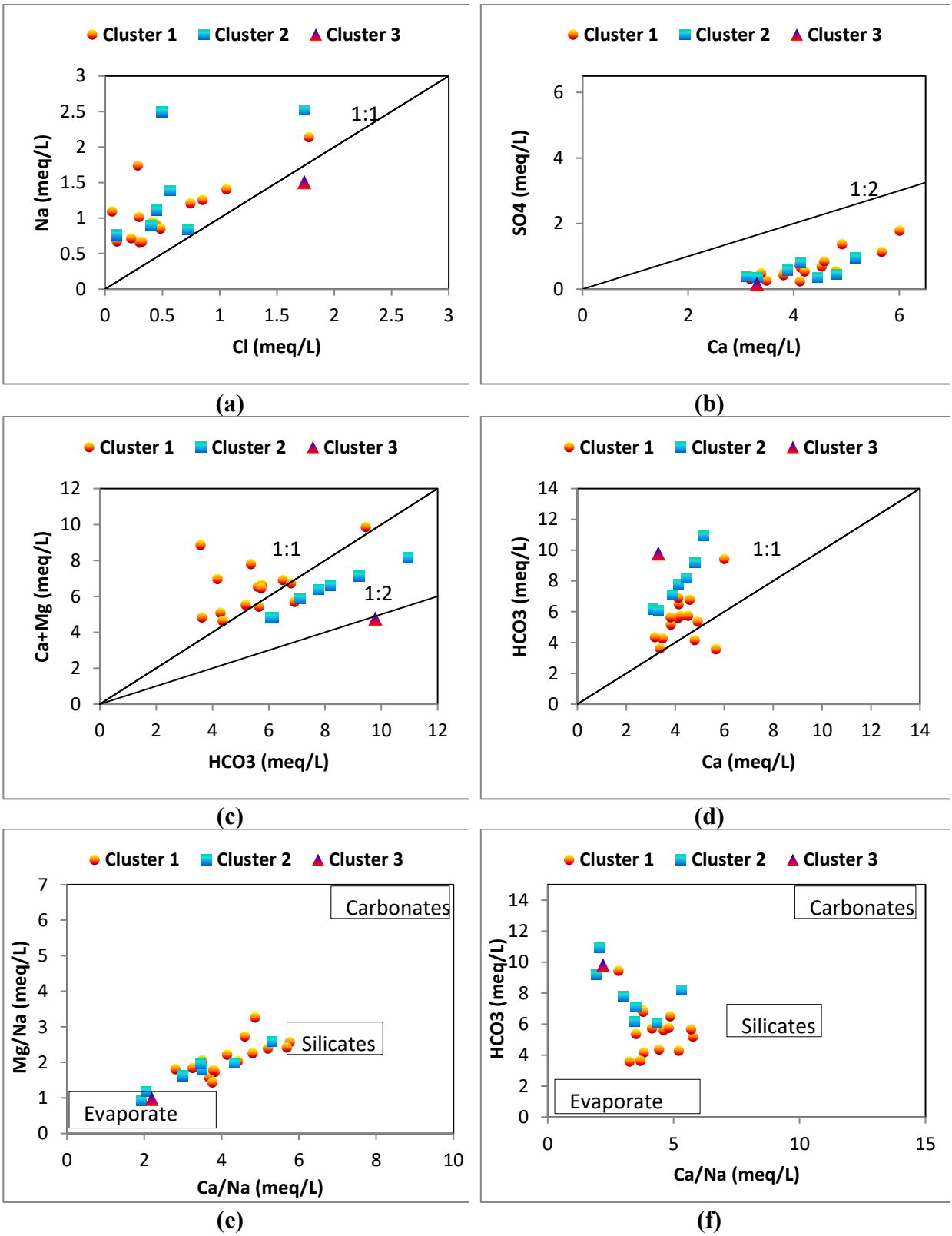

Fig. 3.5. Bivariate plots explaining the mineral weathering and hydrochemistry of shallow aquifers. (a) Na vs Cl, (b) SO4 vs Ca, (c) Ca+Mg vs HCO3, (d) HCO3 vs Ca, (e) Mg/Na vs Ca/Na, and (f) HCO3 vs Ca/Na

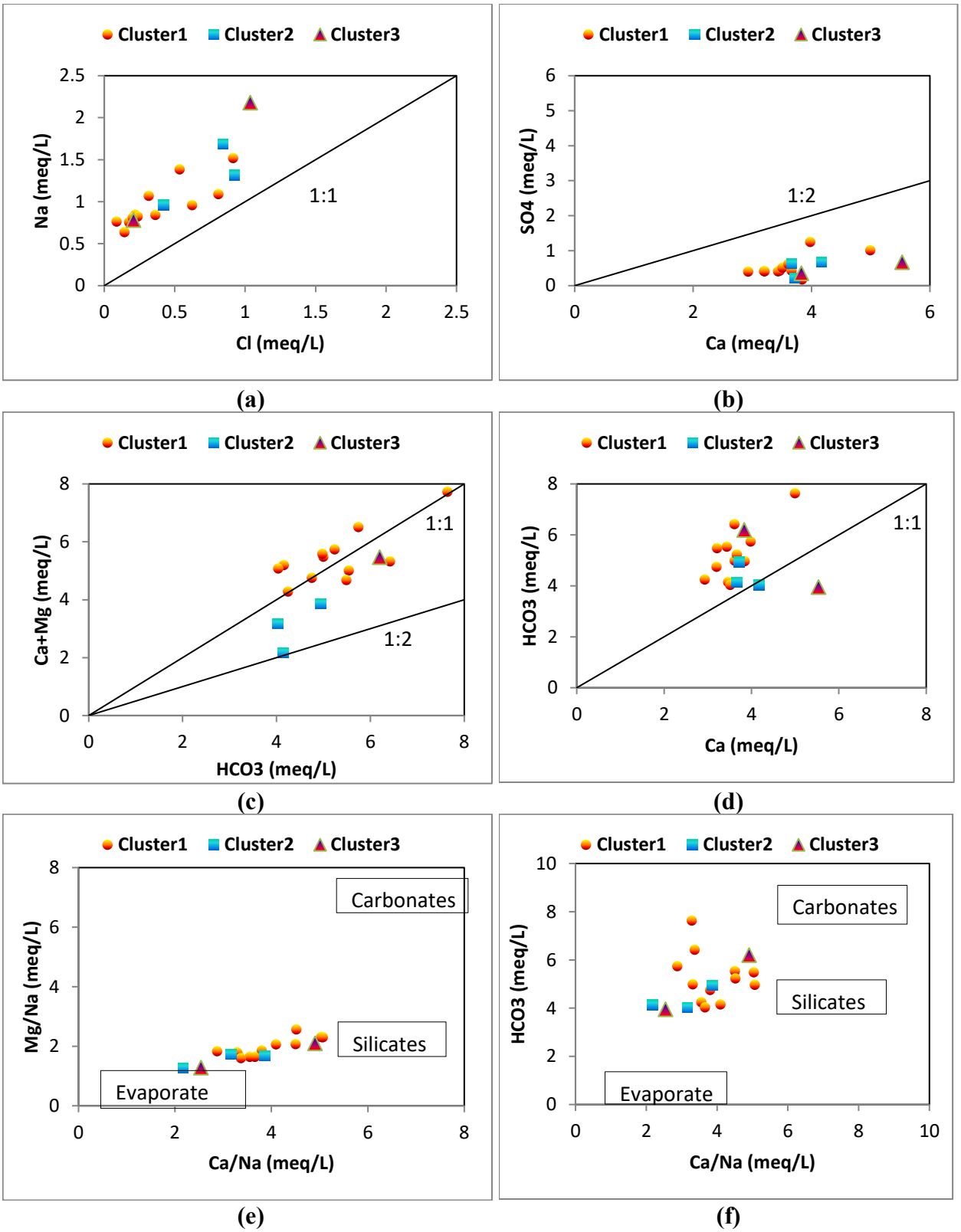

Fig. 3.6. Bivariate plots explaining the mineral weathering and hydrochemistry of deeper aquifers. (a) Na vs Cl, (b) SO4 vs Ca, (c) Ca+Mg vs HCO3, (d) HCO3 vs Ca, (e) Mg/Na vs Ca/Na, and (f) HCO3 vs Ca/Na

Further evidence is provided by Figures 3.5e and 3.5f, which indicate a mixed silicate–carbonate weathering regime in the shallow aquifer. Conversely, Figures 4.6e and 4.6f confirm a stronger influence of silicate weathering in the deep aquifer.

Mineral saturation indices were also assessed to understand groundwater–mineral interactions. The dissolution of calcite ($CaCO_3$) and dolomite ($CaMg(CO_3)_2$) contributed Ca^{2+} and Mg^{2+} to the groundwater, while increased HCO_3^- was attributed to silicate weathering. Saturation index results indicate that Manganite (MnO(OH)) is saturated, Hematite (Fe_2O_3) and Goethite (FeOOH), on the other hand, were found to be supersaturated in the aquifer system. However, Montroydite (HgO_2), Siderite ($FeCO_3$), Arsenolite (As_2O_3), and Uranile Nitrate ($UO_2(NO_3)_2$) are undersaturated, indicating an increase in their concentration with increased contact time and prevalence of favorable weathering/dissolution conditions.

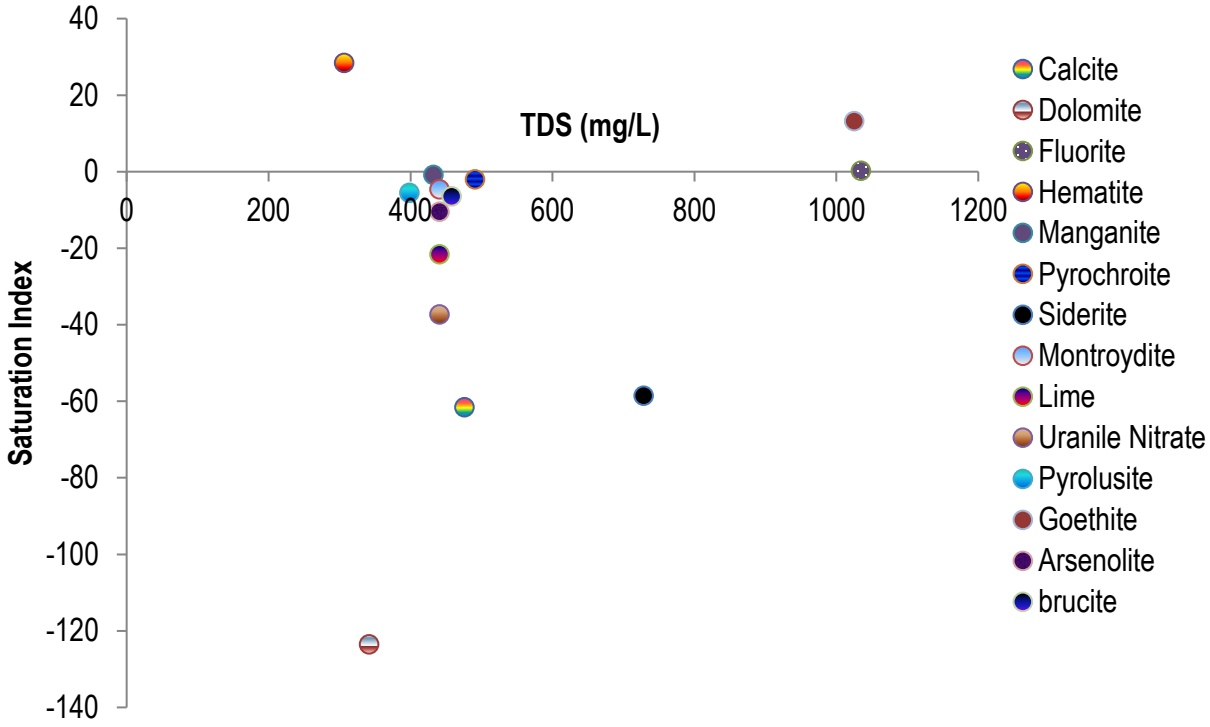

Fig. 3.7. Mineral equilibrium states

In the deep aquifer, the low concentrations of most trace metals, such as Fe, Mn, Hg, and As, suggest limited human interference. However, Uranile Nitrate showed relatively higher presence, possibly due to natural geogenic sources or deeper geological interactions.

Hydrogeochemical analysis reveals that groundwater in Haridwar is primarily influenced by carbonate and silicate weathering, with Ca–Mg–HCO_3-type water dominating. The mineral saturation states further support the natural origin of major ions and trace metals. The deeper

aquifer appears less affected by anthropogenic activities, indicating a relatively pristine geochemical environment.

3.3. Trace Toxic Metals in Groundwater

3.3.1. Arsenic

Arsenic concentrations in shallow groundwater ranged from 0.01 to 267.1 µg/L (mean: 23.9 ± 35.3 µg/L), and in deep groundwater from 0.0 to 77.1 µg/L (mean: 8.8 ± 10.4 µg/L). In the shallow aquifer, 50% of samples exceeded the BIS acceptable limit (10 µg/L), and 16% exceeded the BIS permissible limit of 50 µg/L. In the deep aquifer, 25% of samples exceeded 10 µg/L and 1% exceeded 50 µg/L (Fig. 3.8). Clearly, arsenic contamination is more pronounced in the shallow groundwater compared to the deep.

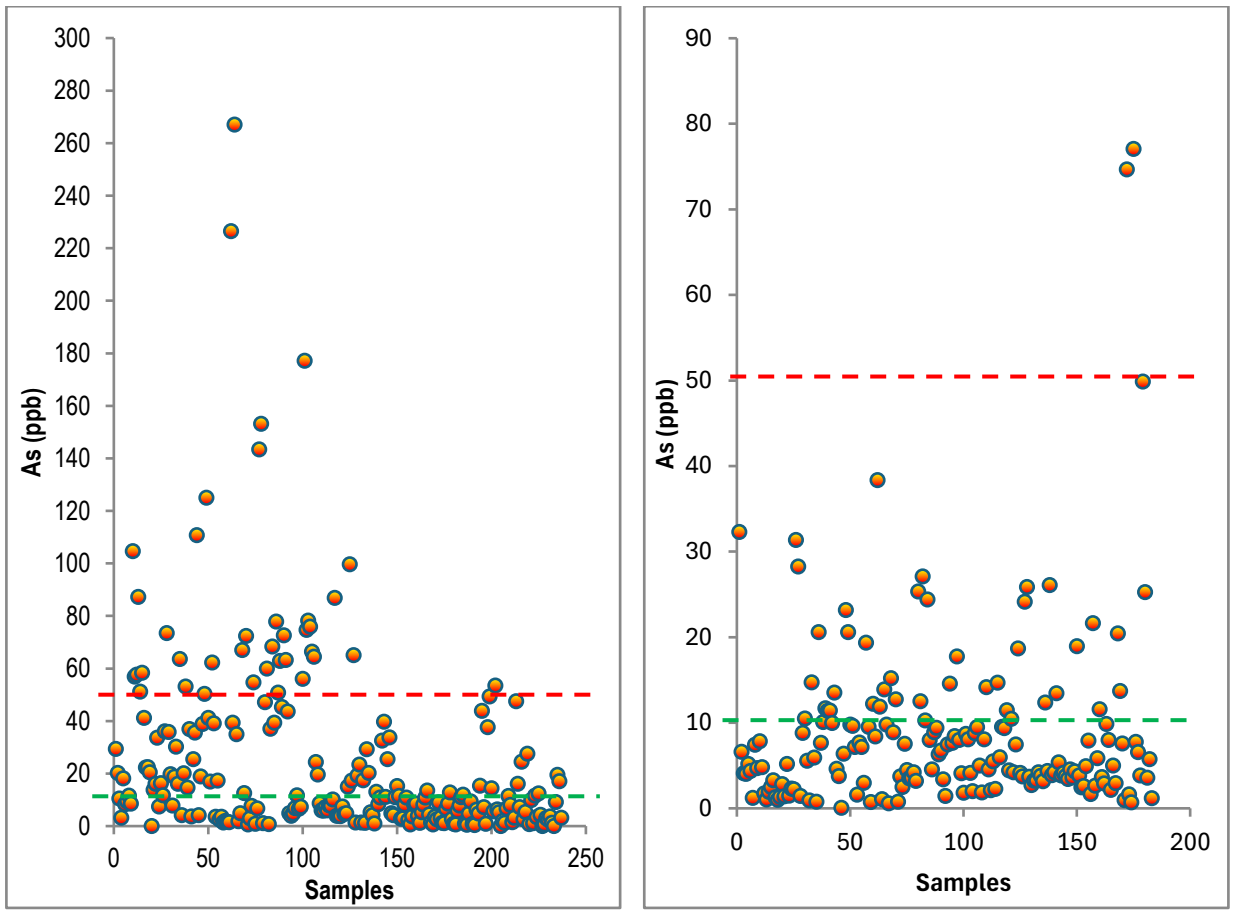

Fig. 3.8. As concentration in shallow (a) and deep (b) aquifers

3.3.2. Iron

Iron is abundant in Earth's crust and often dissolves into groundwater under reducing conditions. Excessive iron concentrations may cause taste, staining, and microbial growth issues, though they are less of a direct health concern. Fe concentration ranged from 0.6 to 24,737.4 µg/L (mean ~2,193 µg/L) in shallow groundwater, with 68% of samples exceeding the BIS limit of 300 µg/L. In deep groundwater, concentrations ranged from 0.6 to 14,379.3 µg/L (mean ~909 µg/L), with 60% exceeding the permissible limit (Fig. 3.9). Iron levels are generally higher in shallow aquifers than in deeper ones.

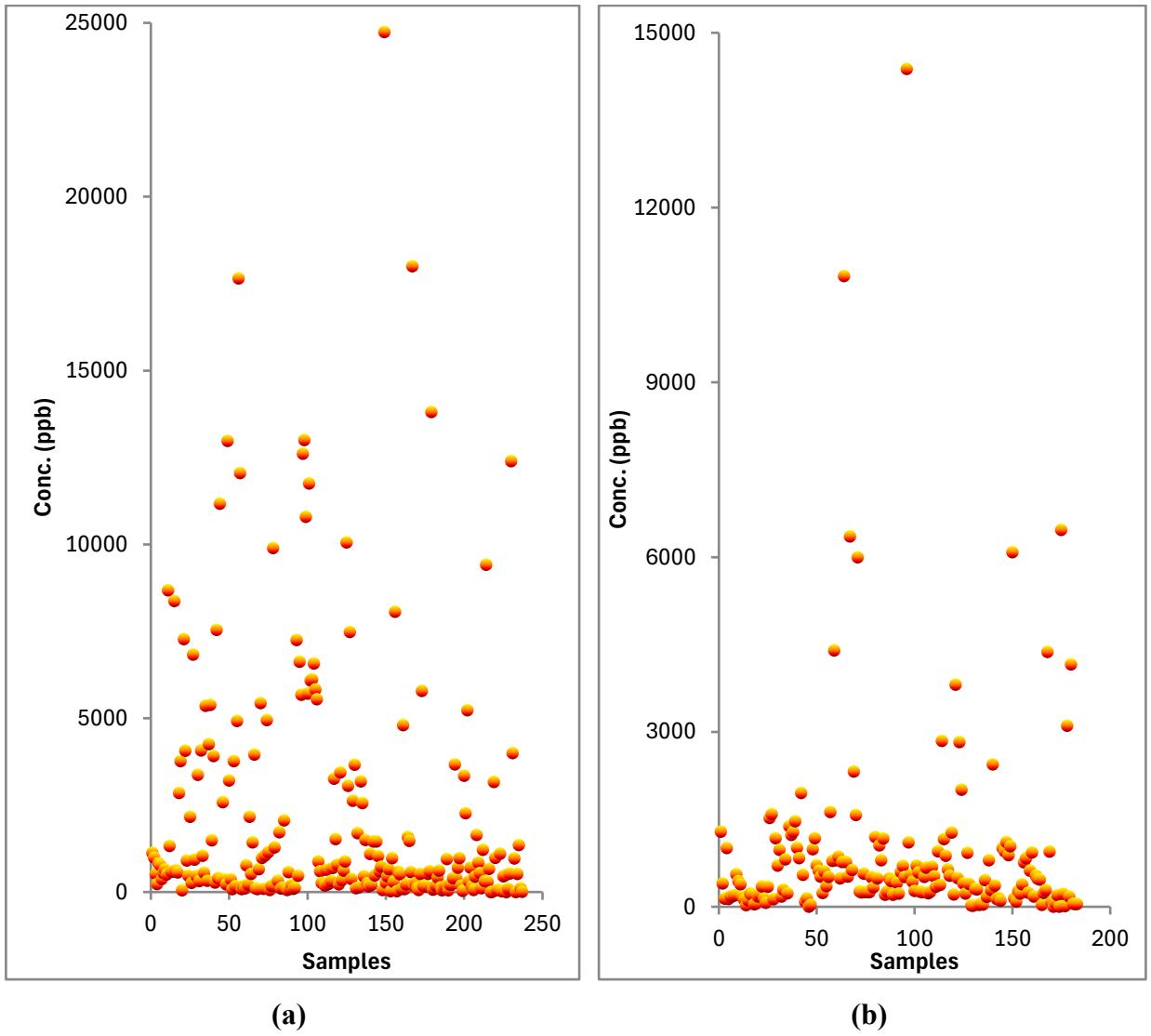

(a) **(b)**

Fig. 3.9. Iron concentration in shallow (a) and deep (b) aquifers

3.3.3. Manganese

Manganese often coexists with iron and is common in groundwater under reducing conditions. In the analyzed samples, Mn ranged from 0 to 2,549 µg/L (mean ~478 µg/L) in shallow groundwater and 0.7 to 1,834.9 µg/L (mean ~333.3 µg/L) in deep groundwater. About 77% of shallow and 67% of deep groundwater samples exceeded the WHO guideline (Figure 3.10).

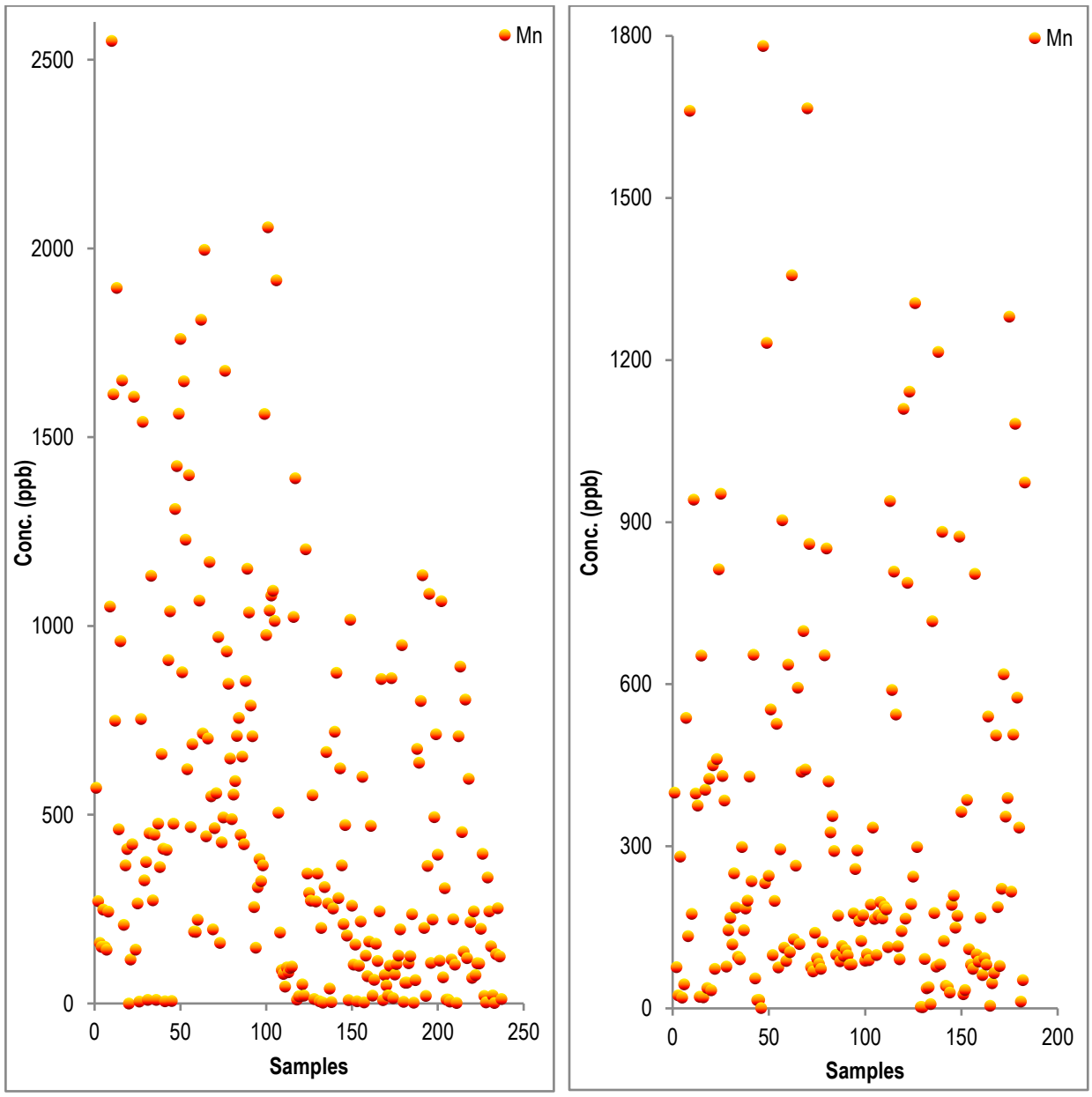

(a) **(b)**

Fig. 3.10. Manganese concentration in shallow (a) and deep (b) aquifers

3.3.4. Copper

Copper is an essential micronutrient but can cause staining or unpleasant taste at elevated levels. Its concentration ranged from 0 to 161.7 µg/L in shallow and 0 to 105.8 µg/L in deep groundwater. Only about 2% of samples exceeded the WHO guideline. Spatially, the distribution of copper is relatively uniform between shallow and deep aquifers (Fig. 3.11).

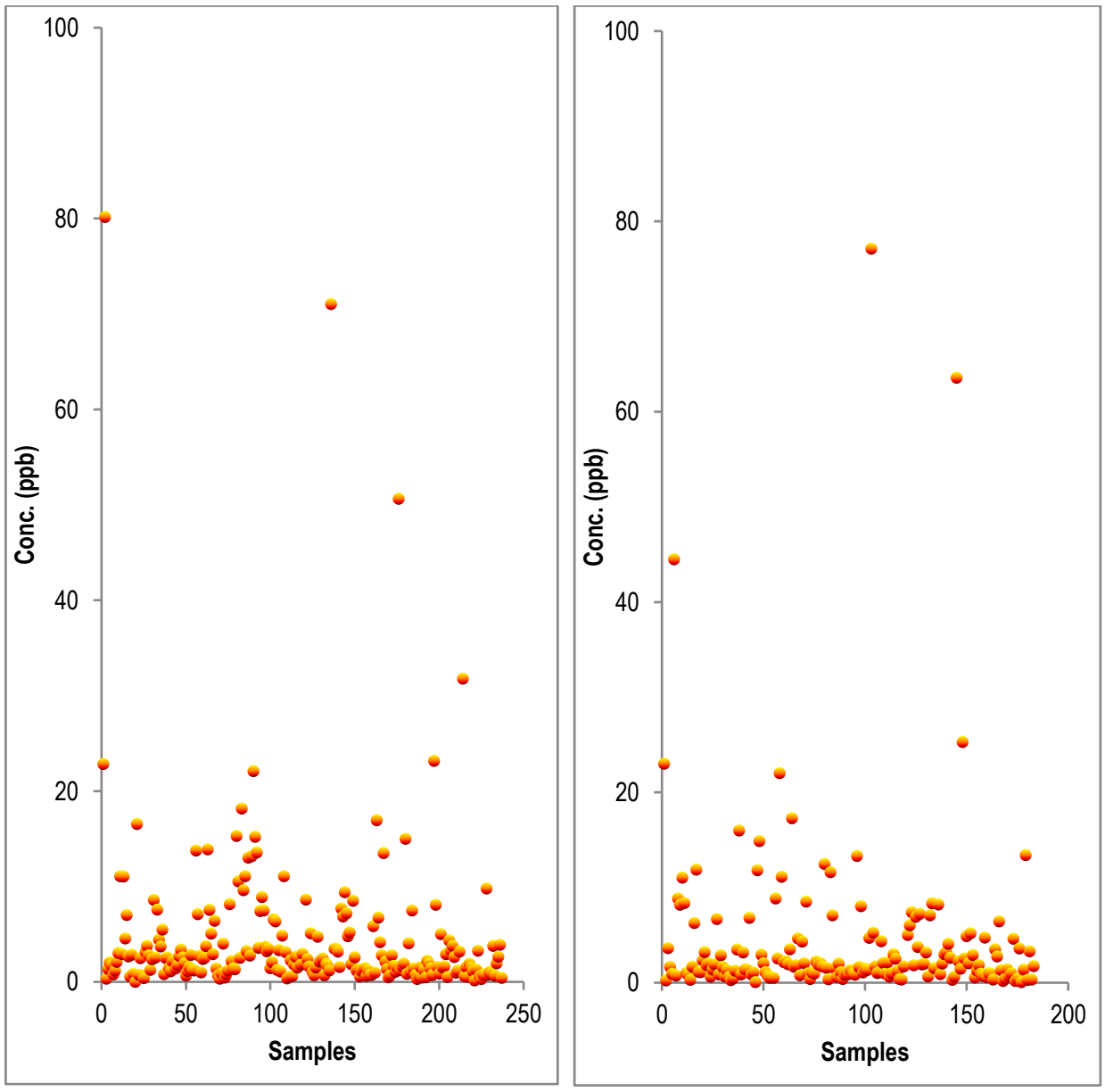

Fig. 3.11. Copper concentration in shallow (a) and deep (b) aquifers

3.3.5. Zinc

Zinc is an essential trace element, generally posing little risk at typical concentrations in drinking water. Zn concentrations in excess of 3-5 mg/l impart an undesirable astringent taste to water and develop a greasy film on boiling. Drinking water usually makes a negligible contribution to zinc intake and is not of health concern at levels found in drinking water. Zn ranged from 0 to 3,350 µg/L (mean ~175.3 µg/L) in shallow and 1 to 1,341 µg/L (mean ~107.6 µg/L) in deep groundwater. All samples remained below the BIS limits (Fig. 3.12).

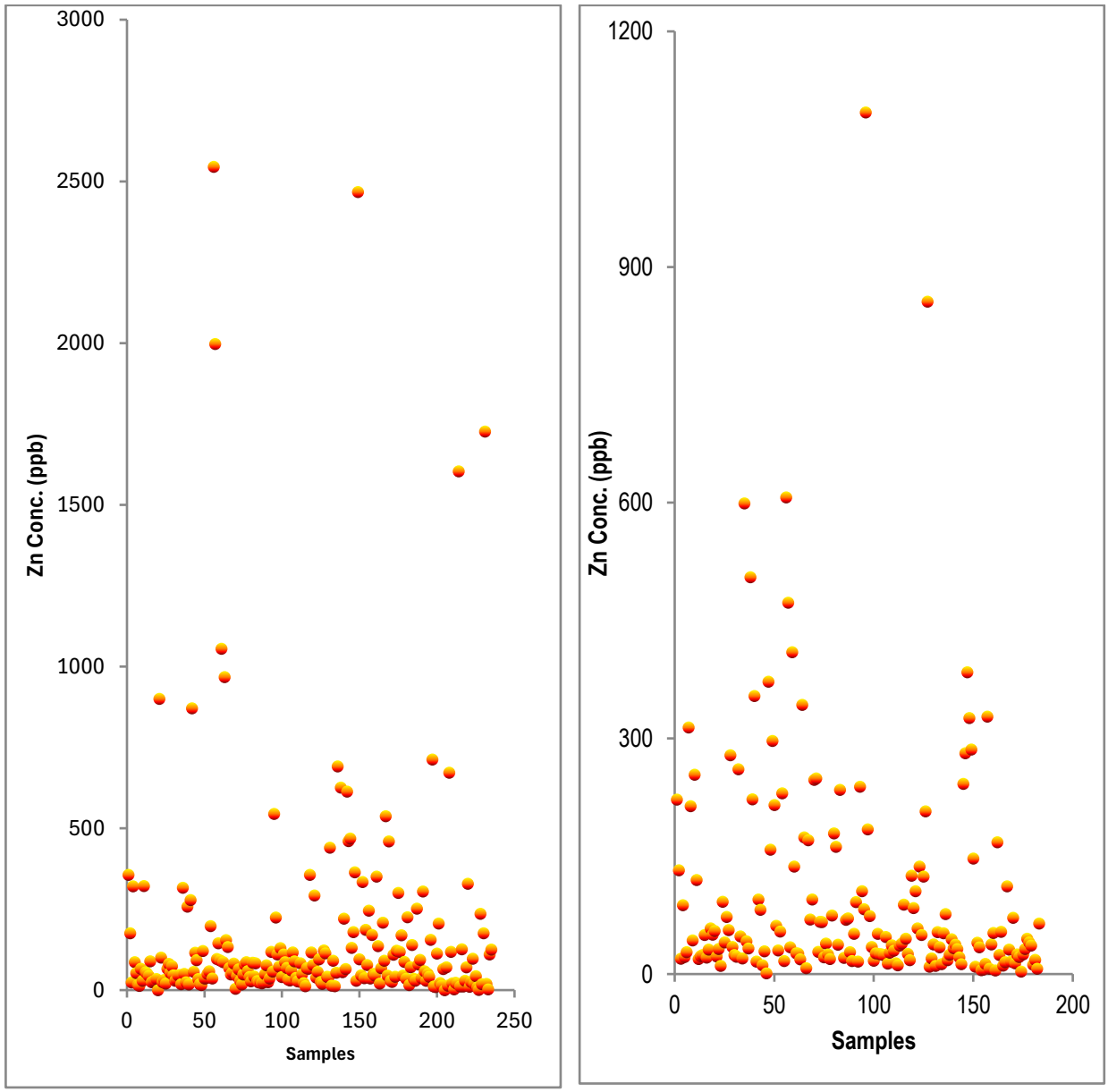

(a) **(b)**

Fig. 3.12. Zinc concentration in shallow (a) and deep (b) aquifers

3.3.6. Aluminum

Aluminum is abundant in the Earth's crust; in drinking water, it can cause discoloration or turbidity but is not acutely toxic. In collected samples, Al ranged from 228.4 to 1,721.8 µg/L (mean ~61.8 µg/L) in shallow groundwater and 0 to 1,972.1 µg/L (mean ~69.2 µg/L) in deep groundwater. About 34% of shallow and 32% of deep groundwater samples exceeded the BIS permissible limit (Fig. 3.13).

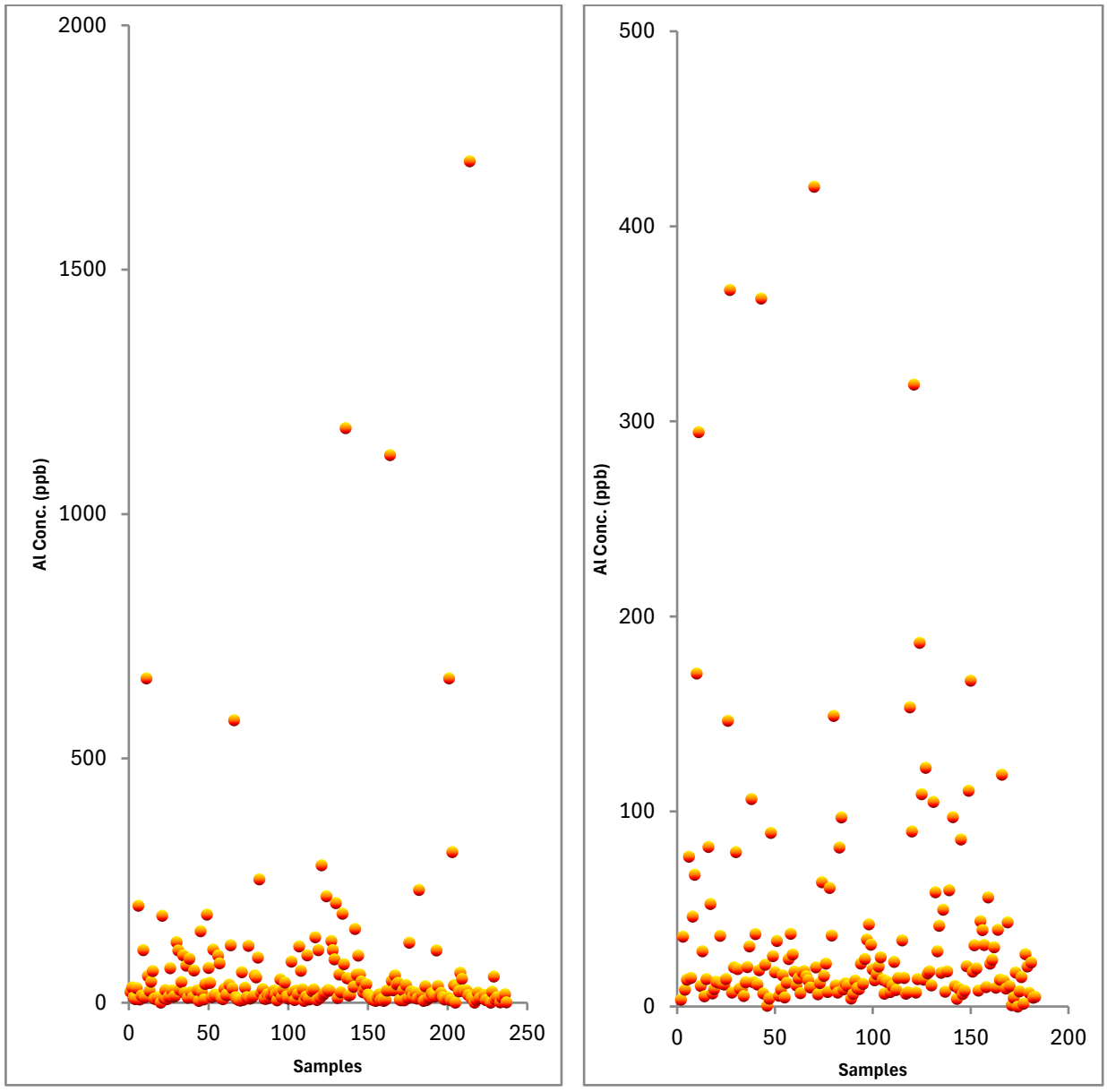

(a) **(b)**

Fig. 3.13. Aluminium concentration in shallow (a) and deep (b) aquifers

3.3.7. Lead

Lead is neurotoxic, especially in children. In shallow groundwater, Pb ranged from 0 to 156.7 µg/L (mean ~3.5 µg/L); in deep water, from 0 to 46.8 µg/L. Approximately 5% of shallow and 4% of deep samples exceeded the WHO guideline (Figure 3.14). Lead's higher presence in shallow aquifers suggests a greater risk near the surface.

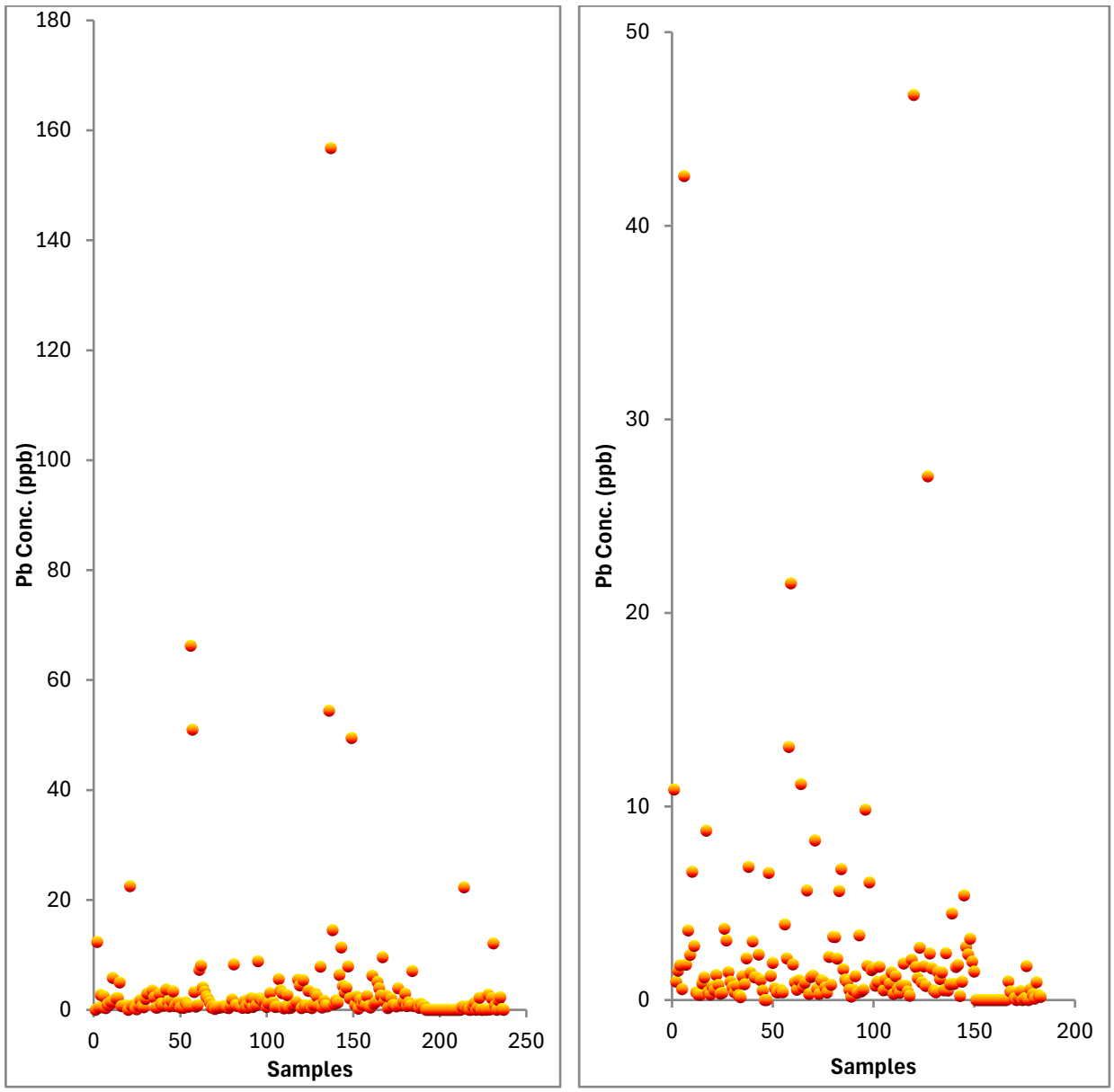

Fig. 3.14. Lead concentration in shallow (a) and deep (b) aquifers

3.3.8. Cadmium

Cadmium is highly toxic and bioaccumulates in organisms. Cd concentrations ranged from 0.06 to 2.4 µg/L (mean ~0.1 µg/L) in shallow water, and 0 to 2.9 µg/L in deep water. All samples remained below the WHO guideline (Figure 3.15), indicating minimal health risk from Cd.

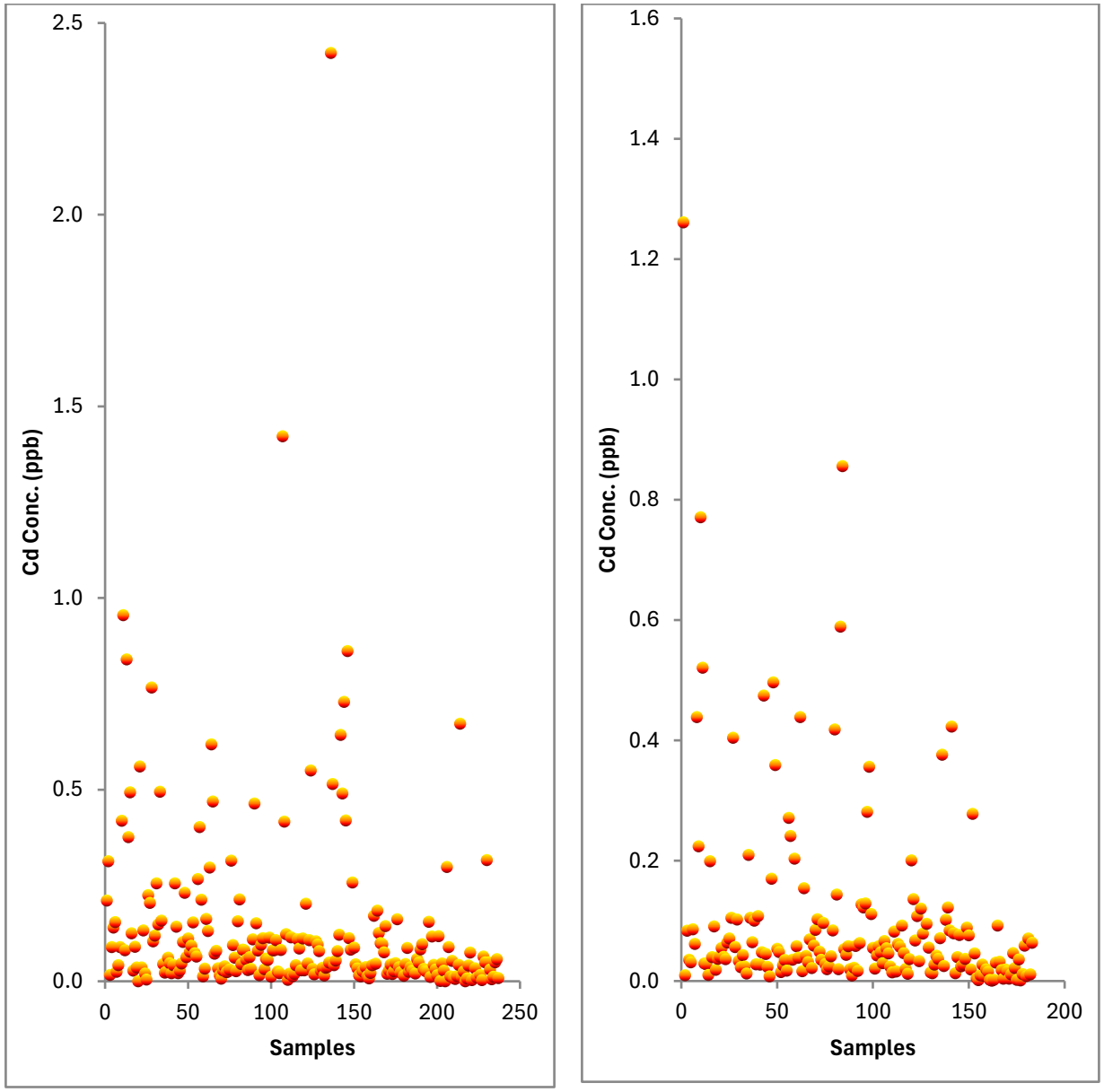

Fig. 3.15. Cadmium concentration in shallow (a) and deep (b) aquifers

3.3.9. Nickel

Nickel is essential in small amounts but can be toxic. The average abundance of nickel in the earth's crust is 1.2 mg/l, in soils it is 2.5 mg/l, in streams it is 1 µg/l and in groundwater it is <0.1 mg/l. Nickel is released to the environment from the burning of fossil fuels and waste discharge from electroplating industries. In general concentration of nickel in water resources is generally below 0.02 mg/l. IARC has included inhaled nickel compounds in Group 1 (carcinogenic to humans) and metallic nickel in Group B (possibly carcinogenic). The concentration of Ni in the analyzed samples ranged from 0.2 to 44.6 µg/L (mean ~1.8 µg/L) in shallow groundwater, and 0 to 309.5 µg/L (mean ~3.4 µg/L) in deep groundwater (Figure 3.16). Interestingly, Ni concentrations were higher in deep groundwater, possibly reflecting deeper geochemical sources.

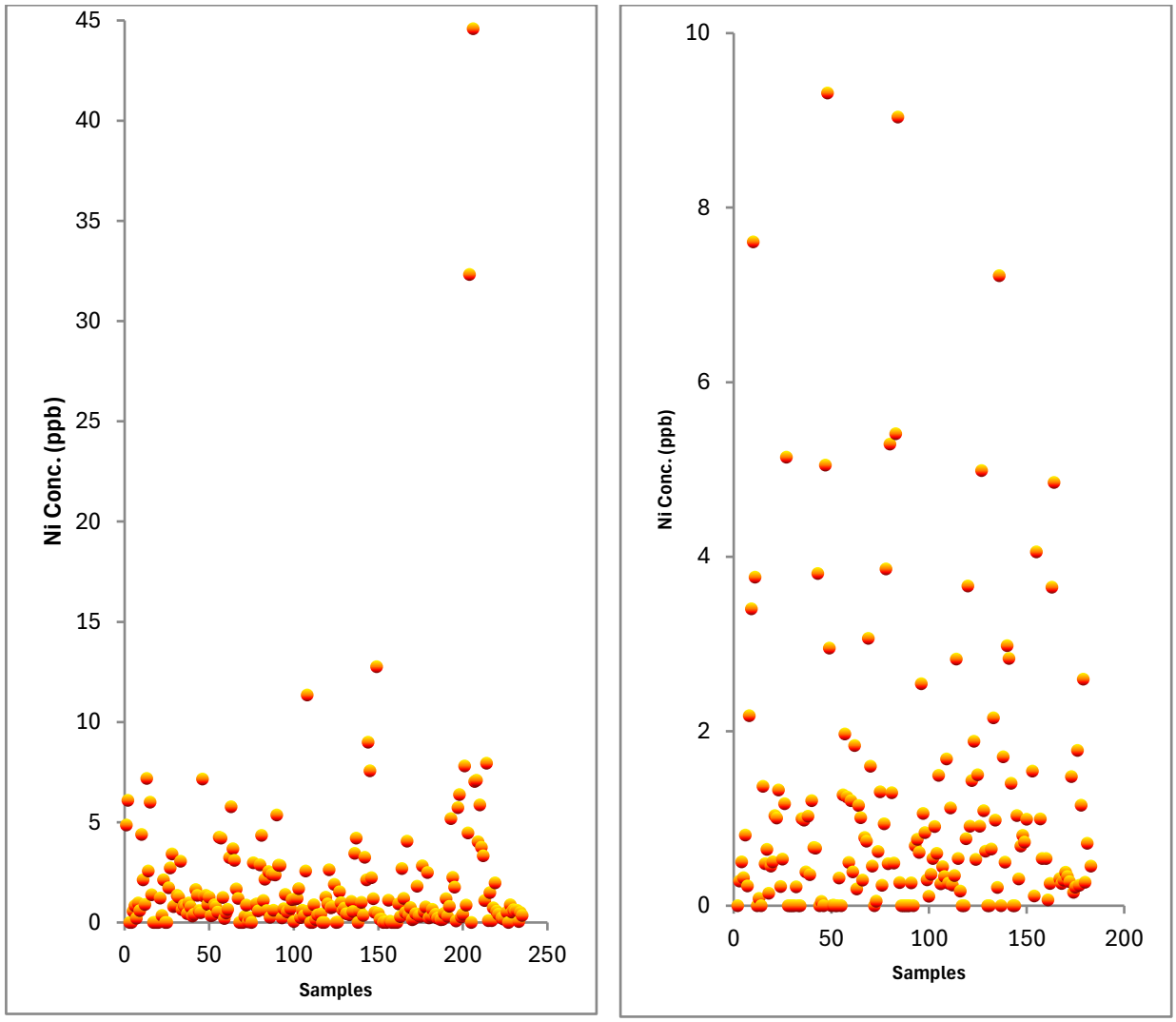

(a) **(b)**

Fig. 3.16. Nickel concentration in shallow (a) and deep (b) aquifers

3.3.10. Cadmium

Cadmium is highly toxic and bioaccumulates in organisms. It is a group XII element, and its compounds are widely used in batteries, pigments, electronic components, and nuclear reactors. It is released to the environment through wastewater, leaching of solid waste, and diffuse pollution from fertilizers and local air pollution. Cadmium accumulates primarily in the kidneys, has a long biological half-life in humans. In analyzed samples, Cd concentrations ranged from 0.06 to 2.4 µg/L (mean ~0.1 µg/L) in shallow water, and 0 to 2.9 µg/L in deep water. All samples remained below the WHO guideline (Figure 3.17), indicating minimal health risk from Cd.

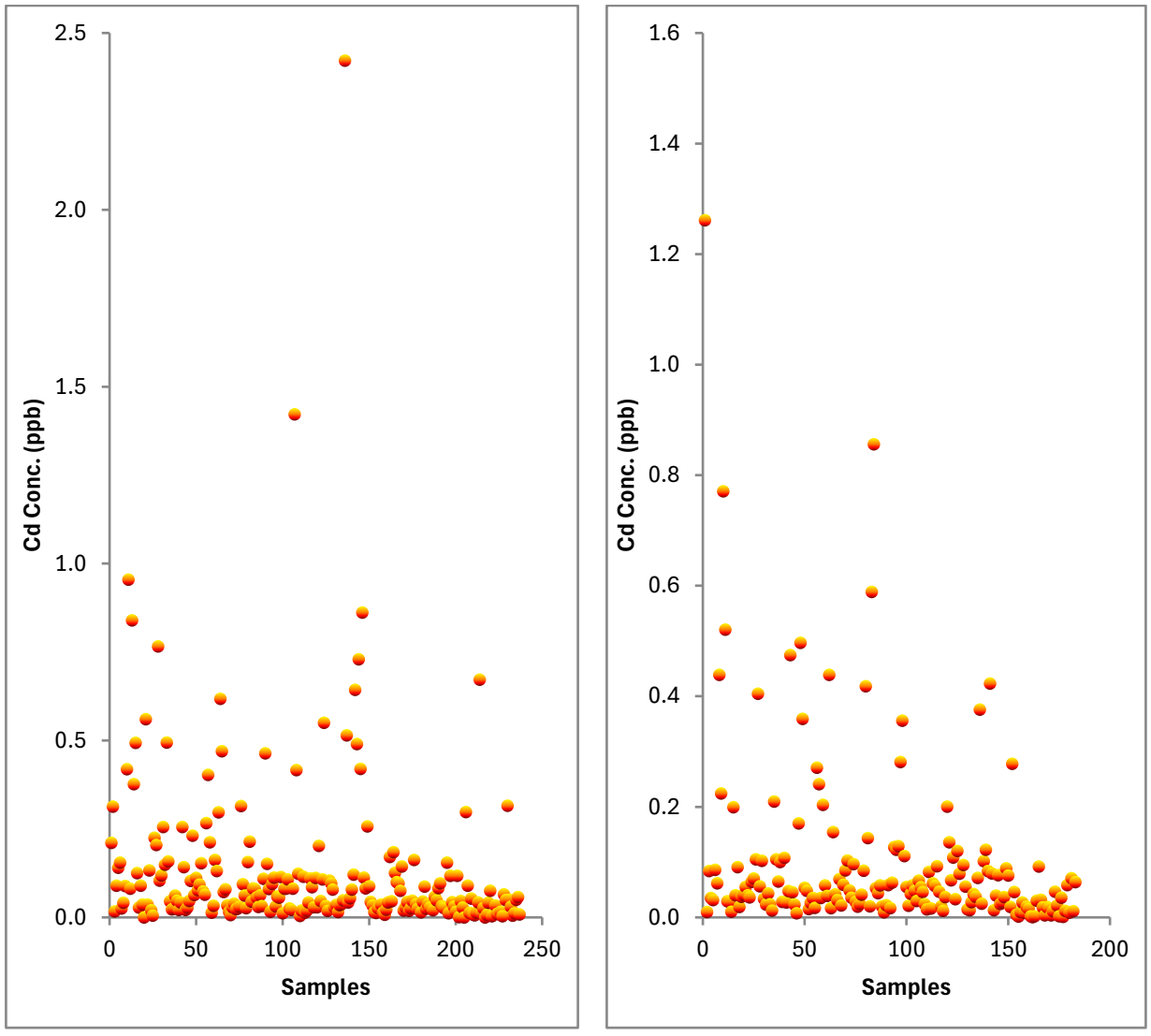

Fig. 3.17. Cadmium concentration in shallow (a) and deep (b) aquifers

3.3.11. Chromium

Cr is widely distributed in Earth's crust. It can exist in valences of +2 to +6. Cr (III) is an essential human dietary element and is found in many vegetables, fruits, meats, grains, and yeast. Cr enters the environment by industrial processes discharge. Further, Cr enters the environment by leakage, poor storage, or inadequate industrial waste disposal practices. IARC has classified chromium (VI) in Group 1 (human carcinogen) and chromium (III) in Group 3 (not classifiable as to its carcinogenicity to humans). The BIS permissible limit for total chromium is 50 µg/L. In collected GW samples, Cr ranged from 0 to 27.9 µg/L (mean ~1.3 µg/L) in shallow and 0 to 12.5 µg/L in deep groundwater (Figure 3.18), all below the permissible limits.

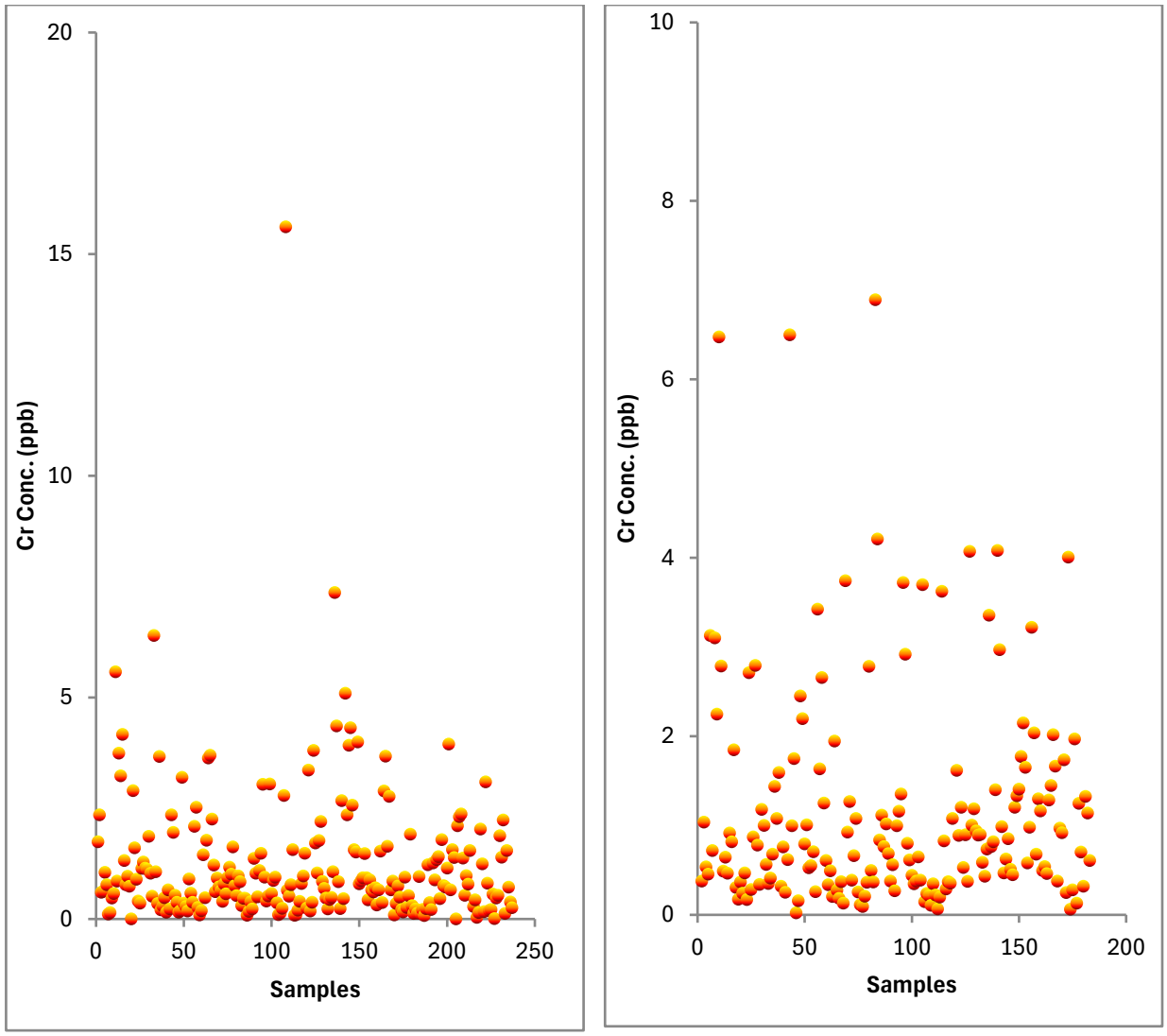

(a) **(b)**

Fig. 3.18. Chromium concentration in shallow (a) and deep (b) aquifers

3.3.12. Cobalt

Cobalt concentrations ranged from 0.3 to 3.3 µg/L in shallow and 0 to 45.7 µg/L in deep groundwater (mean ~0.3 and 0.4 µg/L respectively). The deeper aquifer exhibited somewhat higher Co contamination (Figure 3.19).

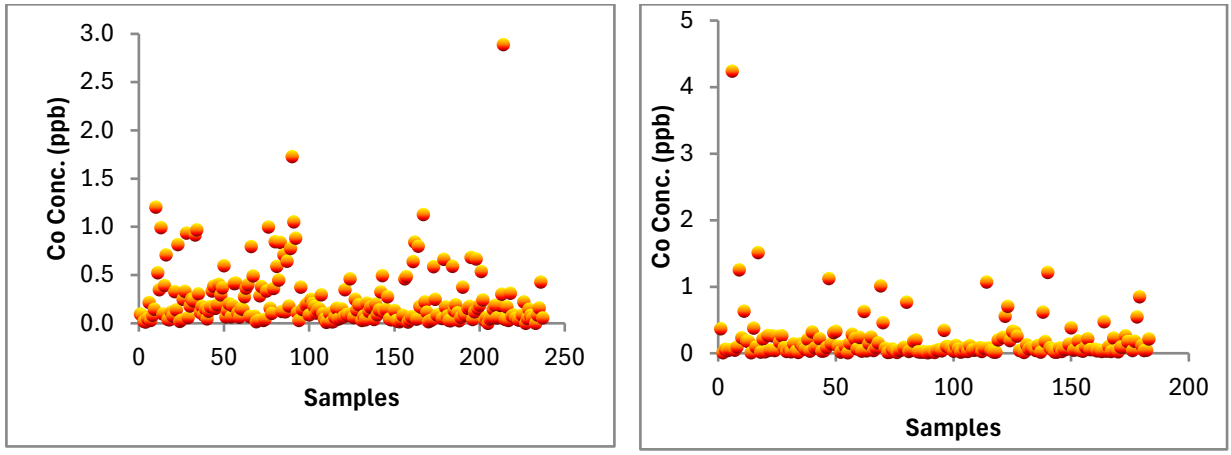

(a) **(b)**

Fig. 3.19. Cobalt concentration in shallow (a) and deep (b) aquifers

3.3.13. Barium

Barium is naturally present in trace amounts and is mainly introduced via rock weathering. Ba concentration ranged from 0.1 to 2,485.5 µg/L (mean ~342.1 µg/L) in shallow and 0.7 to 1,565.4 µg/L (mean ~8.3 µg/L) in deep groundwater. About 12% of shallow and 4% of deep samples exceeded the WHO guideline of 1,300 µg/L (Figure 3.20).

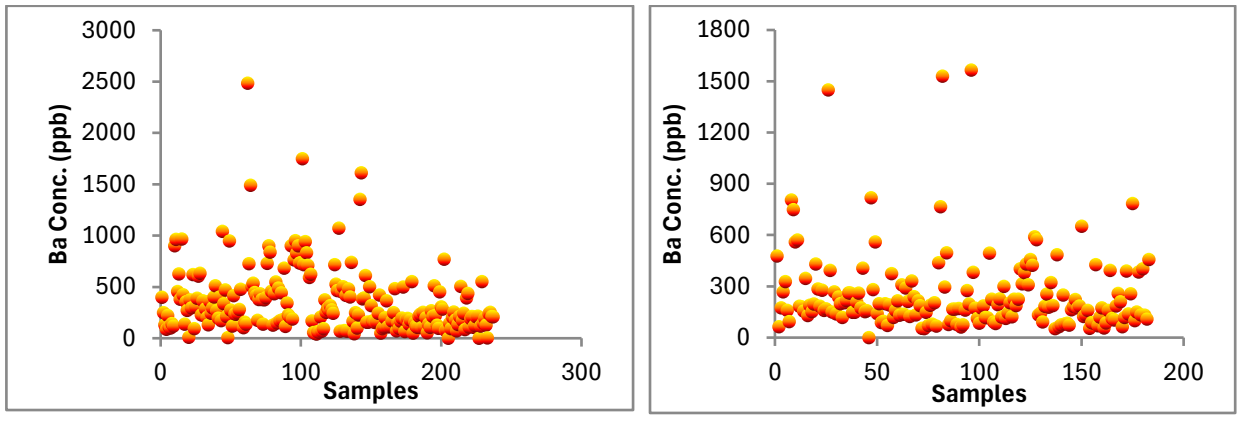

(a) **(b)**

Fig. 3.20. Barium concentration in shallow (a) and deep (b) aquifers

3.3.14. Selenium

Selenium (Se), a metalloid, is a member of group VIA and generally present in elemental form or ionic (selenide (Se-2), selenate (SeO4-2), or selenite (SeO3-2)). It is widely distributed in the Earth's crust, in association with sulfur containing minerals, at a concentration of 50-90 µg/kg. Its concentration in groundwater and surface water ranges from 0.06 µg/l to 400 µg/l. It is an essential element and FAO/WHO recommends daily intake of 6-21 µg/l, 26 µg/l, and 30 µg/l Se for infants/children, females, and males respectively. Se concentration in collected samples ranged from 0 to 4,422.9 µg/L (mean ~19.3 µg/L) in shallow and 0 to 4.8 µg/L (mean ~0.4 µg/L) in deep groundwater. Only 1 sample from shallow aquifer exceeded the WHO permissible limit (Figure 3.21).

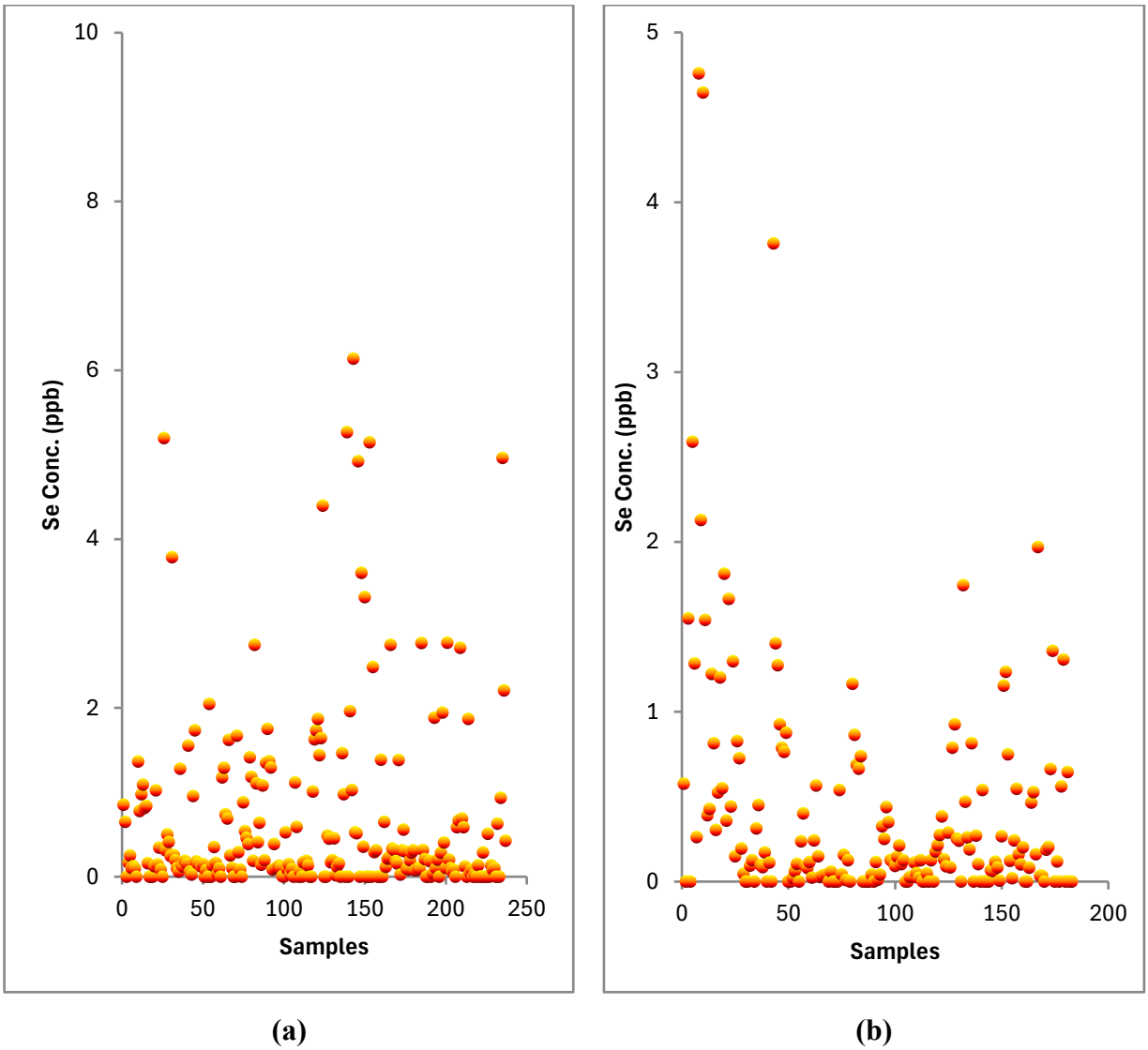

Fig. 3.21. Selenium concentration in shallow (a) and deep (b) aquifers

3.3.15. Strontium

Strontium (Sr) is a trace element, present as ^{84}Sr, ^{86}Sr, and ^{88}Sr stable isotopes, and ^{87}Sr as radioactive isotope formed by the decay of 87Rb (Ladegaard-Pedersen et al., 2020). Sr concentration in the collected samples ranged from 0 to 1,900.6 µg/L in shallow and 0.7 to 1,565 µg/L in deep groundwater (Figure 3.22). Its co-variation with arsenic suggests that Sr-bearing mineral dissolution or geogenic pathways may influence arsenic mobility.

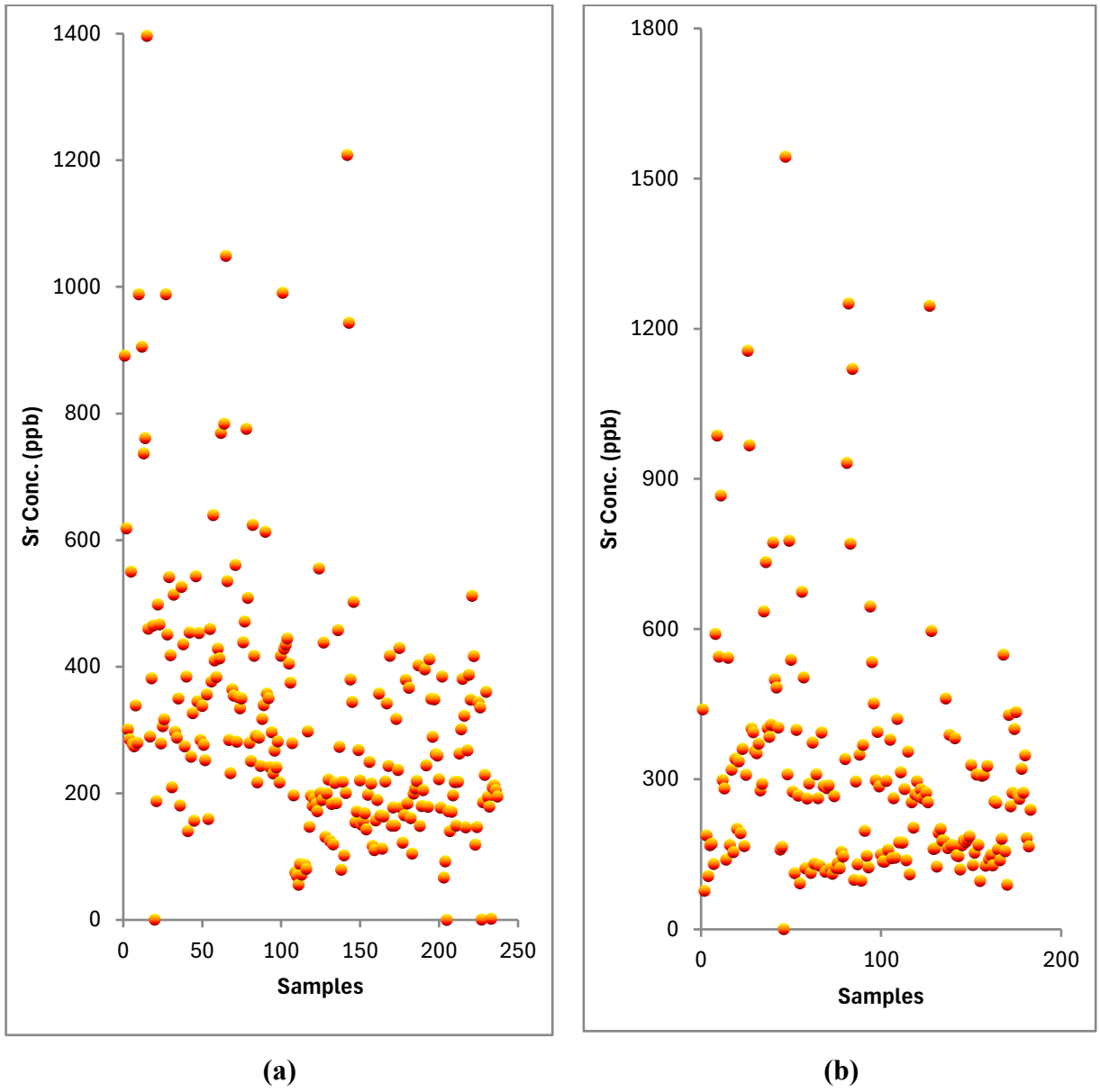

Fig. 3.22. Strontium concentration in shallow (a) and deep (b) aquifers

3.3.16. Boron

Boron (B) is a naturally occurring element and is used in many consumer products like fiberglass, borosilicate glass, soaps and detergents, flame retardants, neutron absorbers for nuclear installations, mild antiseptics, cosmetics, pharmaceuticals (as pH buffers), boron neutron capture therapy (for cancer treatment), pesticides, and fertilizers. The concentration of boron in the earth's crust has been estimated to be <10 mg/kg, Boron enters in the environment mainly through the weathering of rocks and volcanic activity. Boron concentration in groundwater and surface water is generally small, however, the concentration can be significantly increased depending on the anthropogenic activities and surrounding geology. Boron toxicity results in gastrointestinal tract distress, vomiting, abdominal pain, diarrhea, and nausea (Simonnot et al. 2000, Yazbeck et al. 2005, Health Canada 2020). B concentration in analyzed samples ranged from 0 to 125.9 µg/L (mean ~26.2 µg/L) in shallow and 0 to 127.9 µg/L (mean ~21.0 µg/L) in deep groundwater (Figure 3.23). These concentrations remain relatively low and pose minimal direct health risk under current guidelines.

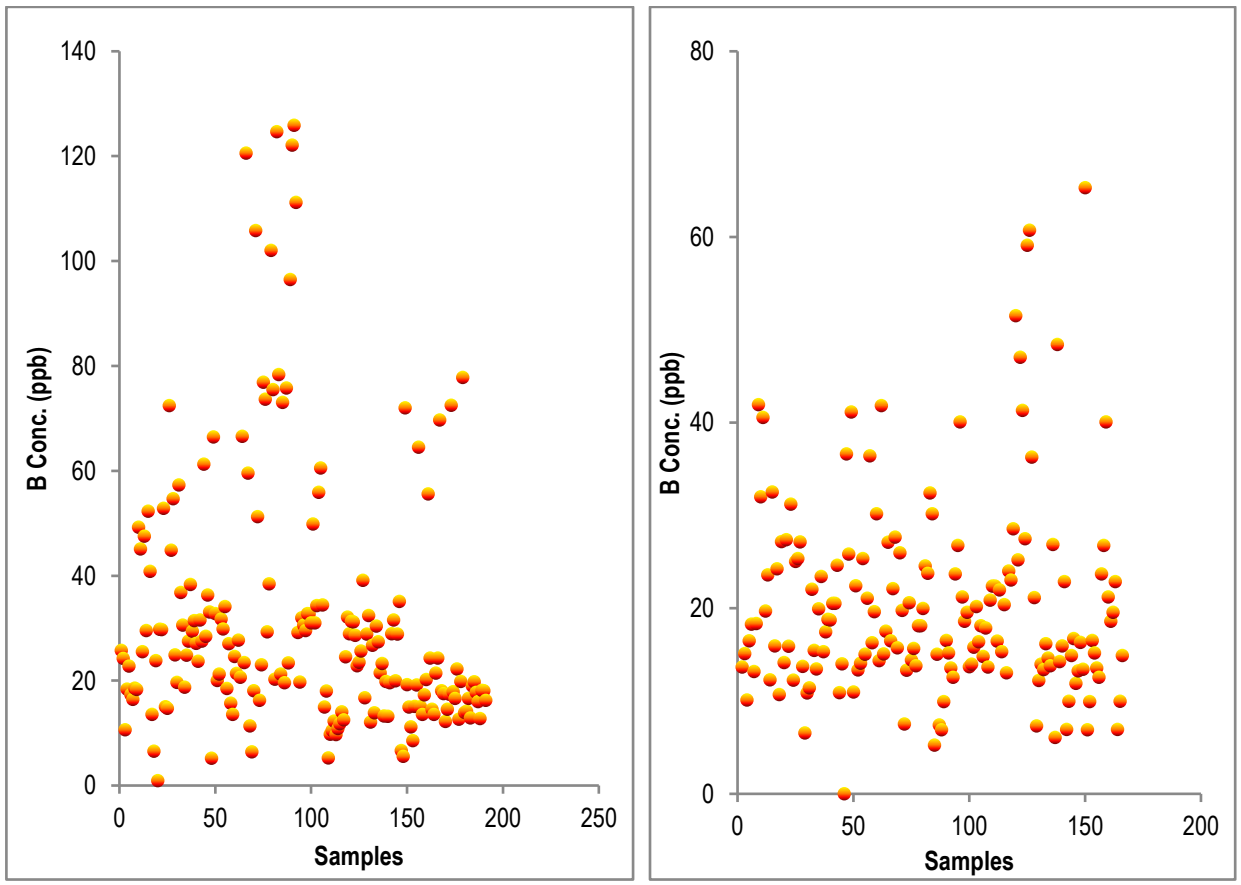

(a) **(b)**

Fig. 3.23. Boron concentration in shallow (a) and deep (b) aquifers

3.3.17. Uranium

Uranium is a naturally occurring radioactive element, usually present as the uranyl ion (UO_2^{2+}). In groundwater, it forms carbonate and other complexes that control solubility (CGWB, 2020). The uranium concentration in the analyzed samples ranged from 0 to 85.1 µg/L in shallow and 0 to 88.1 µg/L in deep aquifers (Figure 3.24). About 5–6% of samples exceeded the WHO permissible limit of 30 µg/L, indicating a health risk and need for further work.

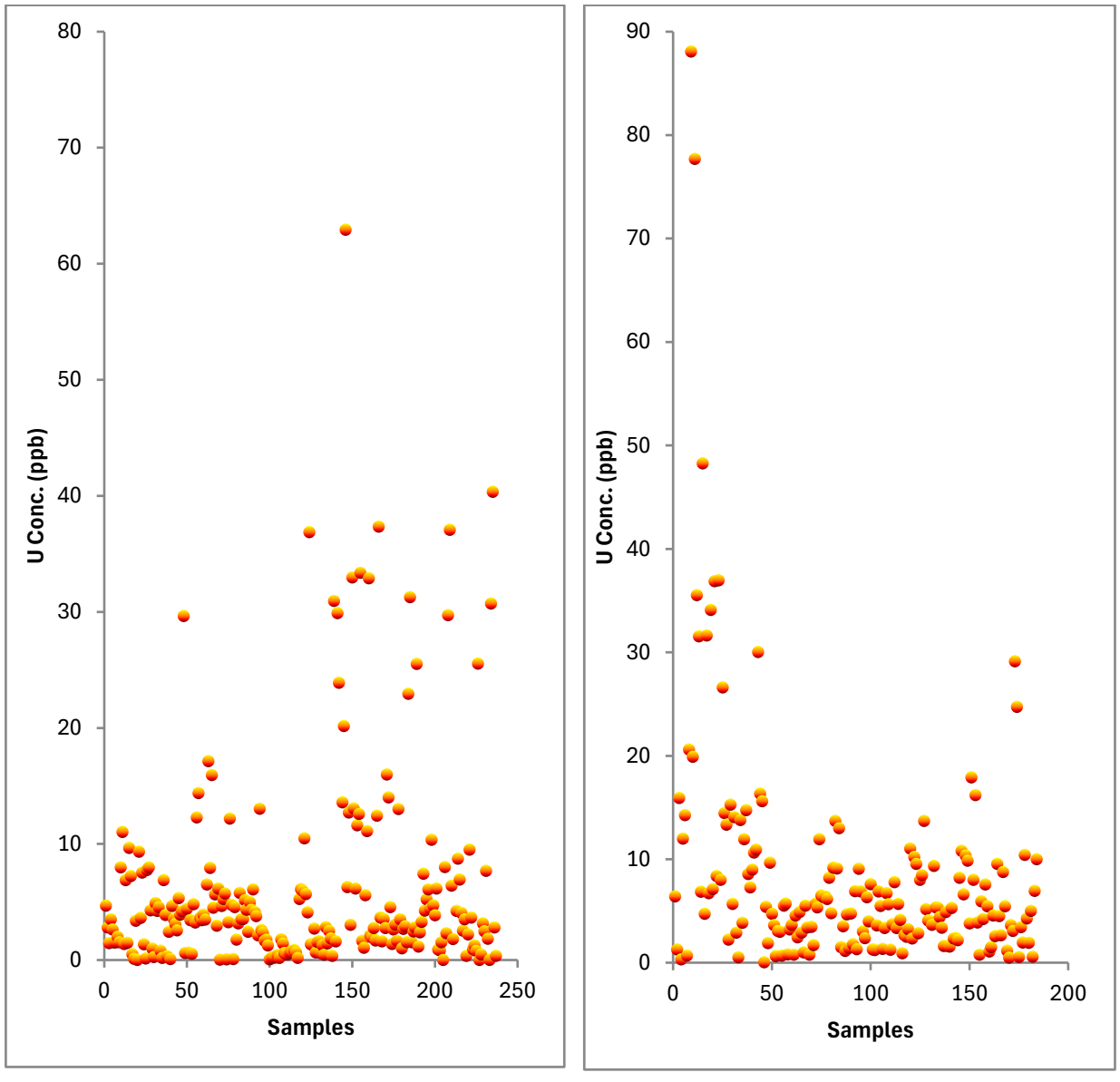

Fig. 3.24. Uranium concentration in shallow (a) and deep (b) aquifers

3.4. Spatial, Seasonal, and Depth-wise Variation of Arsenic in Groundwater

3.4.1. Spatial Variation

The spatial distribution of arsenic and corresponding LULC has been depicted in Figures 3. Elevated arsenic concentrations in shallow groundwater were recorded at locations such as Damanpuri, Kuwakheda, Husainpur, Kalasiya, Fatwa, and Laksar Market, while deep groundwater arsenic contamination was observed at Damanpuri, Jainpur Jhajheri, and Bhogpur.

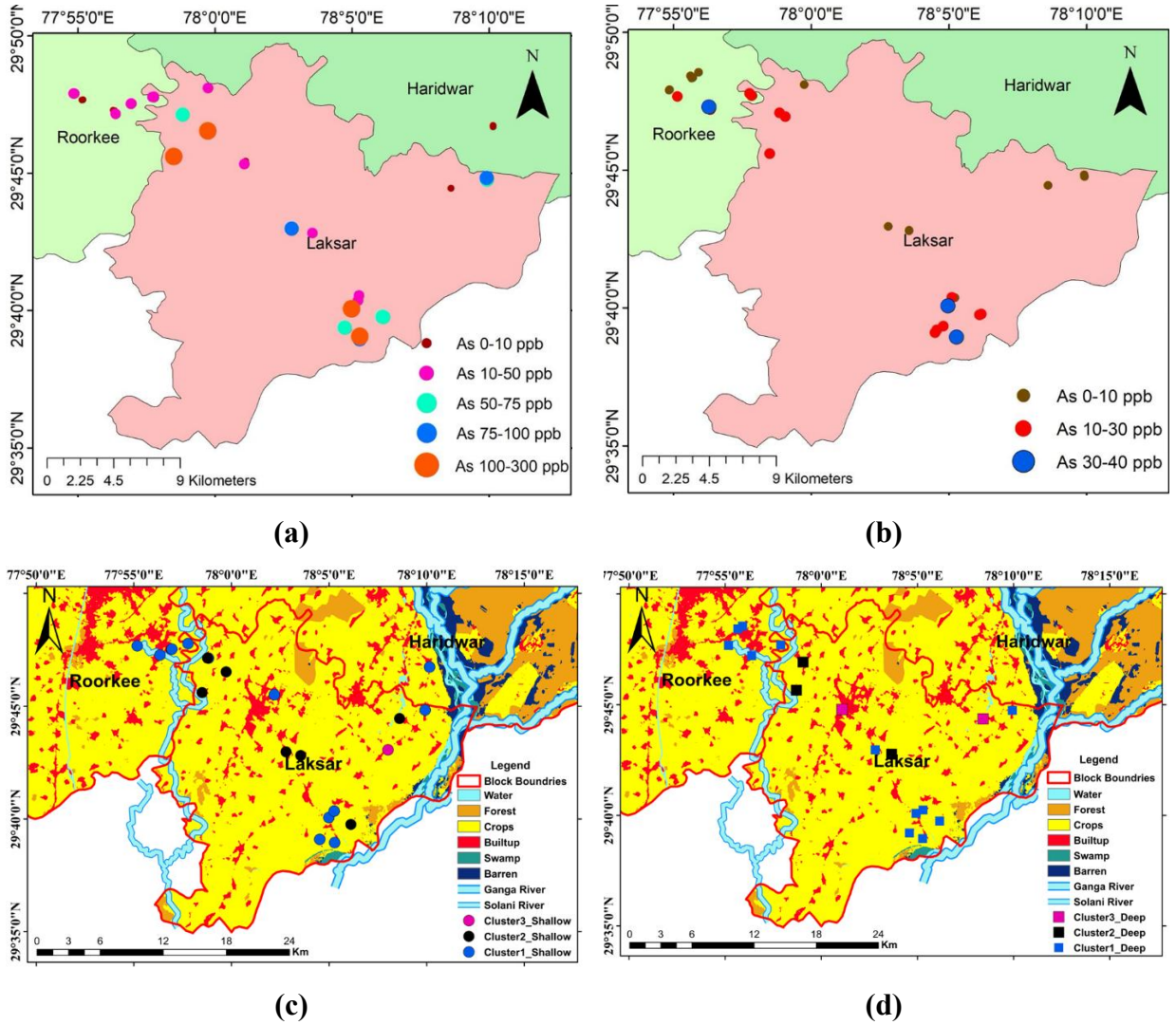

Fig. 3.25. Spatial distribution of As in shallow (a) and deep (b) aquifers, and LULC of sampling sites for shallow (c) and deep wells (d).

These contaminated sites are primarily located within the Laksar and Roorkee blocks, which lie in close proximity to the Ganga and Solani rivers (Figures 3.25c & 3.25d). This proximity suggests significant river–groundwater interaction, likely driven by monsoonal recharge and lateral flow from the riverbanks.

The LULC maps further refines the understanding about As contamination. Cluster 1, representing high arsenic concentrations in shallow aquifers, are mainly in cropland and built-up areas near rivers. Cluster 2 is in agricultural regions, especially along riverbanks, indicating that irrigation practices and sediment–water interaction could promote arsenic release. Cluster 3 is near swampy zones and low-lying areas, possibly linked to stagnant water conditions and reducing environments that favor arsenic dissolution. The majority of high As zones overlap with cropland-dominated areas, especially in Laksar and Roorkee, where floodplain deposits and intensive groundwater extraction may enhance desorption and mobilization processes.

The δ^2H vs $\delta^{18}O$ isotopic plot (Figure 3.26) provides crucial insights into the origin and recharge sources of groundwater. The samples align closely along a regression line with a strong correlation coefficient ($R^2 = 0.96$), indicating a meteoric origin of the groundwater. The regression line ($\delta^2H = 6.2904 \times \delta^{18}O - 3.686$) runs parallel and close to the regression line for the Solani River, suggesting ignificant river water contribution, supporting the inference of river–aquifer interaction as a driver for arsenic mobilization. During the post-monsoon period, when river stages are high, the infiltration of oxygenated surface water into reducing subsurface environments can trigger the reductive dissolution of iron oxyhydroxides, thereby releasing arsenic into groundwater.

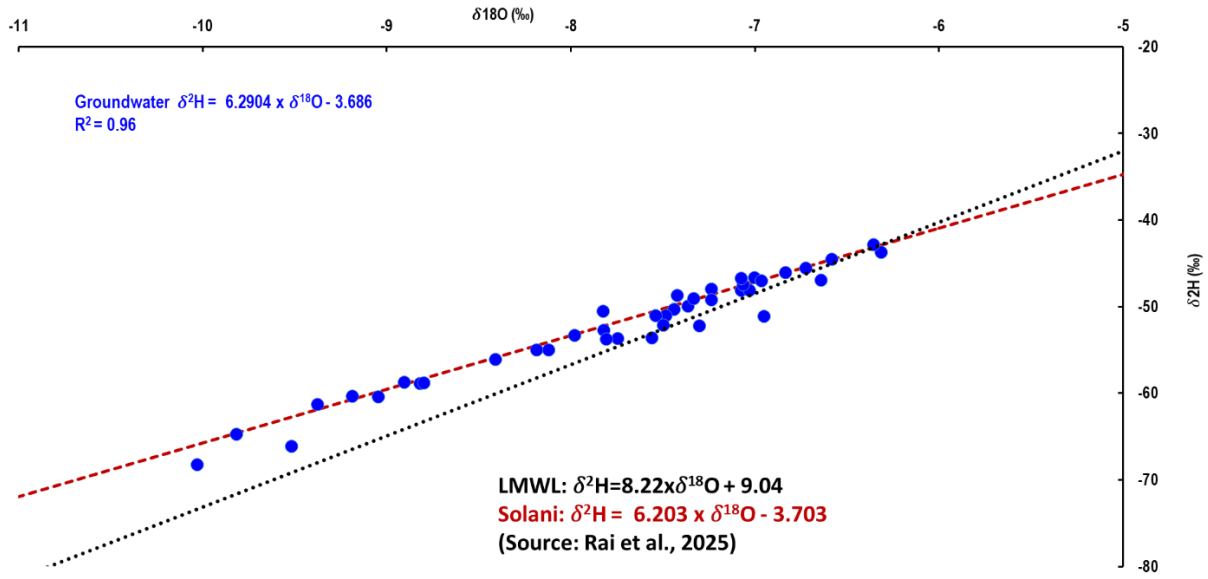

Fig. 3.26. $\delta^{18}O$ vs. δ^2H plot of GW samples

3.4.2. Seasonal Variation

Figure 3.27a (shallow aquifer) and Figure 3.27b (deep aquifer) illustrate the seasonal fluctuations in arsenic concentrations. In both aquifers, post-monsoon shows the highest arsenic levels, followed by pre-monsoon and monsoon periods. This implies that arsenic mobilization intensifies after the rainy season, likely due to increased infiltration of surface water into the aquifers.

In the shallow zone, arsenic concentration declines from pre-monsoon to monsoon, whereas in the deep aquifer, the drop is more pronounced from monsoon to pre-monsoon. Such trends suggest that monsoonal recharge (from rainfall and river water—Ganga and Solani) plays a key role in enhancing arsenic leaching, especially in the post-monsoon period.

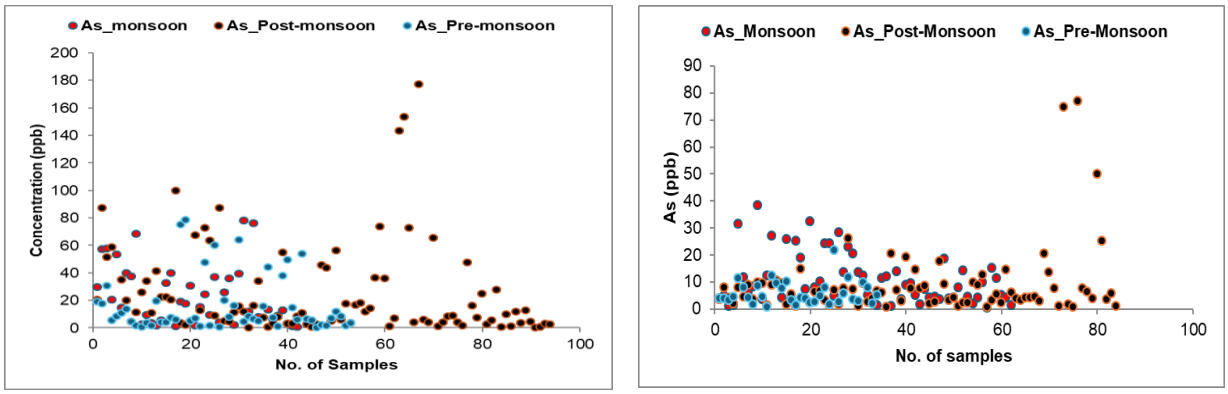

(a) **(b)**

Fig. 3.27. Seasonal variation of arsenic in shallow (a) and deep (b) groundwater

3.4.2. Depth profile of As contamination

Figure 3.28 presents the vertical distribution of arsenic in groundwater across depths. The shallow aquifer exhibits a wide arsenic range (0 to ~267.5 µg/L), which gradually diminishes with depth, often reaching negligible levels below ~50 m. After this depth, concentrations tend to stay below 50 µg/L. This behavior supports the inference that arsenic contamination is largely a shallow aquifer phenomenon, likely driven by surface-derived redox processes or organic matter inputs.

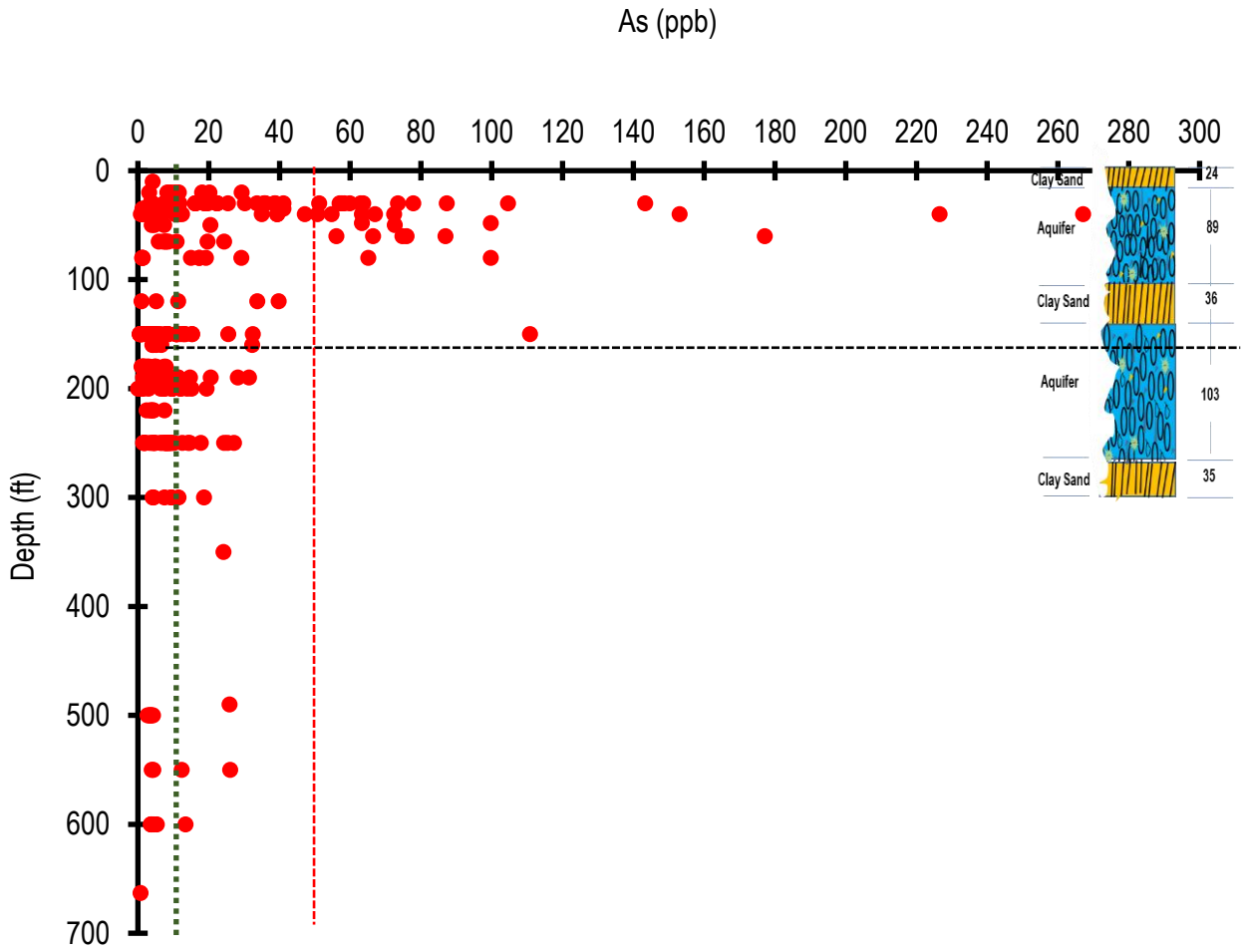

Fig. 3.28. Vertical depth profile of arsenic concentration in groundwater

3.5. Impact of Hydrogeochemical Parameters on As Mobilization

3.5.1. Arsenic vs ORP (Oxidation–Reduction Potential)

ORP is an important indicator of the redox environment in groundwater. A negative correlation between ORP and arsenic was observed in both shallow and deep aquifers, with Pearson correlation values of –0.212 and –0.245, respectively (Tables 3.2a & 3.2b). This suggests that arsenic mobilization increases under reducing conditions, as shown in Figure 3.29. The reducing environment in shallow aquifers is more prominent, which explains the higher arsenic concentrations compared to deeper aquifers.

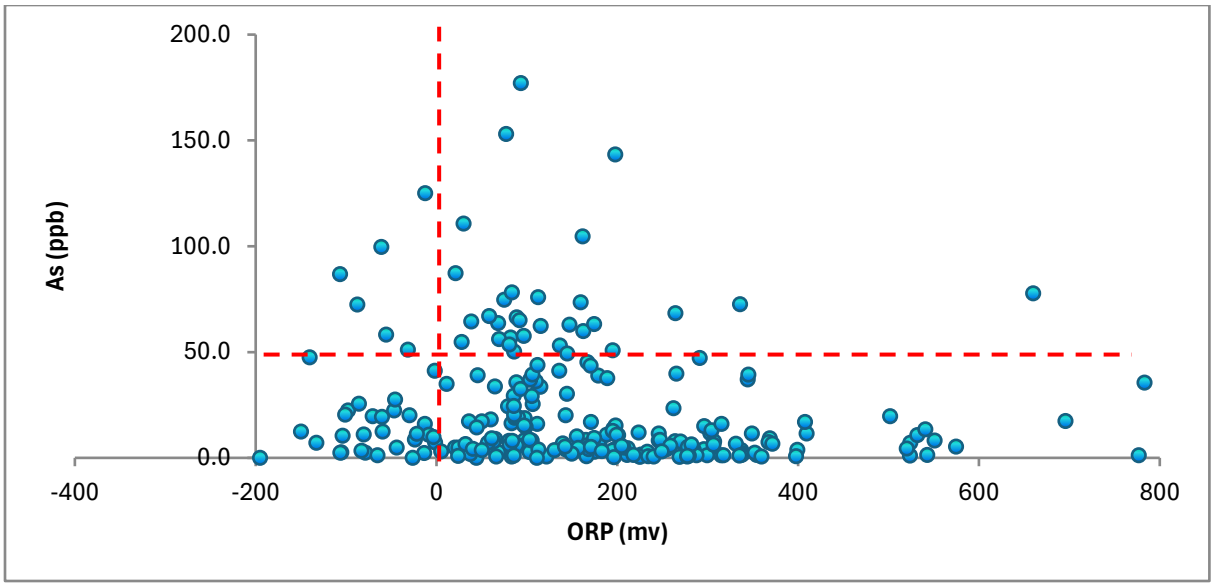

(a)

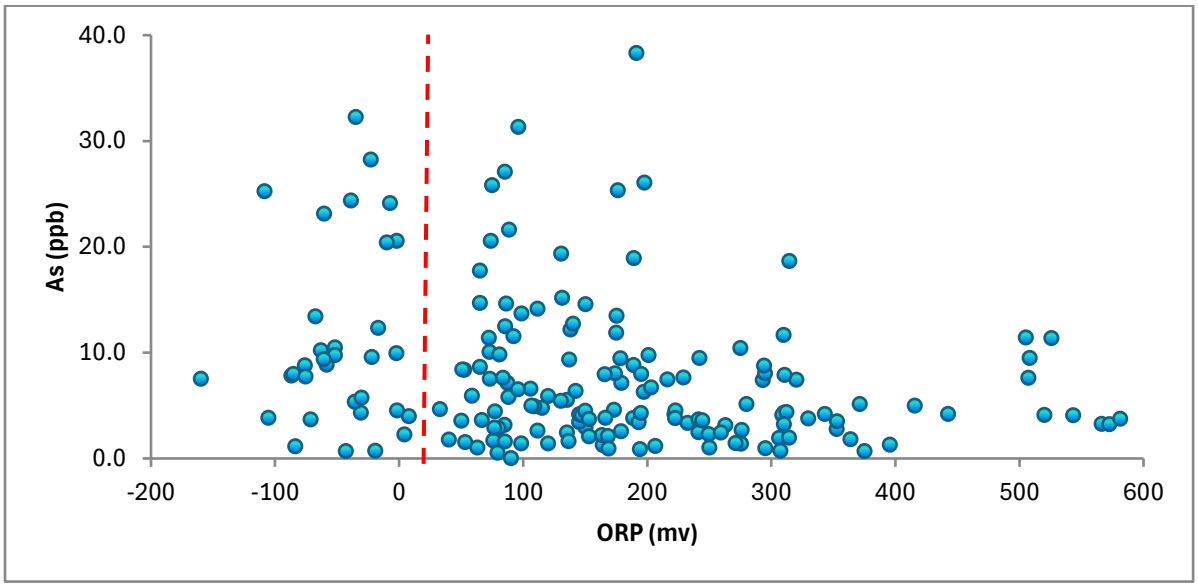

(b)

Fig. 3.29. Variation of Arsenic with ORP in shallow (a) and deep (b) groundwater

3.5.2. Arsenic vs Iron (Fe) and Manganese (Mn)

Iron (Fe) is often regarded as a controlling factor in arsenic mobilization due to the reductive dissolution of iron oxyhydroxides. However, in this study, the correlation between arsenic and iron was weak in both shallow ($r = 0.193$) and deep ($r = 0.087$) aquifers (Tables 3.2a & 3.2b), indicating a limited role of iron in arsenic release in the Laksar and Roorkee blocks. This suggests that

reductive dissolution of Fe-bearing minerals is not the dominant mechanism in these aquifers (Figure 3.30a & b).

Conversely, manganese (Mn) exhibited a stronger correlation with arsenic, particularly in shallow groundwater 0.626), and to a lesser extent in deep aquifers (0.304). This indicates that Mn oxides may play a more active role in arsenic mobilization, possibly through reductive dissolution under anaerobic conditions.

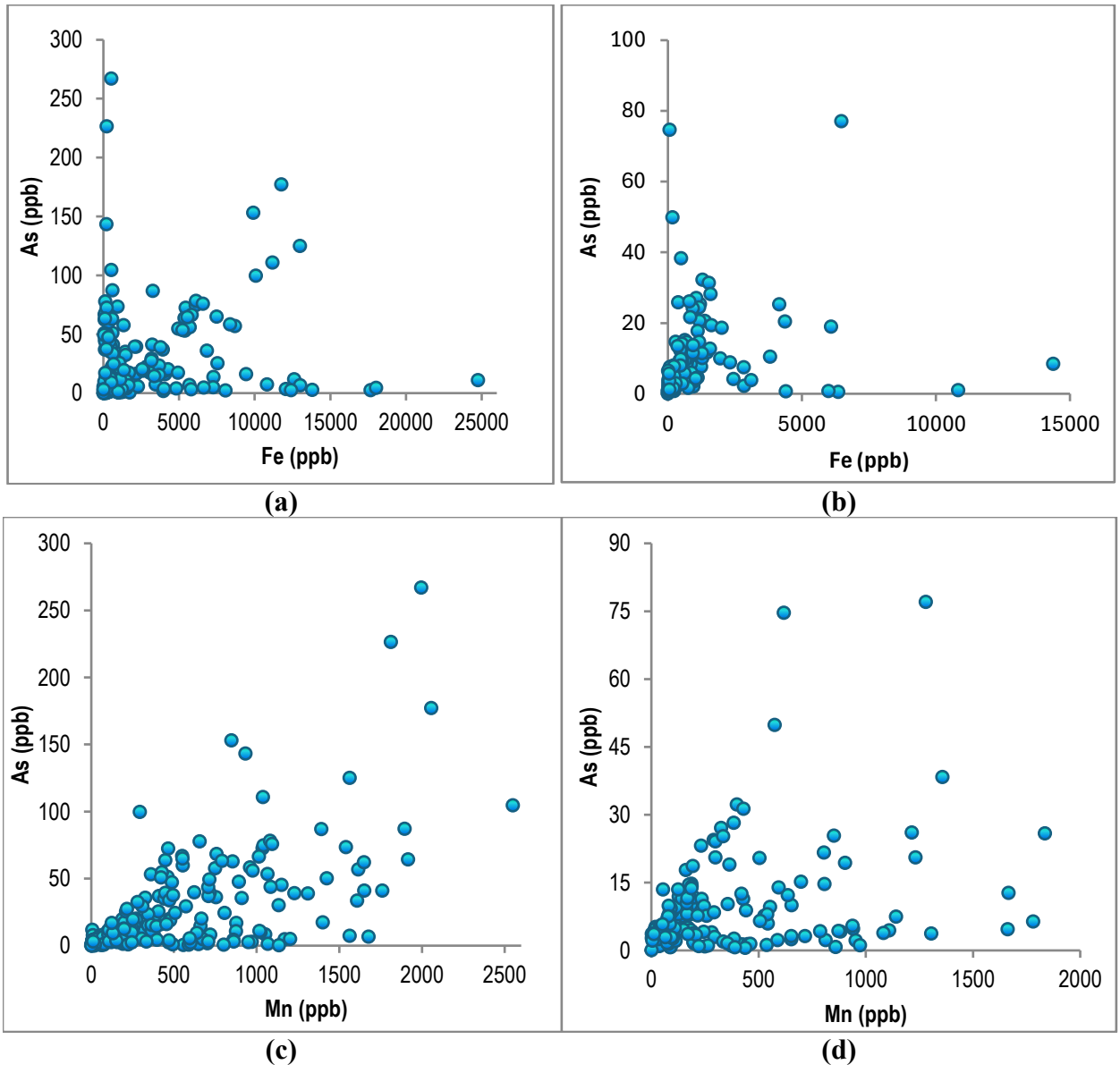

Fig. 3.30. Relationship of As with Fe and Mn in shallow and deep aquifers. (a) As vs Fe in Shallow wells, (b) As vs Fe in deep wells, (c) As vs Mn in Shallow wells, (b) As vs Mn in deep wells

3.5.3. Arsenic vs Barium (Ba)

A strong positive correlation (r = 0.691) was observed between arsenic and barium concentrations in shallow groundwater (Table 3.2a), suggesting a concurrent release mechanism or similar geochemical pathway (Figure 3.31a). In deep aquifers, the correlation was weaker (r = 0.421), but still indicates a potential influence of Ba on arsenic mobility (Figure 3.31b). These results imply that Ba may act as a geochemical indicator or co-mobilizing element during arsenic leaching in the study area.

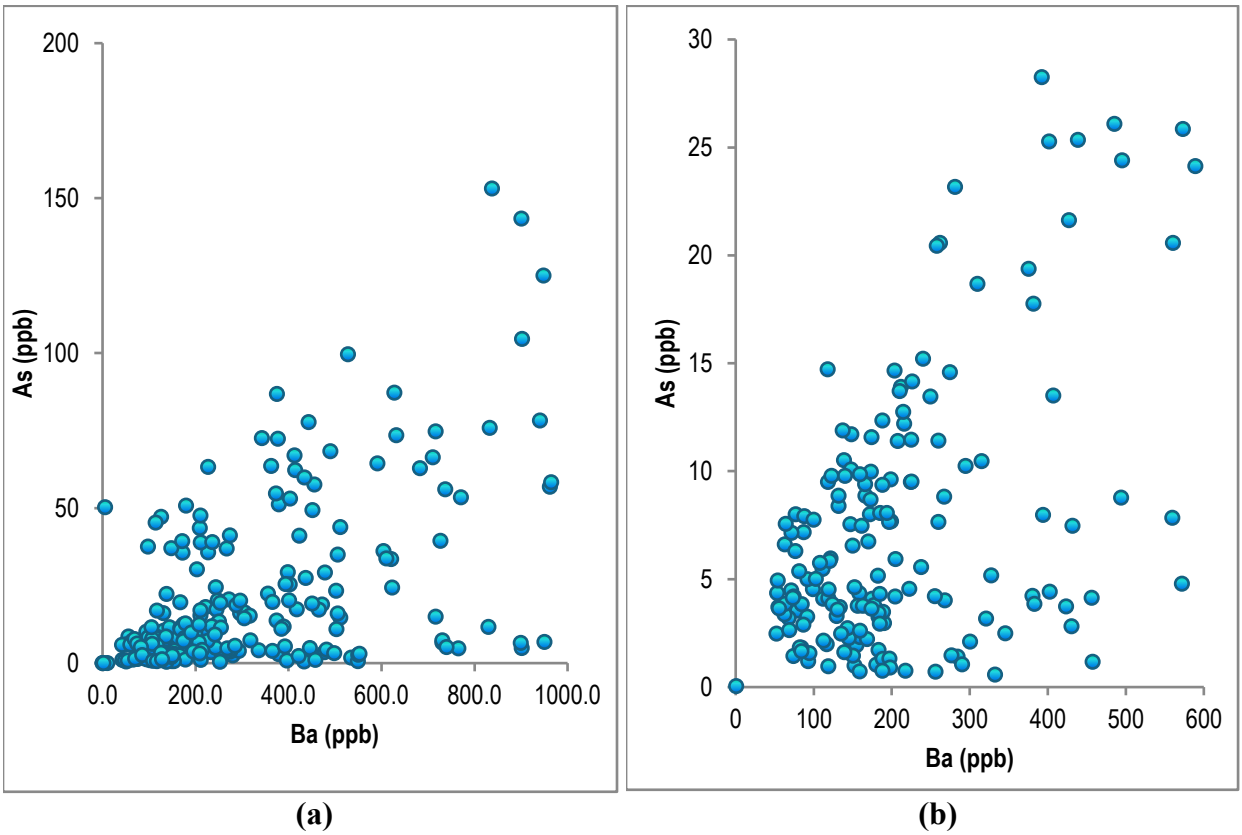

Fig. 3.31. Variation of As with Ba in (a) shallow and (b) deep groundwater

.

3.5.5. Arsenic vs Strontium (Sr) and Bicarbonate (HCO_3)

Strontium (Sr) showed a weak to moderate correlation with arsenic: r = 0.438 in shallow and r = 0.482 in deep aquifers (Tables 3.2a & b). Higher As concentrations were generally associated with higher Sr levels, especially in samples where As exceeded 150 ppb (Figure 3.32a & b). This may suggest that Sr-rich lithologies or ion exchange processes contribute indirectly to arsenic mobilization.

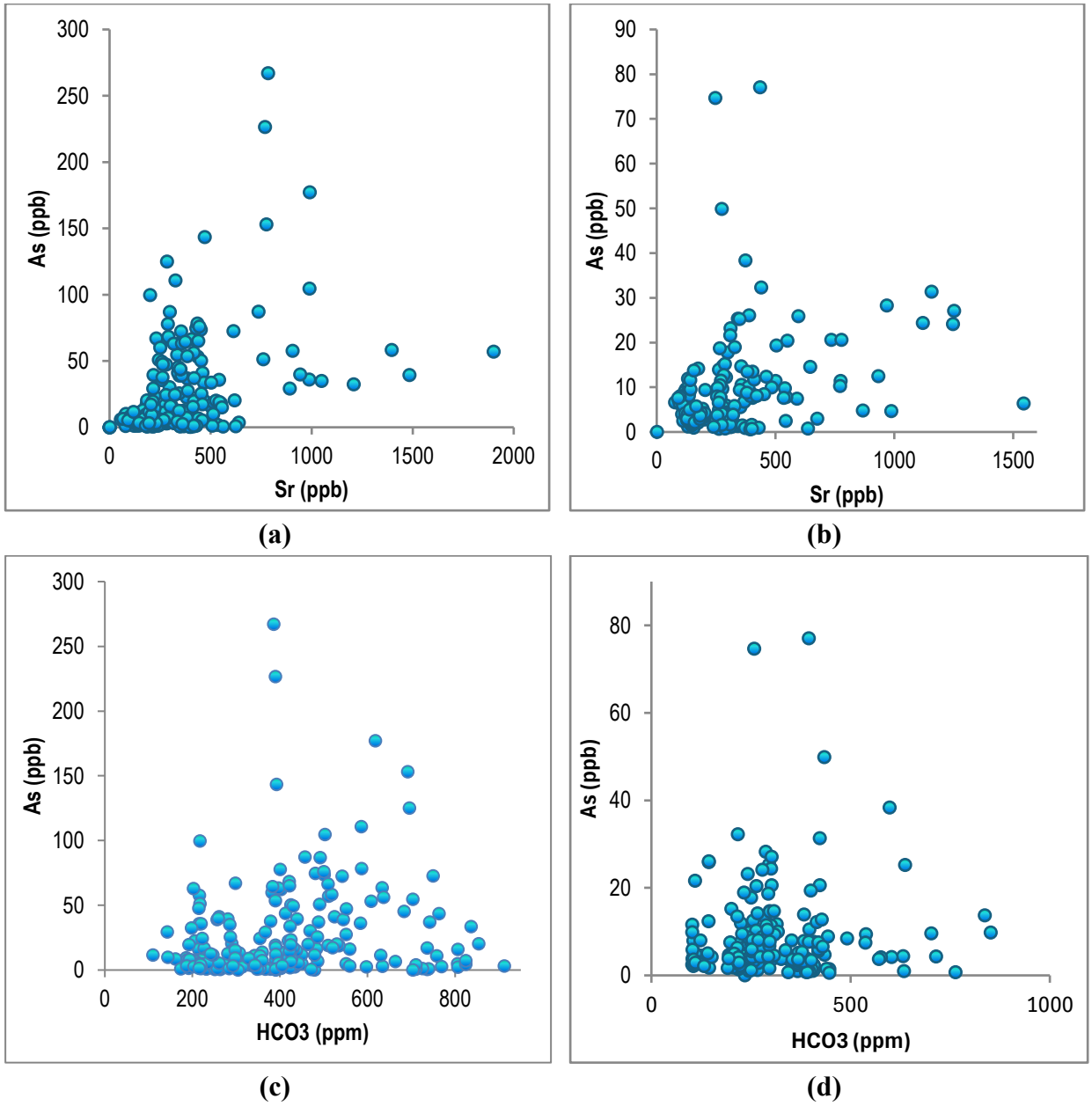

Fig.3.32. Relationship of As with Sr and HCO_3 in shallow and deep aquifers. (a) As vs Sr in Shallow wells, (b) As vs Sr in deep wells, (c) As vs HCO_3 in Shallow wells, (b) As vs HCO_3 in deep wells

Bicarbonate (HCO_3^-) showed a weak positive correlation with arsenic in shallow aquifers (r = 0.230), while the correlation was insignificant in deep aquifers (Figure 3.32c & d). However, the highest observed arsenic concentrations (up to 177.2 ppb) were found in samples with elevated bicarbonate levels, suggesting that high alkalinity may enhance arsenic desorption from mineral surfaces under certain conditions.

3.5.6. Arsenic vs Boron (B)

In shallow groundwater, arsenic showed a moderate positive correlation with boron (r = 0.422), indicating possible co-mobilization under similar geochemical conditions (Figure 3.33a). In contrast, arsenic and boron were weakly correlated in deep groundwater, and their concentrations were comparatively lower (Figure 3.33b). The high concentrations of both arsenic and boron in shallow aquifers suggest that they may be influenced by organic matter degradation and associated reductive processes.

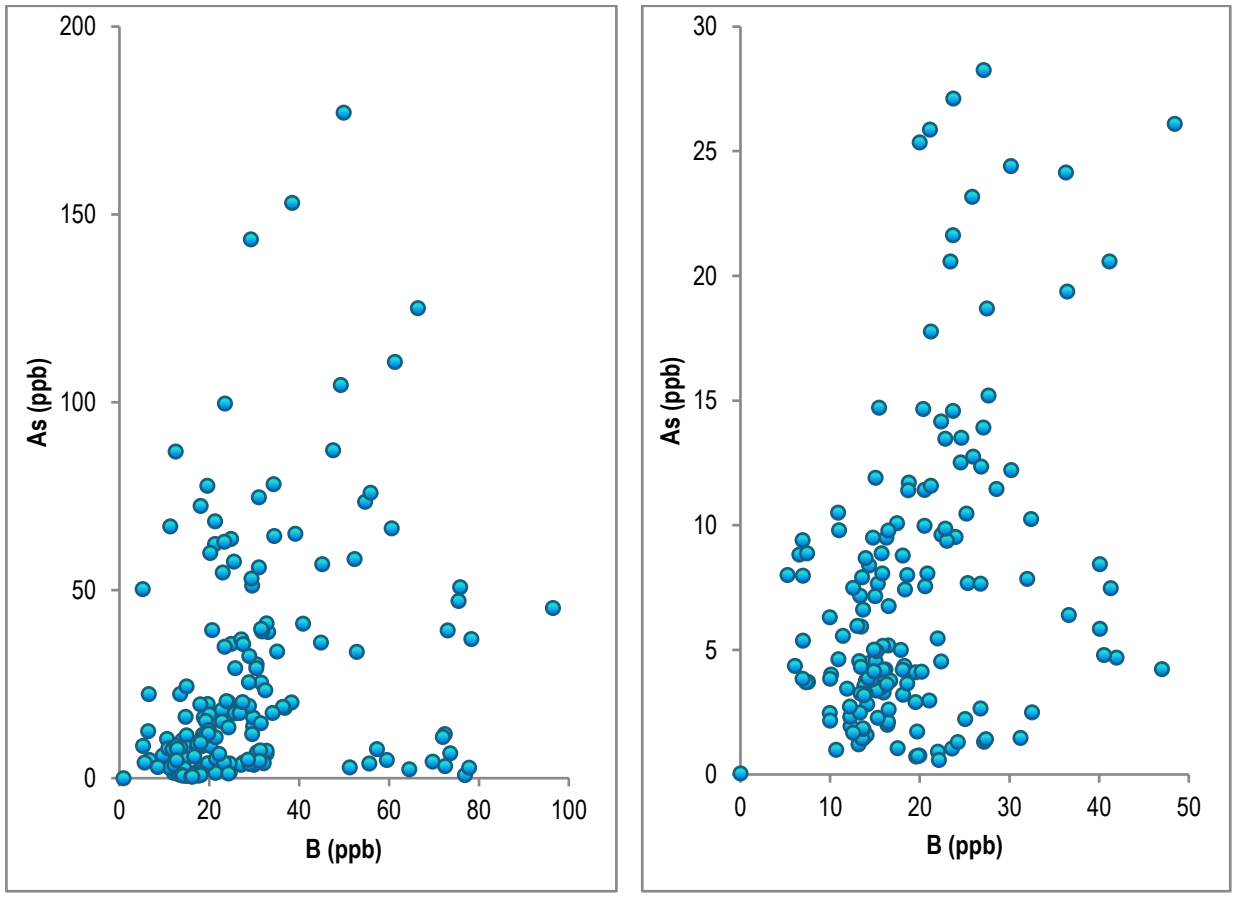

(a) **(b)**

Fig. 3.33. Variation of As with B in (a) shallow and (b) deep groundwater

The mobilization of arsenic in the groundwater of the Laksar and Roorkee blocks is predominantly influenced by reducing conditions, as indicated by negative correlations with ORP and positive correlations with Mn. While Fe shows limited influence, elements like Ba, Sr, and B appear to play supporting roles in arsenic mobilization, especially in shallow aquifers. Elevated bicarbonate levels further suggest that pH and alkalinity could influence arsenic desorption. Overall, shallow

aquifers are more susceptible to arsenic contamination due to stronger reducing conditions and higher concentrations of co-mobilizing elements. A comprehensive understanding of these hydrogeochemical interactions is essential for designing effective mitigation and groundwater management strategies in arsenic-prone regions.

3.6. Bioremediation Potential of Arsenite-Oxidizing Bacteria in Arsenic

3.6.1. Microbial - hydrogeochemical Interactions

The relationships between hydrogeochemical and microbiological parameters across seasonal datasets were evaluated using Principal Component Analysis (PCA). The first two principal components (Dim1 and Dim2) explained more than 65% of the total variance in all seasons, highlighting strong correlations among variables. High cos^2 values (orange to red in biplots) indicated the dominant factors influencing groundwater chemistry and microbial distribution (Figure 3.34).

During the pre-monsoon period, PCA revealed a strong positive correlation of arsenic (As) with Fe, Mn, alkalinity, electrical conductivity (EC), and total coliforms ((Figure 3.34a). These variables clustered together, suggesting a common geochemical regime governed by reductive dissolution of metal oxides under alkaline and reducing conditions. In contrast, arsenite-resistant bacteria (ARBs) and E. coli plotted away from this cluster, showing weaker associations with As and other redox-sensitive metals. Instead, ARBs aligned with pH, oxidation-reduction potential (ORP), and temperature, implying a preference for slightly oxidizing or transitional redox conditions where As(III) remains bioavailable but decoupled from coliform activity. These patterns suggest that pre-monsoon arsenic mobilization is primarily driven by alkaline reducing conditions, with coliforms enhancing reductive processes, while ARBs selectively occupy transitional niches.

During the monsoon season, total coliforms, *E. coli*, and EC clustered closely with As, Fe, Mn, and HCO_3^-, indicating that microbial contamination—likely from surface runoff and sewage infiltration—contributes to enhanced arsenic release (Figure 3.34b). This points to microbially mediated reductive dissolution of Fe/Mn oxides as a key mobilization pathway. As maintained strong correlations with Mn and Fe, underscoring the central role of redox processes. ARBs, however, showed weak correlations with As and geochemical variables, instead clustering near ORP, pH, and Cl^-, suggesting a distinct ecological preference for slightly oxidizing conditions.

Such findings collectively emphasize the complex interplay between geochemical and microbial shifts during pre-monsoon, monsoon, and post-monsoon seasons. This can potentially lead to As mobilisation in groundwater and public health hazards.

In the post-monsoon season, PCA revealed continued strong correlations between As, Mn, Fe, alkalinity, and EC, highlighting the sustained role of redox processes in arsenic mobilization. Notably, E. coli and total coliforms clustered near As and redox-sensitive parameters, reflecting persistent microbial contamination and input of organic matter, likely from sewage or surface runoff. These conditions promote sustained reducing environments, stimulating microbial activity and enhancing reductive dissolution of Fe/Mn oxides, thereby releasing arsenic. Interestingly, ARBs were positioned closer to NO_3^- and Na^+, suggesting a preference for moderately oxidizing niches possibly influenced by agricultural runoff or wastewater infiltration.

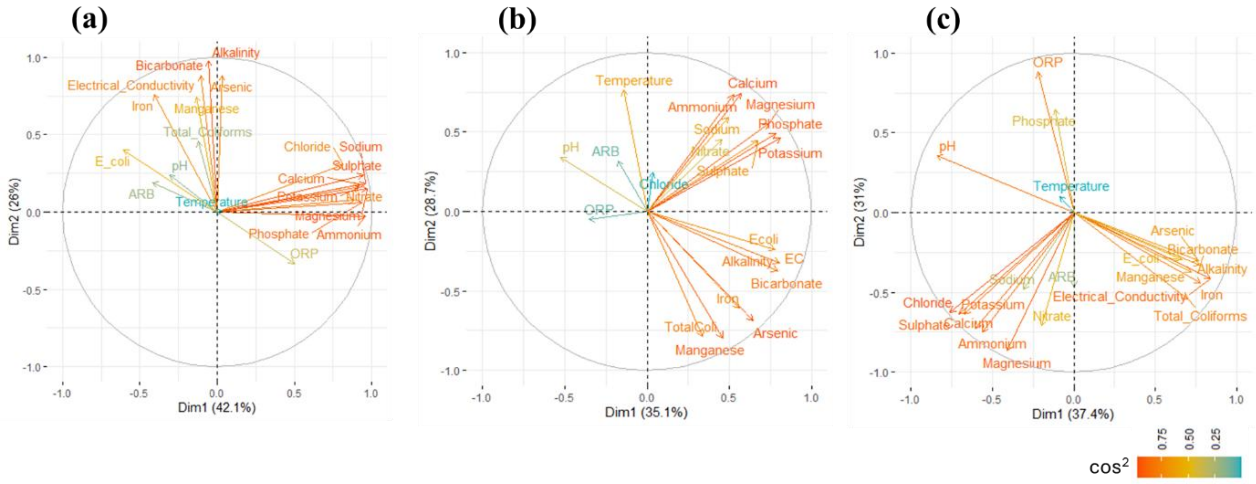

Fig. 3.34. PCA biplots showing the spatial alignment of physicochemical and microbiological parameters during (a) pre-monsoon (June), (b) monsoon (August), and (c) post-monsoon (October) seasons

Overall, PCA highlights a dynamic seasonal interplay between geochemical processes and microbial activity in governing arsenic mobilization. While reductive dissolution of Fe/Mn oxides emerges as the dominant geogenic mechanism, coliform contamination amplifies this process through microbial reduction pathways. Conversely, ARBs act as natural detoxifiers by oxidizing As(III) to the less mobile As(V), occupying transitional niches shaped by redox gradients and anthropogenic inputs. This duality underscores the aquifer's complexity, where mobilization and detoxification processes coexist and shift with seasonal conditions.

3.6.2. Seasonal distribution of Coliforms and As-resistant bacteria in groundwater

The seasonal variation of fecal indicator bacteria (Total coliforms and E. coli), alongwith arsenite-resistant bacteria (ARBs) and As(III)-oxidizing bacteria (AOBs), was assessed across all groundwater sampling sites (Figure 3.35a–c). Groundwater consistently showed elevated levels of coliforms exceeding WHO permissible limits, reflecting poor microbiological quality and unsuitability for direct human consumption. The highest concentrations of total coliforms (46 cells/mL) and *E. coli* (0.78 cells/mL) were observed in June at the Uussainpur site, whereas the Kuwakheda site recorded peak microbial loads during August (75.4 cells/mL total coliforms and 0.97 cells/mL *E. coli*), indicating localized fecal contamination, most likely due to sewage infiltration or runoff.

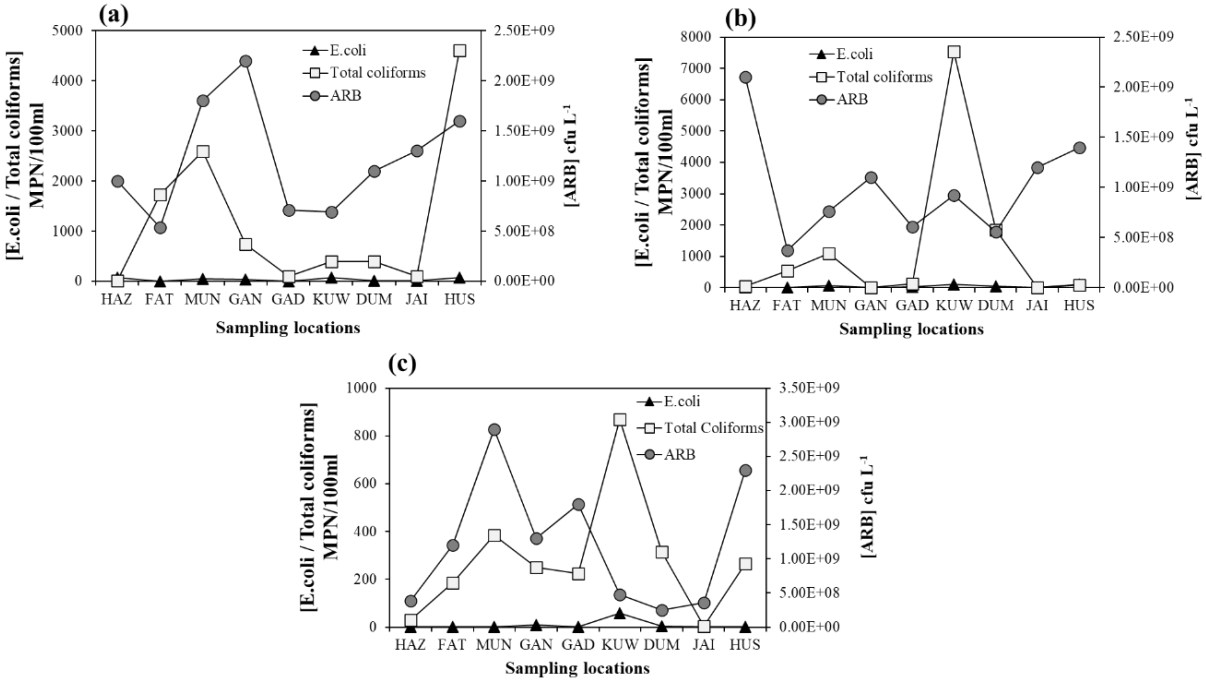

Fig. 3.35. Seasonal data on MPN Index of E. coli, Total coliforms and colony counts of Arsenite resistant bacteria (ARB): (a) Pre-monsoon (June), (b) Monsoon (August), (c) Post-monsoon (October)

Culture based quantification on media supplemented with 1mM As(III) revealed elevated ARBs counts across several sites, notably at Gangdaspur, Mundakheda, and Hazzarpur, where concentrations exceeded 2x109 CFU/L. Interestingly, despite high coliform levels at Kuwakheda in August, ARBs abundance was significantly lower (~9.2 × 10^8 CFU/L), suggesting that organic pollution may suppress ARB proliferation, either through substrate competition, ecological stress, or inhibition by fecal microbial populations. The inverse relationship between coliforms and ARBs

observed at Kuwakheda reinforces the hypothesis that fecal contamination alters microbial community dynamics, reducing the prevalence of naturally occurring arsenic-detoxifying bacteria.

Seasonal monitoring further highlighted the impact of monsoon recharge on groundwater microbiology. Coliforms and *E. coli* peaked during the monsoon and post-monsoon periods, consistent with surface runoff and sewage effluent infiltration into shallow aquifers. This contamination not only poses direct health risks but also promotes arsenic mobilization through microbial reductive processes, exacerbating groundwater quality concerns.

By contrast, ARBs exhibited spatial and seasonal variability. They thrived in groundwaters of Gangdaspur and Mundakheda but were consistently suppressed at Kuwakheda, where fecal contamination was dominant. Seasonal recharge likely plays a regulatory role by influencing redox conditions and nutrient availability, further shaping ARB abundance. The observed negative association between fecal bacteria and ARBs underscores the vulnerability of aquifer detoxification potential to anthropogenic pressures. In essence, while coliforms enhance arsenic release through reductive pathways, ARBs represent a natural detoxification mechanism that can be compromised in areas of intense pollution.

3.6.3. Arsenite-resistant bacteria (ARB) oxidation potential for bioremediation

A total of 152 ARB isolates were recovered from nine arsenic-contaminated groundwater sites and evaluated for their As(III)-oxidizing potential in a chemically defined medium (CDM). Na-acetate and bicarbonate (HCO_3^-) were provided as carbon sources, with As(III) serving as the sole electron donor. Most isolates grew only with Na-acetate, indicating a predominantly heterotrophic metabolism, while three anaerobic isolates showed growth with bicarbonate, suggesting autotrophic As(III) oxidizers.

Qualitative screening using $AgNO_3$ identified 28 isolates capable of As(III) oxidation, confirmed by the appearance of brown precipitates (Figure 3.36a). A complementary $KMnO_4$-based colorimetric microplate assay validated these findings: pink coloration indicated oxidation of As(III) to As(V). All 28 isolates oxidized 5 mM As(III) under aerobic conditions (Figure 3.36b), demonstrating their potential as arsenite-oxidizing bacteria (AOBs) with applications in arsenic bioremediation.

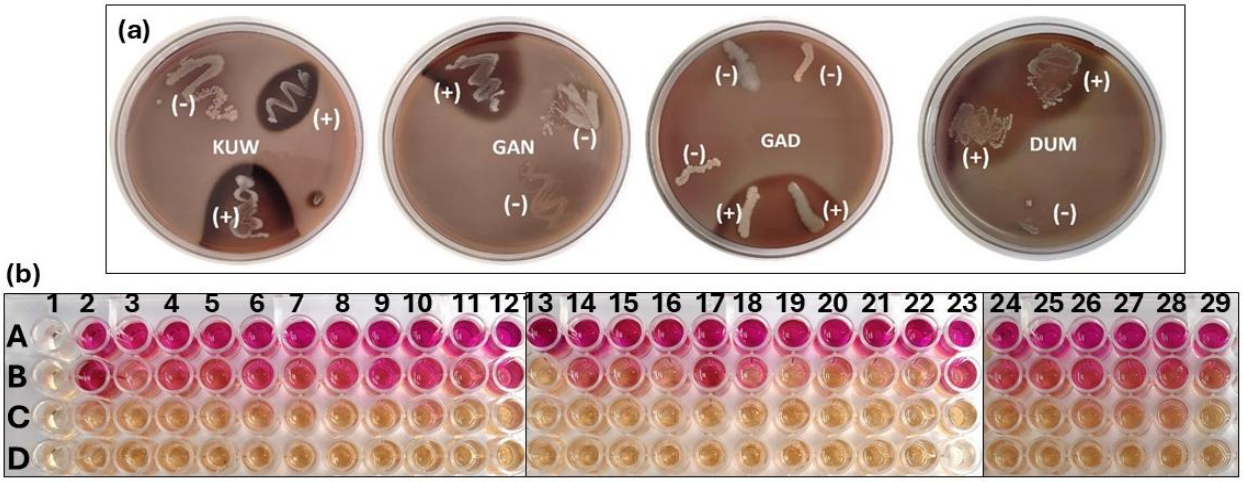

Fig. 3.36. Qualitative test for determination of AOBs: (a) AgNO3 test in agar plates for screening of bacterial isolates: Arsenite oxidizing bacteria (+) positive, (-) negative; (b) KMnO4 method in 96 well microtiter plate to determine oxidation potential of isolates against varying As(III) concentration. [A1 to D1: control without As(III), 2-29 represents isolates; A, B, C and D represent different As (III) concentrations as 1.33, 5, 10 and 20mM]

Growth and tolerance assays revealed concentration-dependent inhibition by As(III). At 1.33 mM, most isolates exhibited growth comparable to controls, while moderate inhibition was observed at 5 mM. At 10 mM, most isolates showed marked growth suppression, and at 20 mM, growth was nearly absent except in isolates D1 and KUW18, which retained measurable activity (Figure 3.37a). Quantitative oxidation assays normalized to dry cell weight (mM As(III) mg^{-1} d^{-1}) showed strong inter-strain variability (Figure 3.37b). Strains D1, KUW18, and C5 recorded the highest oxidation rates (~1.13 mM As(III) mg^{-1} d^{-1}), followed by GAN and KUW10 (0.7–0.93 mM As(III) mg^{-1} d^{-1}). Other isolates, such as FAT2, KUW23, and KUW29, displayed lower activities. These findings underscore the diversity of tolerance and detoxification efficiency among indigenous microbial populations.

ARB occurrence varied across sites. They were abundant in moderately oxidizing aquifers (e.g., Gangdaspur, Mundakheda) but suppressed in areas of heavy fecal contamination (e.g., Kuwakheda). PCA indicated co-localization of coliforms with arsenic and conductivity, suggesting anthropogenic pollution promotes arsenic mobilization while reducing AOB activity. Persistent fecal inputs may further shift microbial communities toward iron-reducing bacteria (IRBs), dissimilatory arsenate-reducing prokaryotes (DARPs), and sulfate-reducing bacteria (SRBs), which facilitate arsenic release but inhibit detoxifying AOBs.

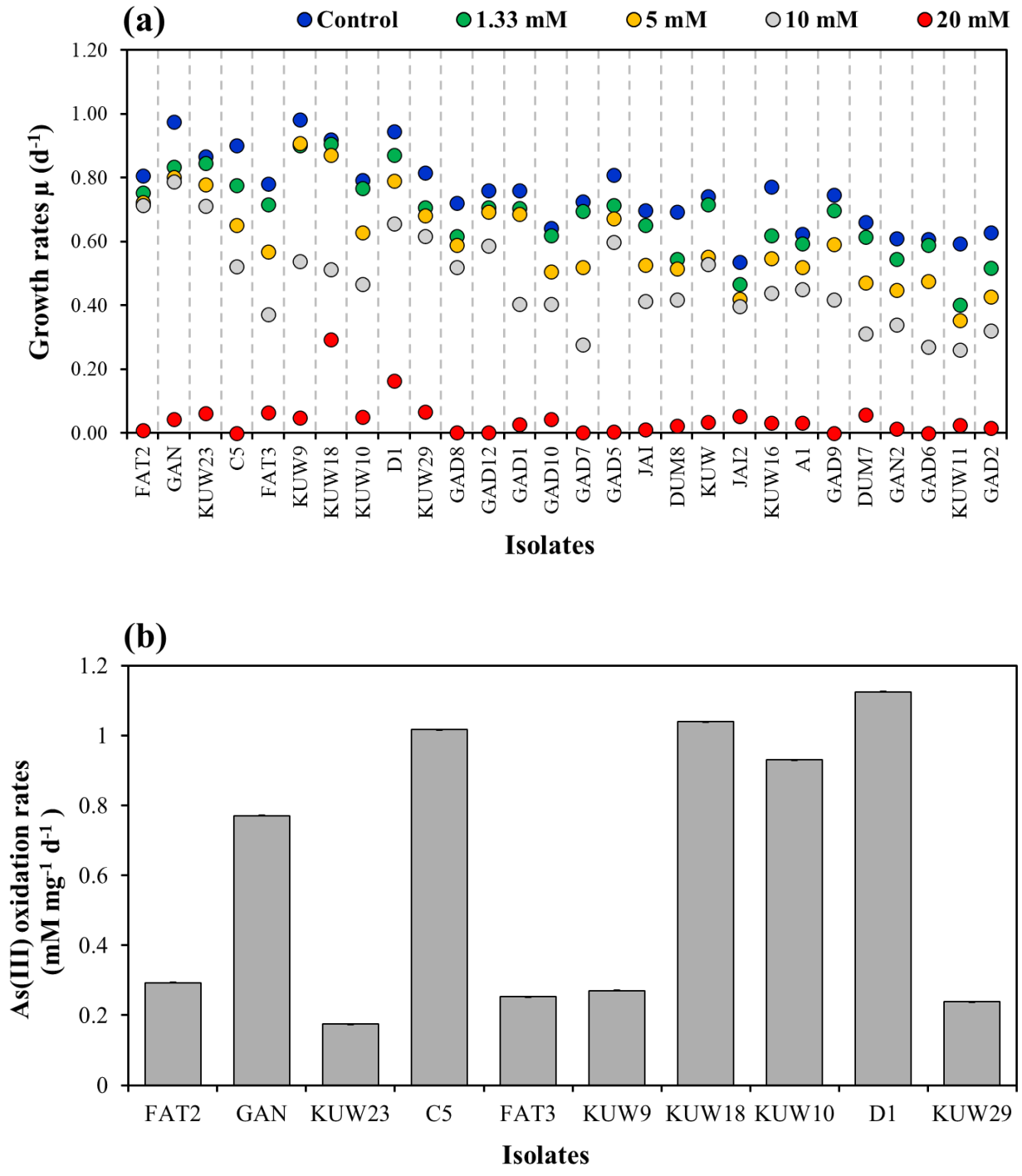

Fig. 3.37. As (III) tolerance and oxidation potentials of bacteria isolated from groundwater. (a) Effects of added As(III) on growth rates of isolates in minimal media with Na-acetate as C source; (b) As(III) oxidation rates of isolated strains normalised to dry-weight of cells.

Taxonomic analysis revealed dominance of Acinetobacter, Stenotrophomonas, and Bacillus, all known for metal resistance, biofilm formation, and enzymatic detoxification (Song et al., 2022). These genera also exhibited the highest oxidation rates (~1.3 mM As(III) mg^{-1} hr^{-1}). Brevundimonas sp. demonstrated dual oxidation–reduction capability, conferring flexibility under variable redox conditions (Banerjee et al., 2021). Additional genera such as Rhodococcoides and Nocardioides are associated with xenobiotic degradation and arsenic transformation (Kumari et al., 2019; Ma et al., 2023).

The role of arsenite oxidase (aioA) genes was strongly suggested. Inhibition assays with DEPC suppressed As(III) oxidation in selected isolates (Figure 3.38), pointing to enzymatic mediation. Reports confirm aioA presence in *Acinetobacter* and *Stenotrophomonas* from arsenic-contaminated aquifers (Dutta et al., 2023, 2024a; Singh et al., 2025). Phylogenetic analysis confirmed a diverse assemblage of AOBs, forming clades with *Acinetobacter johnsonii* and *A. haemolyticus* with strong bootstrap support (>70%) (Figure 3.39).

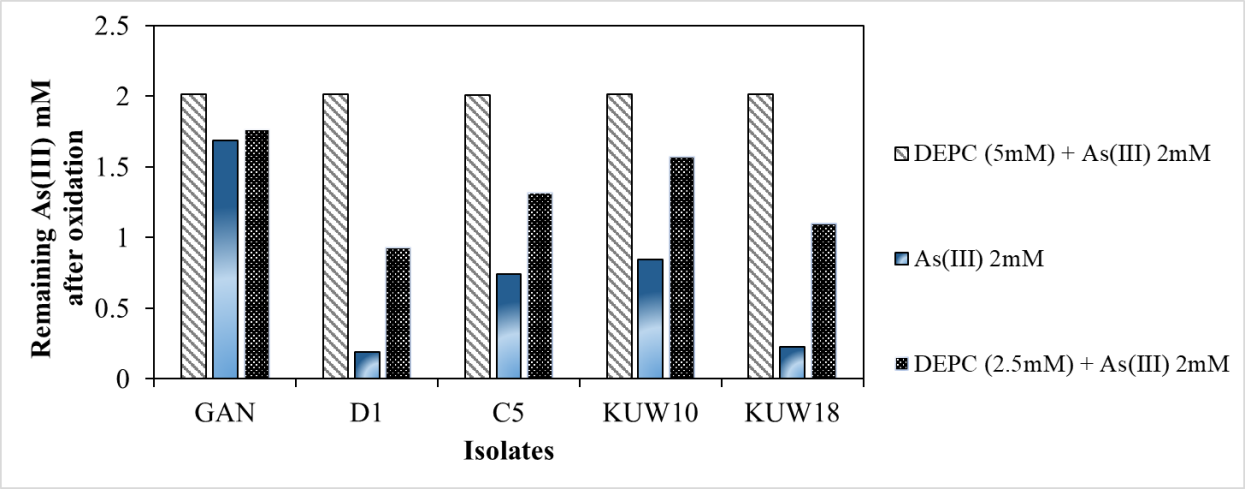

Fig. 3.38. AioA arsenite oxidase enzyme inhibition assay using DEPC (Di-ethyl pyrocarbonate)

Overall, 28 AOB strains, both heterotrophic and autotrophic, were confirmed as efficient As(III) oxidizers. Several isolates tolerated concentrations up to 20 mM, while most maintained growth and oxidation capacity up to 10 mM. Their resilience highlights the ecological importance of AOBs as natural detoxifiers and their strong potential for in situ bioremediation. Importantly, their metabolic versatility makes them suitable candidates for microbial-based interventions such as Subterranean Arsenic Removal (SAR), where stimulation of native AOB and Fe-oxidizers can enhance arsenic remediation efficiency (Gupta et al., 2024).

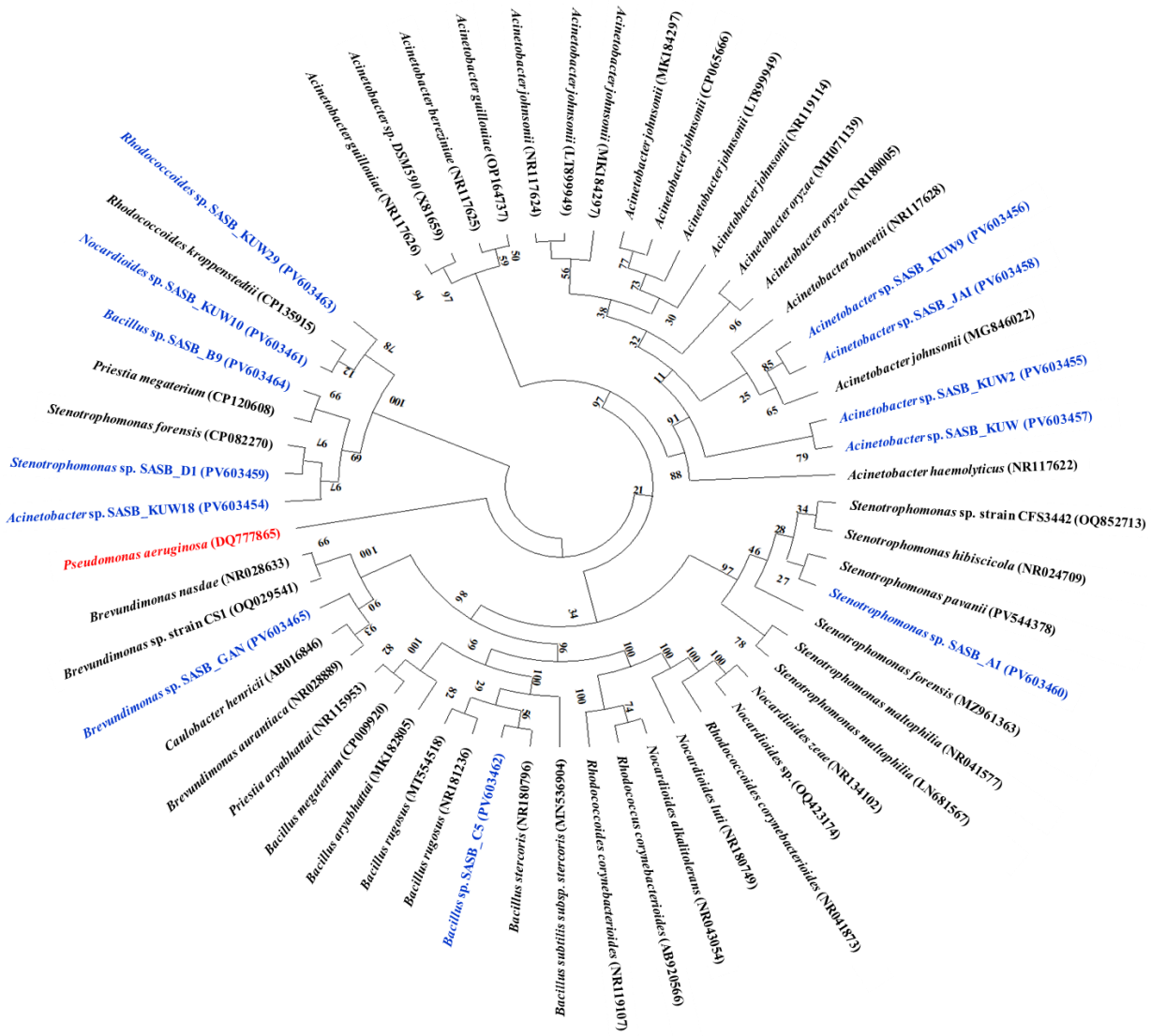

Fig. 3.39. Phylogenetic relationships of AOBs isolated from groundwater aquifers based on 16S rRNA gene sequences. GenBank accession numbers are shown in blue parentheses. The tree was constructed using the neighbor-joining method with maximum likelihood analysis. Bootstrap values (1000 replicates) are indicated at the branch nodes.

In summary, indigenous ARBs represent a diverse and adaptable microbial community with significant As(III) oxidation capacity. While their activity can be compromised by anthropogenic contamination, particularly fecal pollution, the identified strains demonstrate robust tolerance and enzymatic detoxification potential. These findings provide a strong foundation for developing sustainable, microbially driven arsenic remediation strategies and emphasize the need for further genomic and functional characterization of aioAB gene diversity to fully harness their biotechnological potential.

4. CONCLUSIONS & WAY FORWARD

Water remains the most critical natural resource, with human health and ecosystems directly dependent on its availability and quality. In the Laksar region of Haridwar, this study demonstrates how a combination of natural geochemical processes and anthropogenic activities threatens groundwater integrity. Rapid urbanization, agricultural intensification, and poor waste management have accelerated aquifer degradation, with arsenic mobilization emerging as a significant concern for shallow aquifers. The study highlights the following key conclusions:

- Groundwater chemistry in Haridwar is largely shaped by carbonate and silicate weathering, with Ca–Mg–HCO_3-type water dominating. Deeper aquifers appear less affected by anthropogenic activities, while shallow aquifers are more vulnerable to external influences.

- Trace metal contamination is most pronounced in shallow aquifers than in deeper ones, where arsenic, iron, manganese, aluminum, and uranium frequently exceed guideline values, posing serious health risks. Other metals such as copper, zinc, cadmium, chromium, and boron generally remain within safe limits, though sporadic exceedances of lead, nickel, cobalt, barium, selenium, and strontium highlight localized risks.

- Spatial and isotopic analysis reveal that river–aquifer interactions, intensive agricultural practices, and floodplain processes are key drivers of arsenic mobilization in the region. The combined spatial, seasonal, and depth-wise assessment shows that contamination is primarily restricted to shallow aquifers, where it is strongly influenced by surface recharge and land-use dynamics. Post-monsoon peaks highlight the role of infiltration-driven redox changes in enhancing arsenic release.

- Arsenic mobilization in groundwater is primarily governed by reducing conditions, with negative ORP correlations ($r = –0.212$ to $–0.245$) and strong positive associations with Mn ($r = 0.626$ in shallow, $r = 0.304$ in deep aquifers). Among co-occurring elements, Ba shows the highest correlation with arsenic ($r = 0.691$ shallow, $r = 0.421$ deep), followed by Sr ($r \approx 0.44$–0.48) and B ($r = 0.422$ shallow). Elevated bicarbonate levels were also linked to peak arsenic concentrations (~177.2 µg/L), suggesting alkalinity-driven desorption.

- Indigenous arsenite-resistant bacteria (ARBs) in the aquifers exhibit strong detoxification potential, with several isolates capable of oxidizing high concentrations of As(III). Taxonomic analysis confirmed dominance of Acinetobacter, Stenotrophomonas, and Bacillus, all harboring aioA-mediated enzymatic pathways. These findings establish ARBs as key natural regulators of arsenic cycling and highlight their promising role in sustainable in situ remediation strategies through biological oxidation.

Way Forward

Safeguarding groundwater in Haridwar requires an integrated and adaptive approach that bridges scientific understanding with policy implementation. Strengthening the connection between hydrogeochemical and microbial research and translating that knowledge into practical interventions is essential for long-term water security. Coordinated research, technological innovation, and strong governance mechanisms are needed to ensure safe and sustainable water resources for future generations. The following key directions are proposed:

- **Advance scientific understanding:** Conduct in-depth research on microbe–geochemistry interactions, focusing on the role of indigenous arsenite-resistant bacteria (ARBs) in natural attenuation and their potential for bio-augmentation. Pilot studies for in situ remediation of arsenic mobilization should be prioritized to validate field-scale feasibility.

- **Develop predictive and risk assessment tools:** Create integrated predictive models that combine hydrogeochemical data, land-use information, and microbial ecology to identify contamination hotspots, forecast future risks, and guide mitigation efforts.

- **Establish groundwater protection frameworks:** Policymakers should delineate and regulate vulnerable shallow aquifer zones, enforcing stricter controls on agricultural chemical use, fertilizer application, and wastewater discharge within recharge areas.

- **Institutionalize regular monitoring:** Implement routine testing of groundwater for key parameters, including trace metals, major ions, and microbial indicators, through a decentralized monitoring framework. Exceedances should be promptly reported, mapped, and made publicly accessible to enhance transparency and accountability.

- **Promote community-based management:** Strengthen community participation in groundwater governance through awareness programs, local water user committees, and citizen science initiatives to ensure collective ownership and sustainable practices.

REFERENCES

Adimalla, N. 2020 Controlling factors and mechanism of groundwater quality variation in semiarid region of south India: an approach of Water Quality Index (WQI) and Health Risk Assessment (HRA). Environmental Geochemistry and Health 42 (6), 1725–1752.

Amini, M., Abbaspour, K. C., Berg, M., Winkel, L., Hug, S. J., Hoehn, E., Yang, H., & Johnson, C. A. (2008a). Statistical modeling of global geogenic arsenic contamination in groundwater. Environmental Science & Technology, 42(10), 3669–3675.

Appelo, C.A.J., Postma, D., 2005. Geochemistry, Groundwater and Pollution, second ed. CRC Press, Taylor & Francis Group, Boca Raton.

Aullón Alcaine A, Schulz C, Bundschuh J, Jacks G, Thunvik R, Gustafsson J-PP, Mörth C-MM, Sracek O, Ahmad A, Bhattacharya P: Hydrogeochemical controls on the mobility of arsenic, fluoride and other geogenic co-contaminants in the shallow aquifers of northeastern La Pampa Province in Argentina. Sci Total Environ 2020, 715:136671.

Baloch MYJ, Talpur SA, Talpur HA, Iqbal J, Mangi SH, Memon S: Effects of arsenic toxicity on the environment and its remediation techniques: a review. J Water Environ Technol 2020, 18:275–289.

Bissen, M. and Frimmel, F. H. "Arsenic: a review—part I: occurrence, toxicity, speciation, mobility," Acta Hydrochimica etHydrobiologica, vol. 31, no. 1, pp. 9–18, 2003.

CGWB, 2016, Aquifer Mapping Report Haridwar District, Uttarakhand Central Ground Water Board Ministry Of Water Resources, River Development and Ganga Rejuvenation, Government of India, Uttaranchal Region, Dehradun

Chakraborti, D. *et al.* (2003) "Arsenic groundwater contamination in Middle Ganga Plain, Bihar,India: a future danger?," *Environmental health perspectives*, 111(9), pp. 1194–1201. doi:10.1289/ehp.5966.

Chakraborty, M., Mukherjee, A., & Ahmed, K. M. (2015). A Review of Groundwater Arsenic in the Bengal Basin, Bangladesh and India: from Source to Sink. Current Pollution Reports, 1(4), 220–247.

Dowling, C. B., Poreda, R. J., Basu, A. R., Peters, S. L., & Aggarwal, P. K. (2002). Geochemical study of arsenic release mechanisms in the Bengal Basin groundwater. Water Resources Research, 38(9), 12-1-12–18.

Egbueri, J. C., Mgbenu, C. N. & Chukwu, C. N. 2019 Investigating the hydrogeochemical processes and quality of water resources in Ojoto and environs using integrated classical methods. Modeling Earth Systems and Environment, 5 (4), 1443–1461.

Fakhreddine S, Prommer H, Scanlon BR, Ying SC, Nicot J: Mobilization of arsenic and other naturally occurring contaminants during managed aquifer recharge: a critical review. Environ Sci Technol 2021, 55:2208–2223.

Fan, H., Su, C., Wang, Y., Yao, J., Zhao, K., Wang, Y., & Wang, G. (2008). Sedimentary arsenite-oxidizing and arsenate-reducing bacteria associated with high arsenic groundwater from Shanyin, Northwestern China. Journal of Applied Microbiology, 105(2), 529–539.

Gautam, A., Rai, S.C., Rai, S.P., Ram, K., 2022. Impact of Anthropogenic and Geological Factors on Groundwater Hydrochemistry in the Unconfined Aquifers of Indo- Gangetic Plain. Physics and Chemistry of the Earth. Parts A/B/C, 103109.

Goyal, V. C., Singh, O., Singh, R., Chhoden, K., Kumar, J., Yadav, S., Singh, N., Shrivastava, N. G. & Carvalho, L. 2021 Ecological health and water quality of village ponds in the subtropics limiting their use for water supply and groundwater recharge. Journal of Environmental Management, 277, 111450.

Hug SJ, Winkel LHE, Voegelin A, Berg M, Johnson AC: Arsenic and other geogenic contaminants in groundwater – a global challenge. Chimia 2020, 74:524.

Islam, F. S., Gault, A. G., Boothman, C., Polya, D. A., Charnock, J. M., Chatterjee, D., & Lloyd, J. R. (2004). Role of metal-reducing bacteria in arsenic release from Bengal delta sediments. Nature, 430(6995), 68-71.

Jain CK, Ali I: Arsenic: occurrence, toxicity and speciation techniques. Water Res 2000, 34:4304–4312.

Jha, R., Singh, V. P., & Vatsa, V. (2008). Analysis of urban development of Haridwar, India, using entropy approach. *KSCE journal of Civil Engineering*, *12*(4), 281-288.

Jiang, Z., Li, P., Wang, Y., Liu, H., Wei, D., Yuan, C., & Wang, H. (2019). Arsenic mobilization in a high arsenic groundwater revealed by metagenomic and Geochip analyses. Scientific Reports, 9(1), 1–10.

Kaiser, H. F. 1958 The varimax criterion for analytic rotation in factor analysis. Psychometrika, 23 (3), 187–200.

Khan, M.U., Rai, N. Arsenic and selected heavy metal enrichment and its health risk assessment in groundwater of the Haridwar district, Uttarakhand, India. *Environ Earth Sci* **81**, 337 (2022).

Kulkarni, H. V., Mladenov, N., Johannesson, K. H., & Datta, S. (2017). Contrasting dissolved organic matter quality in groundwater in Holocene and Pleistocene aquifers and implications for influencing arsenic mobility. Applied Geochemistry, 77, 194–205.

Kumar, M., Das, N., Tripathi, S., Verma, A., Jha, P. K., Bhattacharya, P., & Mahlknecht, J. (2023). Global co-occurrences of multi-(emerging)-contaminants in the hotspots of arsenic polluted

groundwater: A pattern of menace. *Current Opinion in Environmental Science & Health*, *34*, 100483.

Kumar, S., Joshi, S.K., Pant, N., Singh, S., Chakravorty, B., Saini, R.K., Kumar, V., Singh, A., Ghosh, N.C., Mukherjee, A., Rai, P., Singh, V., 2021a. Hydrogeochemical evolution and groundwater recharge processes in arsenic enriched area in central Gangetic plain, India. Appl. Geochem. 131, 105044.

Lapworth, D.J., Das, P., Shaw, A., Mukherjee, A., Civil, W., Petersen, J.O., MacDonald, A. M., 2018. Deep urban groundwater vulnerability in India revealed through the use of emerging organic contaminants and residence time tracers. Environ. Pollut. 240, 938–949.

Lapworth, D.J., Das, P., Shaw, A., Mukherjee, A., Civil, W., Petersen, J.O., MacDonald, A. M., 2018. Deep urban groundwater vulnerability in India revealed through the use of emerging organic contaminants and residence time tracers. Environ. Pollut. 240, 938–949.

Lapworth, D.J., Krishan, G., MacDonald, A.M., Rao, M.S., 2017. Groundwater quality in the alluvial aquifer system of northwest India: new evidence of the extent of anthropogenic and geogenic contamination. Sci. Total Environ. 599–600, 1433–1444.

Maciag, B. J., Brenan, J. M., Parsons, M. B., & Kennedy, G. W. (2023). Sources of geogenic arsenic in well water associated with granitic bedrock from Nova Scotia, Canada. *Science of The Total Environment*, *887*, 163943.

McArthur, J. M., Ravenscroft, P., Safiulla, S., & Thirlwall, M. F. (2001). Arsenic in groundwater: Testing pollution mechanisms for sedimentary aquifers in Bangladesh. Water Resources Research, 37(1), 109–117.

Mukherjee, A., Bhattacharya, P., Savage, K., Foster, A., Bundschuh, J., 2008. Distribution of geogenic arsenic in hydrologic systems: controls and challenges. J. Contam. Hydrol.

National Green Tribunal (NGT), 2019, District Environmental Plan of Haridwar, 2019, G.B. Pant National Institute of Himalayan Environment (NIHE), HQ, Kosi-Katarmal Almora-263643, Uttarakhand, India.

Nijesh, P., Akpataku, K.V., Abhinav, Rai, P., Rai, S.P., 2021. Spatial variability of hydrochemical characteristics and appraisal of water quality in stressed phreatic aquifer of Upper Ganga Plain, Uttar Pradesh, India. Environ. Earth Sci. 80 (5), 185.

Oremland, R. S., & Stolz, J. F. (2005). Arsenic, microbes and contaminated aquifers. Trends in Microbiology, 13(2), 45–49.

Pal, S.C., Islam, A.R.M.T., Chakrabortty, R., Islam, M.S., Saha, A., Shit, M., 2022. Application of data-mining technique and hydro-chemical data for evaluating vulnerability of groundwater in Indo-Gangetic Plain. J. Environ. Manag. 318, 115582.

Pant, N., Rai, S.P., Singh, R., Kumar, S., Saini, R.K., Purushothaman, P., Pratap, K., 2021. Impact of geology and anthropogenic activities over the water quality with emphasis on fluoride in water scarce Lalitpur district of Bundelkhand region, India. Chemosphere 279, 130496.

Parul, A. and Saraswat, H. (2024). Arsenic Metal Analysis at Selective Region of West Bengal, Department of Chemistry, Mangalaytan University, (Thesis).

Podgorski J, Berg M: Global threat of arsenic in groundwater. Science (80-.) 2020, 368:845–850.

Raessler, M., Michalke, B., Schulte-Hostede, S., Kettrup, A., 2000. Long-term monitoring of arsenic and selenium species in contaminated groundwaters by HPLC and HG-AAS. Sci. Total Environ. 258, 171 – 181.

Rai, D., Saini, R., Kumar, S., Arya, S., Noble, J., & Singh, D. (2025). Stable isotopic characterization and estimation of canal recharge to the groundwater in a part of the Ganga Plain, North India. *Journal of Hydrology*, *655*, 132962.

Sarkar, A., & Paul, B. (2016). The global menace of arsenic and its conventional remediation - A critical review. Chemosphere, 158, 37–49.

Sarkar, A., & Paul, B. (2016). The global menace of arsenic and its conventional remediation - A critical review. Chemosphere, 158, 37–49.

Schreiber, M.E., Simo, J.A., Freiberg, P.G., 2000. Stratigraphic and geochemical controls on naturally occurring arsenic in groundwater, eastern Wisconsin, USA. Hydrogeol. J. 8, 161 – 176.

Sharma, B., Savera, K. K., Kausik, S., Saini, P., Bhadula, S., Sharma, V., & Singh, P. (2016). Assessment of Ground Water Quality of Bhagwanpur Industrial Area of Haridwar in Uttarakhand, India. *Applied Ecology and Environmental Sciences*, *4*(4), 96-101.

Singh, A. L., & Singh, V. K. (2015). Arsenic contamination in ground water of Ballia, Uttar Pradesh state, India. Journal of Applied Geochemistry, 17(1), 78-85.

Singh, K., Singh, R., & Pandey, G. (2023). Hydrogeochemistry, solute source identification, and health risk assessment of groundwater of cancer-prone region in India. Water Supply, 23(1), 317-342.

Slyemi, D., & Bonnefoy, V. (2012). How prokaryotes deal with arsenic. Environmental Microbiology Reports, 4(6), 571–586.

Smedley PL, Kinniburgh DG: A review of the source, behaviour and distribution of arsenic in natural waters. Appl Geochem 2002, 17:517–568.

Smedley, P. L., & Kinniburgh, D. G. (2002). A review of the source, behaviour and distribution of arsenic in natural waters. Applied Geochemistry, 17(5), 517–568.

Slides of Sampling Sites

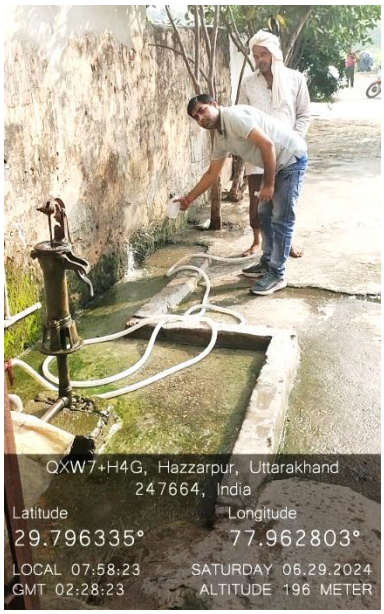


राजकीय प्राथमिक विद्यालय गंगदासपुर
वि. क्षे. लक्सर जिला हरिद्वार उत्तराखण्ड
M463+V2M, Gangdaspur, Mansoorpur Urf Kapooro, Uttarakhand 251327, India
Latitude
29.662332°
Longitude
78.102570°
LOCAL 11:48:32
GMT 06:18:32
THURSDAY 06.27.2024
ALTITUDE 202 METER


M39J+7X6, Kaputo, Raghunathpur Urf Balawali, Uttarakhand 247671, India
Latitude
29.668117°
Longitude
78.082183°
LOCAL 11:14:54
GMT 05:44:54
THURSDAY 06.27.2024
ALTITUDE 187 METER


Unnamed Road, Mansoorpur Urf Kapooro, Damanpuri, Uttarakhand 251327, India
Latitude
29.649146°
Longitude
78.087881°
LOCAL 09:11:42
GMT 03:41:42
FRIDAY 06.28.2024
ALTITUDE 186 METER

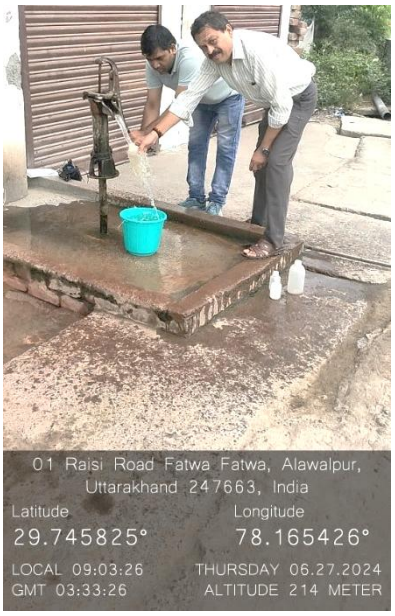
01 Raisi Road Fatwa Fatwa, Alawalpur, Uttarakhand 247663, India
Latitude
29.745825°
Longitude
78.165426°
LOCAL 09:03:26
GMT 03:33:26
THURSDAY 06.27.2024
ALTITUDE 214 METER

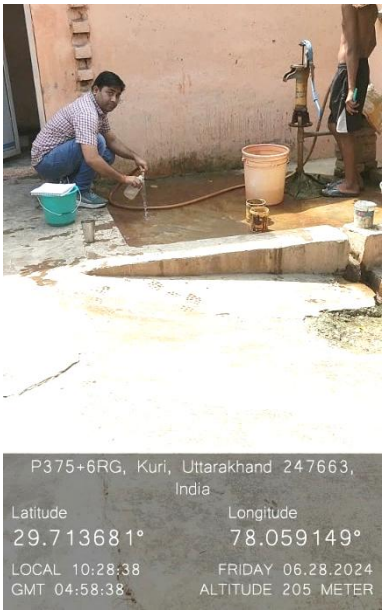
P375+6RG, Kuri, Uttarakhand 247663, India
Latitude
29.713681°
Longitude
78.059149°
LOCAL 10:28:38
FRIDAY 06.28.2024
GMT 04:58:38
ALTITUDE 205 METER

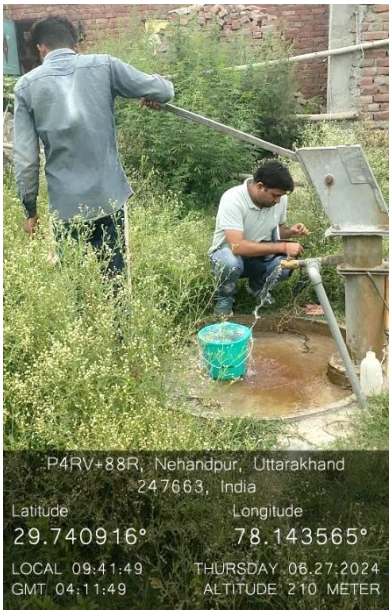
P4RV+88R, Nehandpur, Uttarakhand 247663, India
Latitude
29.740916°
Longitude
78.143565°
LOCAL 09:41:49
THURSDAY 06.27.2024
GMT 04:11:49
ALTITUDE 210 METER


01 Raisi Road Fatwa Fatwa, Alawalpur, Uttarakhand 247663, India
Latitude
29.745720°
Longitude
78.165587°
LOCAL 09:10:33
THURSDAY 06.27.2024
GMT 03:40:33
ALTITUDE 214 METER

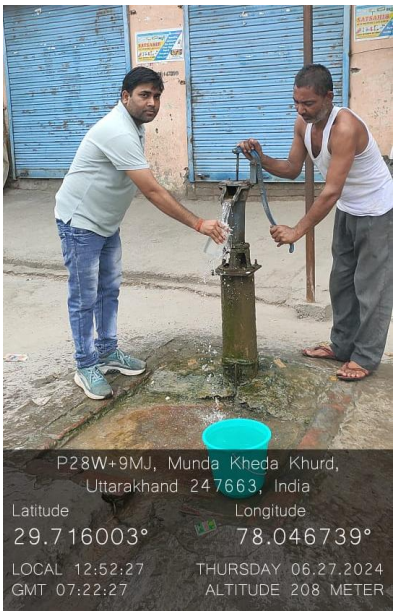
P28W+9MJ, Munda Kheda Khurd, Uttarakhand 247663, India
Latitude
29.716003°
Longitude
78.046739°
LOCAL 12:52:27
THURSDAY 06.27.2024
GMT 07:22:27
ALTITUDE 208 METER


P5W8+W44, Alawalpur, Uttarakhand 247663, India
Latitude
29.747242°
Longitude
78.165347°
LOCAL 10:23:05
TUESDAY 12.24.2024
GMT 04:53:05
ALTITUDE 210 METER


M39V+44R, Kur, Kapuro, Uttarakhand 247671, India
Latitude
29.667976°
Longitude
78.082734°
LOCAL 12:20:48
TUESDAY 12.24.2024
GMT 06:50:48
ALTITUDE 176 METER


P4RV+88R, Nehandpur, Uttarakhand 247663, India
Latitude
29.740949°
Longitude
78.143555°
LOCAL 11:13:40
TUESDAY 12.24.2024
GMT 05:43:40
ALTITUDE 210 METER


P28W+MMJ, Laksar - Balawali Rd, Munda Kheda Khurd, Uttarakhand 247663, India
Latitude
29.716511°
Longitude
78.046617°
LOCAL 12:49:25
TUESDAY 12.24.2024
GMT 07:19:25
ALTITUDE 203 METER


P28W+9MJ, Munda Kheda Khurd,
Uttarakhand 247663, India
Latitude
29.715989°
Longitude
78.046772°
LOCAL 12:56:54
GMT 07:26:54
TUESDAY 12.24.2024
ALTITUDE 203 METER


M39M+44R, Kuri, Kaputo, Uttarakhand
247671, India
Latitude
29.667829°
Longitude
78.083137°
LOCAL 12:26:19
GMT 06:56:19
TUESDAY 12.24.2024
ALTITUDE 177 METER


Akodaa mukrmtpurR7 Haridwar, Laksar,
Kuri, Uttarakhand 247663, India
Latitude
29.713950°
Longitude
78.059208°
LOCAL 13:15:09
GMT 07:45:09
TUESDAY 12.24.2024
ALTITUDE 204 METER


P376+X8J, Kuri, Uttarakhand 247663,
India
Latitude
29.712781°
Longitude
78.061023°
LOCAL 13:26:38
GMT 07:56:38
TUESDAY 12.24.2024
ALTITUDE 204 METER


M39M+44R, Kur, Kaputo, Uttarakhand 247671, India
Latitude
29.667829°
Longitude
78.083137°
LOCAL 12:26:19
TUESDAY 12.24.2024
GMT 06:56:19
ALTITUDE 177 METER


M463+V2M, Gangdaspur, Mansoorpur Urf Kapooro, Uttarakhand 251327, India
Latitude
29.662957°
Longitude
78.103078°
LOCAL 12:23:45
THURSDAY 12.26.2024
GMT 06:53:45
ALTITUDE 179 METER


QXPH+7P3, Majri Akbarpur, Uttarakhand 247663, India
Latitude
29.785626°
Longitude
77.979640°
LOCAL 13:22:45
FRIDAY 12.27.2024
GMT 07:52:45
ALTITUDE 191 METER


Unnamed Road, Uttarakhand 247666, India
Latitude
29.794639°
Longitude
77.919562°
LOCAL 11:00:11
FRIDAY 12.27.2024
GMT 05:30:11
ALTITUDE 229 METER


Shiri Guru Ravidas Mandir Khanpur ,
brahampur, P48V+V7M, Rasoolpur Urf
Kankarkhata, Uttarakhand 247671, India
Latitude
29.717849°
Longitude
78.133689°
LOCAL 15:17:45
GMT 09:47:45
FRIDAY 12.27.2024
ALTITUDE 205 METER


M3CQ+X7J, Panditpuri, Uttarakhand
247671, India
Latitude
29.672757°
Longitude
78.087677°
LOCAL 13:02:14
GMT 07:32:14
THURSDAY 12.26.2024
ALTITUDE 186 METER